Effective Porosity and Longitudinal Dispersivity of Sedimentary Rocks Determined by Laboratory and Field Tracer Tests

December 1994

HIROYUKI II

Graduate School of Science and Technology
CHIBA UNIVERSITY

千葉大学学位申請論文

Effective Porosity and Longitudinal Dispersivity of Sedimentary Rocks Determined by Laboratory and Field Tracer Tests

１９９４年１２月１日

千葉大学大学院自然科学研究科

環境科学専攻環境動態学

井伊博行

Contents

ABSRACT 1

1. INTRODUCTION 2

2. TRACERS 6

3. TOKI FIELD TRACER TEST

3.1 Method 8

3.2 Gelhar method 9

3.3 FEM analysis 11

1) Seepage analysis 11

2) Migration analysis 12

3) Numerical results 15

4. TOKI ROCK SAMPLE LABORATOTRY TRACER TESTS

4.1 Method 17

4.2 Analysis 17

4.3 Results 19

5. MATSUMOTO FIELD TRACER TEST

5.1 Study area 20

5.2 Tracer test 22

5.3 Analysis 23

1) Seepage analysis 23

2) Migration analysis 26

5.4 Numerical results 27

1) $K = 6.4 \times 10^{-3}$ m hour^{-1} 28

2) $K = 2.4 \times 10^{-4}$ m hour^{-1} 30

3) $K = 4.1 \times 10^{-2}$ and 6.8×10^{-2} m hour^{-1} 30

4) $K = 8.6 \times 10^{-2}$ and 1.1×10^{-1} m hour^{-1} 30

5) $K = 1.5 \times 10^{-1}$ and 2.8×10^{-1} m hour^{-1} 31

6. BENTONITE AND QUARTZ-SAND MIXTURE LABORATORY TRACER TESTS

6.1 Material 33

6.2 Method 34

6.3 Results 35

7. PORE SIZE MEASUREMENT OF BENTONITE QUARTZ-SAND MIXTURE

7.1 Method 36

7.2 Results and discussion 37

8. DISCUSSION 40

9. CONCLUSION 43

10. ACKNOWLEDGMENT 44

11. REFERENCE 45

12. TABLES AND FIGURES 49

ABSTRACT

Effective porosity is defined as the proportion of pores through which water flows and consists of only continuous pores. Effective porosity is estimated from results of tracer tests in order to calculate the actual velocity of groundwater. However, there is little data concerning effective porosity determined by tracer test in Japan. Dispersion is also an essential phenomenon for estimating mass transport in groundwater. Therefore we performed both laboratory (Toki sedimentary rocks, bentonite and quartz-sand mixture) and field (Toki and Matsumoto sites) tracer tests using conservative tracers in order to estimate the effective porosity and longitudinal dispersivity (dispersion) of a sedimentary rock. Both the laboratory and field tracer test results indicate that as test scale increases from 1.0 cm to 130 m, effective porosity decreases and longitudinal dispersivity increases. The following empirical relationship has been found for the sedimentary formation : longitudinal dispersivity equals one tenth of scale. This is in agreement with the relationship presented in the paper by Domenico and Robbins. The relationship is useful for estimating mass transport in groundwater.

The decrease in effective porosity may be attributed to the loss of continuous pore connectivity at the laboratory scale and the increase of selective flow path such as cracks and fissures from laboratory scale to field scale. The existence of selective flow paths such as cracks and fissures has been suggested based on the results of field permeability tests. The lower effective porosity encountered at the field scale may be attributed to the existence of selective flow paths not present in the laboratory samples. The existence of cracks at the field scale explain also effects of longitudinal dispersivity because heterogeneities may be encountered and a higher longitudinal dispersivity would be expected.

1. INTRODUCTION

Groundwater fills all of the interstices in the saturated zone, hence the porosity is a direct measure of the water contained per unit volume. Not all of this water may be removed from the ground by drainage or pumping from a well, however, as molecular and surface tension forces will hold a portion of the water in place. Thus, retained water is that held in place against gravity. The specific retention of a rock or soil is the ratio expressed as a percentage of the volume of water it will retain after saturation against the force of gravity to its own volume. If Sr is the specific retention, then Sr is 100wr/V. Where wr is the volume occupied by retained water, and V is the gross volume of the rock or soil. On the other hand, the water which can be drained is expressed as the specific yield Sy. It may be defined as the ratio expressed as a percentage of the volume of water which, after being saturated, can be drained by gravity to its own volume. Therefore, Sy is 100wy/V, where wy is the volume of water drained.(Linsley *et al.* 1958)

As porosity is defined as the total pore proportion of a rock or soil sample, porosity includes closed pores, branches and continuous pores. Effective porosity is defined as the proportion of pores through which water flows and consists of only continuous pores. The term, effective porosity, has a synonymous meaning of specific yield in the unconfined groundwater. Figure 1.1 shows schematics of effective porosity and porosity. Effective porosity is estimated from results of tracer tests in order to calculate the actual velocity of groundwater (Freeze and Cherry 1979). However, porosity is sometimes used as an effective porosity due to the difficulty and cost involved in measuring effective porosity. According to Ii *et al.*(1993b) and Ii (1994a, 1994b), in most cases porosity is larger than effective porosity. As the actual

velocity of groundwater is an essential parameter for the estimation of mass transport in groundwater, especially accurate estimation of effective porosity for aquifers surrounding radioactive waste repository is particularly important.

Quantitative information on specific yield was obtained from an intensive field investigation of the South Coastal Basin in the Los Angeles area of California (Eckis 1934). Numerous samples were taken from surface exposures test holes, and wells. Porosity and specific retentions were determined in the laboratory and specific yield were obtained as the difference. Mean curves showing porosity, specific yield, and specific retention variation with grain size appear in Figure 1.2. Linsley *et al.*(1958), in another investigation, estimated porosity and specific yield for clay, sand, gravel, sandstone, limestone, shale, chert, and granite in Table 1.1. However, there is little data concerning effective porosity determined by tracer test in Japan. Therefore, we estimated effective porosity by tracer tests.

Dispersion is also an essential phenomenon for estimating mass transport in groundwater (Saffman 1959, Fukui and Katsura 1975). Longitudinal dispersivity is used as the parameter which represents dispersion. Longitudinal dispersivity is defined as the dispersion coefficient divided by actual velocity. The phenomenon of dispersive mixing of solutes in aquifers has been the subject of considerable research interest over the past 10 years. Characterizing the dispersivity at a particular field site is essential to any effort in predicting the subsurface movement and spreading of a contaminant plume at that location. Both theoretical and experimental investigations have found that field-scale dispersivities are several orders of magnitude greater than laboratory-scale values for the same material ; it is generally agreed that this different is a reflection of the influence of natural heterogeneities which produce irregular flow patterns at the field scale. Consequently, laboratory

measurements of dispersivity cannot be used to predict field values of dispersivity. Instead field-scale tracer tests are sometimes conducted to estimate dispersivity at a particular site.

Early efforts to document the scale dependence of dispersivity were based on field values of dispersivity reported in the literature and the test scales associated with those values (Lallemand and Peaudecerf 1978, Anderson 1979, Pickens and Grisak 1981, Beims 1983 and Neretnieks 1985). These studies were useful in that they indeed documented field evidence of the scale effect, but they were lacking in that they did not assess the reliability of the data presented. Gelhar *et al.*(1985) assembled the dispersivity data along with related information from the original sources and evaluated the reliability or quality of these data. The graphical results of that work have been widely used by both practitioners and theoreticians, often without appropriate consideration of the reliability of the data. According to Harleman and Rumer (1963), Day (1975), Schwartz (1977) and Domenico and Robbins (1984), several reasons were offered to explain scale effects of longitudinal dispersivity, most of which relied on heterogeneity and modeling. The heterogeneity argument relates to the number, size, and arrangement of heterogeneities in the porous medium. Gelhar *et al.* (1992) stated also the variations in dispersivity reflected the influence of differing degrees of aquifer heterogeneity at different sites. I feel that it is important to focus on relationship of the heterogeneity and longitudinal dispersivity from the laboratory scale to the field scale.

We will discuss effective porosity and longitudinal dispersivity as estimated by laboratory tracer tests and field tracer tests (Table 1.2). For this paper, a field tracer test and laboratory tracer tests using core samples were performed on a Neogene sedimentary rock in the Toki area. In the Matsumoto area, a

field tracer tests alone was performed on a Miocene sedimentary rock using the Matsumoto tunnel.

The Toki field test site was located in the Tono uranium mine, southern part of Gifu prefecture, central Japan. There was a permeable zone composed of Neogene coarse sandstone and weathered granite which contained uranium ore minerals above the unconformity (Ishikawa and Sugihara 1991). Ishikawa and Sugihara studied the transmissivity of the permeable zone using pumping tests.

The Matsumoto tunnel, approximately 2000 m in length, was being constructed within a plateau north of Matsumoto city in central Japan. There is a Qurternary period river terrace sedimentary layer on the top of the plateau. The plateau mainly consists of andesite tuff breccia formed in the Miocene period. The groundwater chemistry in this area was studied by Ii and Misawa (1994a, 1994b).

We can compare values of effective porosity and longitudinal dispersivity from the laboratory tests with those from the field tracer test and study the effect of test scale on these two parameters. In the laboratory tests no cracks appeared in the samples because latent cracks in the core sample separated during boring. However selective flow paths, such as cracks, may have existed during the field tests. Therefore, we performed laboratory tracer tests using bentonite and quartz sand mixtures with the same conditions of porosity but different pore geometry in order to estimate the influence of selective flow paths on hydraulic conductivity, effective porosity and longitudinal dispersivity.

2. TRACERS

Conservative tracers were suitable for the tracer test which was carried out to estimate effective porosity and longitudinal dispersivity, as it was not necessary to consider adsorption of tracers into the rocks and soil. We selected Br^- and Cl^- as tracers, and performed batch experiments to confirm that Br^- and Cl^- would not be adsorbed by the core samples of the sedimentary rock at the Toki and the Matsumoto field tracer test site or the bentonite and quartz sand mixtures. Distribution coefficients (Kd) of the tracers were calculated from batch-experiment data, according to the following formula :

$$Kd(ml\ g^{-1}) = \frac{q(g\ g^{-1})}{Cq(g\ ml^{-1})} \qquad (1)$$

The quantity q, representing mass of tracer on the sample per unit mass of the sample, was calculated by comparing the initial concentration (C_0) of Br^- or Cl^- in the solution with the equilibrium concentration (C_q) of Br^- or Cl^-. The solution reached equilibrium concentration several days after the addition of the rock sample. q can be calculated as follows :

$$q = \frac{(C_0 - C_q) \times V_s}{W_b} \qquad (2)$$

where V_s : Volume of tracer solution W_b : Weight of rock sample

The initial concentration of the solution was 13 ppm for Cl^- and 21 ppm for Br^-. The weight ratio of sample to solution ranged from 3.1 to 4.4 per 100. Table 2.1 indicates Kd values for the rock samples at the Toki and the Matsumoto field test site and the bentonite and quartz sand mixtures. In all cases, q was calculated to be approximately 0. The results suggested that Br^- and Cl^- could be regarded as conservative tracers in the tracer tests.

3. TOKI FIELD TRACER TEST

The field test site was located in the Tono uranium mine, southern part of Gifu prefecture, central Japan. In this area, several kinds of sedimentary rocks unconformably cover granite bed rock. There was a permeable zone composed of Neogene coarse sandstone and weathered granite which contained uranium ore minerals above the unconformity (Ishikawa and Sugihara 1991). Ishikawa and Sugihara studied the transmissivity of the permeable zone using pumping tests.

3.1 Method

Figure 3.1, 3.2 and 3.3 show schematic figures of the field tracer test. There were two boreholes 7 m apart and each about 90 m in depth. Figure 3.4 shows geological columns at the boreholes. A permeable layer consisting mainly of weathered granite and coarse sandstone, which was formed in the Neogene period, existed from 80 to 90 m in depth. This layer was sandwiched between impermeable layers of siltstone above and fresh granite below. The boreholes were fully lined from 0 to 80 m in depth and perforated in the zone of permeable coarse sandstone. Therefore, the thickness of permeable layer was assumed to be 10 m.

Before the tracer was injected, groundwater was pumped out at the recovery borehole and reinjected at the injection borehole. Groundwater was circulated until a steady-state groundwater flow was obtained. Before tracer test, we determined the circulation flow rate and mass of Br^- tracer. Table 3.1 indicates the maximum concentration and its elapsed time estimated by the Gelhar

method. From the results, the circulation flow rate was determined to be 7800 cm^3 and NaBr 2 kg ($0.0014 \times 79.9/102.9 = 2.2$ ppm) by the Gelhar method in order to detect Br^- tracer at the recovery borehole and for a month. Figure 3.5 shows the groundwater table at the recovery borehole. At this point the groundwater table at the recovery borehole was maintained to be -15 m from natural water table. The original volume of tracer solution was 180000 cm^3. Br^- tracer solution was injected at the injection borehole. During the test, groundwater was sampled regularly at the recovery borehole to measure the concentration of Br^- by ion exchange chromatography.

3.2 Gelhar method

In this analysis we used the Gelhar method and numerical analysis and compared the results. From the breakthrough curve for Br^- in the field tracer test, effective porosity and longitudinal dispersivity were calculated based on the following analytical solution of the two dimensional dispersion equation for a two-well (pumping-injection) flow system (Gelhar 1982) :

$$C_w = \frac{M}{Q}\int_{\hat{\varphi}=0}^{1} \frac{Q\exp[-(a-T)^2/4eb]}{\varepsilon h L^2 (4\pi eb)^{\frac{1}{2}}} d\hat{\varphi}$$

$$T = \frac{Qt}{\varepsilon h L^2} \qquad e = \frac{\alpha}{L}$$

$$a(\beta) = \frac{\pi(\sin\beta - \beta\cos\beta)}{\sin^3\beta} \qquad : \beta = \pi\varphi$$

$$b(\gamma,\beta) = \pi^2 \frac{[(\frac{\gamma+\beta}{2}) + \frac{(\sin\gamma\cos\gamma)}{2} + \frac{(\sin\beta\cos\beta)}{2} - 2\cos\beta(\sin\gamma + \sin\beta) + (\gamma+\beta)\cos^2\beta]}{2\sin^5\beta}$$

(3)

where Cw : concentration at the recovery borehole, t : time,

ε : effective porosity, Q : flow rate, h : thickness of permeable layer,

M : mass of tracer, γ : displacement of the tracer pulse,

φ : stream function ; $\hat{\varphi}=2h\varphi/Q$, L : distance between boreholes, and

α : longitudinal dispersivity.

Table 3.2 shows the system parameters used in the analysis of the field tracer test. Figure 3.6 shows the correlation between the concentration of Br^- at the recovery borehole and the time elapsed from the start of tracer injection. The analytical solution of the dispersion equation for the two well pumping system found effective porosity and longitudinal dispersivity to equal 4.5 % and 3.5 m.

3.3 FEM analysis

Initially, the velocity distribution of the flow field and layer permeability were analyzed as a seepage problem using finite element method (FEM). Next, the advection-dispersion equation was used to numerically analyze the tracer test results.

1) Seepage analysis

The equation governing steady-state groundwater flow in a horizontal two-dimensional system is generally given as (Ii *et al.* 1993a),

$$\frac{\partial^2 \phi}{\partial x^2} + \frac{\partial^2 \phi}{\partial y^2} = 0 \qquad (4)$$

where

ϕ : piezometric head,

x, y : Cartesian coordinates

The system boundaries are impermeable excepting the injection and recovery boreholes. Boundary conditions can be given as follows;

$\phi = \phi_0$ at the recovery borehole

$Q = Q_0$ at the injection borehole (5)

ϕ_0 : steady-state piezometric head level (-15 m from natural water table)

Q : flow rate, Q_0 : constant flow rate (3900 $cm^3\ min^{-1}$)

A seepage analysis was performed using FEM on equation (4). The analysis was simplified using the boundary conditions described by equation (5).

Figure 3.7 displays an analytical model for the seepage analysis of half of the horizontal section of the analytical region. The circulation pipe connecting the pumping injection boreholes was not included in the analysis. Table 3.3 shows the parameters and boundary conditions used in the seepage analysis. The injection flow rate and the piezometric head level were agreed with the observed values.

Figure 3.8 shows the distribution of analyzed piezometric-head values. When hydraulic conductivity of the layer becomes 2×10^{-5} cm sec^{-1}, the analyzed piezometric head at the injection borehole agrees with the head calculated from the observed injection pressure (7.7 kg cm^{-2}) on the ground. Natural groundwater table was under -21 m. The piezometric head level was 98 m (77 + 21 m). The analyzed hydraulic conductivity agrees with those presented in the paper by Ishikawa and Sugihara (1991). Therefore, the hydraulic conductivity of the layer was determined to be 2×10^{-5} cm sec^{-1}. Ishikawa and Sugihara studied the transmissivity of the layer using pumping tests. The transmissivity values around the two boreholes were $1\sim2\times10^{-5}$ cm sec^{-1}.

2) Migration analysis

A coupled equation governing groundwater flow and advection-dispersion in a horizontal two-dimensional system is given as follows (Ii *et al.* 1993a),

$$\frac{\partial C}{\partial t} = \frac{\partial}{\partial x}(Dij\,\frac{\partial C}{\partial x}) + \frac{\partial}{\partial y}(Dij\,\frac{\partial C}{\partial y}) - \frac{\partial}{\partial x}(VxC) - \frac{\partial}{\partial x}(VyC) \qquad (5)$$

$Vx = vx/\varepsilon, Vy = vy/\varepsilon$

where ε : effective porosity, C : concentration,

Dij : tensor of dispersion coefficient,

Vx, Vy : actual velocity in the x and y directions, and

vx, vy : apparent velocity in the x and y directions.

Two different dispersion coefficients are given as follows,

$$D1 = \alpha\,|V| + Dm, \qquad D2 = Dm \qquad (7)$$

where D1 : dispersion coefficient parallel to groundwater flow direction,

D2 : dispersion coefficient perpendicular to groundwater flow direction

$|V| : \sqrt{Vx^2+Vy^2}$, α : longitudinal dispersivity, and

Dm: molecular diffusion coefficient (2.8×10^{-9} cm^2 sec^{-1}).

Using D1 and D2, tensor Dij is given as follows,

$$\begin{bmatrix} D_{xx} & D_{xy} \\ D_{yx} & D_{yy} \end{bmatrix} = \begin{bmatrix} \cos\theta & -\sin\theta \\ \sin\theta & \cos\theta \end{bmatrix} \begin{bmatrix} D_1 & 0 \\ 0 & D_2 \end{bmatrix} \begin{bmatrix} \cos\theta & \sin\theta \\ -\sin\theta & \cos\theta \end{bmatrix}$$

$$= \begin{bmatrix} D_1\cos^2\theta + D_2\sin^2\theta & D_1\sin\theta\cos\theta - D_2\sin\theta\cos\theta \\ D_1\sin\theta\cos\theta - D_2\sin\theta\cos\theta & D_1\sin^2\theta + D_2\cos^2\theta \end{bmatrix} \quad (8)$$

where θ = arctan (Vy/Vx)

Using equation (8), equation (6) becomes;

$$\frac{\partial C}{\partial t} = \frac{\partial}{\partial x}(Dxx\frac{\partial C}{\partial x}) + \frac{\partial}{\partial x}(Dxy\frac{\partial C}{\partial y}) + \frac{\partial}{\partial y}(Dyx\frac{\partial C}{\partial x}) + \frac{\partial}{\partial y}(Dyy\frac{\partial C}{\partial y}) - \frac{\partial}{\partial x}(VxC) - \frac{\partial}{\partial y}(VyC) \quad (9)$$

This is a two dimensional advection-dispersion equation. The dispersion coefficient depends on actual velocity and is anisotropic. The system boundaries are impermeable except at the injection and recovery boreholes.

$C = C_0$ at the injection borehole

$F = F_0$ at the recovery borehole (10)

Where C_0 : initial concentration at the injection borehole, F : flux of mass ($\partial C / \partial t$) , and

F_0 : steady state flux of mass at the recovery hole.

A migration analysis was performed using FEM and the boundary conditions described by (10). The computer code used was developed by

Utsugida *et al.*(1984).

Figure 3.7 shows an analytical model for the migration analysis of half of the horizontal section of the analytical region including the circulation pipe. The flow velocity through the circulation pipe was 0.065 cm sec^{-1} (3900 cm^3 min^{-1} ÷ 10 cm (width) ÷ 1000 cm (height) = 0.39 cm min^{-1}). Table 3.4 displays the parameters and boundary conditions used in the migration analysis.

Before the 180000 cm^3 tracer solution containing 8300 ppm Br^- (NaBr : 2 kg) was injected at the injection borehole, there were 700000 cm^3 of water in the injection borehole. Therefore we assumed that the tracer concentration was 1700 ppm (180000 cm^3 × 8300 ppm ÷ (700000 + 180000) cm^3) and the injection time was 112.8 min ((700000 + 180000) cm^3 ÷ 7800 cm^3 min^{-1}).

3) Numerical results

Figure 3.6 shows the correlation between the concentration of Br^- at the recovery borehole and the time elapsed from the start of tracer injection. The relationship was obtained from the two-dimensional FEM migration analysis. The analytical solution of the dispersion equation for the two well pumping system (Gelhar method) found effective porosity and longitudinal dispersivity to equal 4.5 % and 3.5 m. Effective porosity and longitudinal dispersivity were determined to be 7 % and 3.5 m respectively referred to the results of the analytical solution. The difference between the 4.5 and 7 % effective porosity values is thought to relate to the difference between the initial tracer-concentration values used by the two methods. In the Gelhar method, the tracer solution was assumed to be injected in a moment. The

effective porosity values (4.5 % and 7 %) determined by the Gelhar method and FEM were smaller than porosity values (6～32 % : Table4.1).

Figure 3.9, 3.10 and 3.11 show the analyzed Br^- concentration distributions by FEM using 3.5 m longitudinal dispersivity and 7 % effective porosity, 2, 36 and 100 hours after the start of tracer injection (Ii *et al.* 1993a). Figure 3.9 indicates concentric spreading of Br^- at the beginning of tracer injection. Figure 3.10 and 3.11 indicate the presence of two Br^- concentration peaks around the injection borehole and these concentration peaks reduce in progression.

4. TOKI ROCK SAMPLE LABORATORY TRACER TESTS

4.1 Method

Porosities of the core samples taken from the permeable layer were determined by weighing the samples in both water saturated and dry conditions. Table 4.1 shows that the porosity of core samples from the recovery borehole values ranged from 6～47 % and were mainly concentrated in the range of 25～30 % (Ii *et al.* 1993b, Ii 1994c). Table 4.2 shows three core samples (T1, T2 and T3) of different porosities and used in laboratory tracer tests. Table 4.1 and 4.2 indicate that hydraulic conductivities ranged from 2×10^{-8}～3×10^{-6} cm sec^{-1} and were mainly concentrated in the range of 2×10^{-8}～4×10^{-7} cm sec^{-1}. The length of the laboratory tracer test samples ranged from 1 cm to 6 cm and the diameter of these samples was 4.3 cm. The core sample was placed in an acrylic resin cylinder with an inner diameter of 5 cm. The gap between the core sample and the cylinder was filled with epoxy resin in order to seal. Figure 4.1 shows the laboratory test apparatus. To determine effective porosity, tracer solutions containing 100 to 300 ppm Br^- or Cl^- were pumped into the column under constant flow rates. Flow rate was maintained at a constant level through the manual adjustments of the nitrogen cylinder valve. The volume of effluent solution was measured to determine the flow rate. The tracer concentration of the effluent solution was analyzed using ion exchange chromatography.

4.2 Analysis

Laboratory tests, conducted under several constant head conditions,

resulted in the production of tracer breakthrough curves. Actual velocity and dispersion coefficients were calculated using breakthrough-curve data with the following analytical solution of the one-dimensional advection-dispersion equation (Ogata 1970, Shimooka *et al.* 1989):

$$\frac{C}{C_0} = \frac{1}{2}\left\{\mathrm{erfc}\left(\frac{L - Vt}{2\sqrt{Dt}}\right) + \mathrm{erfc}\left(\frac{L + Vt}{2\sqrt{Dt}}\right) \times \exp\left(\frac{VL}{D}\right)\right\} \qquad (11)$$

where; C : concentration, C_0 : initial concentration , L : length of sample, D : dispersion coefficient, t : time, and V : actual velocity.

The initial and boundary conditions are given as;

C_0 = constant, V = constant

C = 0, X = ∞, at all times

C = 0, X > 0, at t = 0.

From the actual velocity (V) and the monitored constant flow rate (Q), the cross-sectional area of void through which the pore water passed (A) was calculated by the equation $A = Q\,V^{-1}$. The effective porosity (ε) was then calculated, using the equation $\varepsilon = A\,A'^{-1}$ based on the Depuit-Forchheimer assumption. A' represents the total area of the sample cross section (Ii and Sugiyama 1991).

4.3 Results

Figure 4.2～4.21 show breakthrough curves obtained from laboratory tracer test data. The line represents the regression curve using the analytical solution. Using equation (11), the actual velocity and the dispersion coefficient for the tracer were calculated according to the relationship between elapsed time and the effluent tracer concentration normalized by initial tracer concentration. Table 4.2 gives the conditions and results of the Toki laboratory tests. When the length of sample was 1.0 cm, effective porosity reached its maximum value and equaled porosity. As the length of samples increased from 1.0 to 6.0 cm, effective porosity decreased. Effective porosity in the field results was smaller than those in the laboratory results. Hydraulic conductivity (2×10^{-5} cm sec^{-1}) in the field results was larger than those (2×10^{-8}～4×10^{-7} cm sec^{-1}) in the laboratory results.

5. MATSUMOTO FIELD TRACER TEST

5.1 Study area

Figure 5.1 shows the location of study area. The Matsumoto tunnel, approximately 2000 m in length, was being constructed within a plateau north of Matsumoto city in central Japan. The plateau was surrounded by the Sai river on the west side, Metoba river on the east side and south side and a small river on the north side and extended in a south-north direction. There is a Qurternary period river terrace sedimentary layer on the top of the plateau. The plateau mainly consists of andesite tuff breccia formed in the Miocene period. These sediments strike NE-SW and N-S and dips 50° west. There are small faults which strike N-S, NE-SW and NW-SE.

The groundwater chemistry in this area was studied by Ii and Misawa (1994a, 1994b). As this plateau was separated from other mountains, the water found in the pond, river, well and springs on the plateau as well as in the tunnel originated from precipitation on the plateau. Therefore we studied the change in groundwater chemistry from the recharge points to the tunnel seepage points and the deep well. Figure 5.2 shows changes in groundwater chemistry within the plateau. The concentrations of HCO_3^-, Ca^{2+} and Na^+ in the tunnel seepage water was higher than those of other water samples. The dissolution of feldspar which was representative of this area's rock weathering was thought to cause CO_2 gas pressure to decrease and HCO_3^-, Ca^{2+} and Na^+ concentrations to increase. The relationship between the concentration of NO_3^- and the Eh and pH values in the groundwater indicated that in an oxidative condition NO_3^- and H^+ were produced in the river, pond and spring on the plateau by ammonia oxidizing and nitrite oxidizing bacteria, and in a reductive

condition NO_3^- and H^+ were decomposed and OH^- was produced through the rock to the tunnel by denitrifying bacteria.

The relationship between δD and $\delta^{18}O$ indicated the water in this area originated from the precipitation on the plateau. The δD and $\delta^{18}O$ and the recharge time determined by ^3H concentration indicated temperature has increased for more than 60 years because tunnel seepage and deep well water ages were greater than 60 years and δD and $\delta^{18}O$ values in the tunnel seepage and deep well water were lower than the surface water on the plateau. The $\delta^{13}C$ values and the concentration of HCO_3^- in the groundwater originated from organic matter in soil and the HCO_3^- in the deep well water originated from the dissolution of carbonate minerals in rock.

Tunnel construction began in October 1990 and finished in April 1992. Figure 5.3 shows that the total volume of seepage water at the west side of the tunnel from November 1991 to August 1992 was 1.3 million tons. The flow rate was 2.9 m^3 min^{-1} on the average and the maximum volume reached was 6.8 m^3 min^{-1} when the cutting face reached a point 500 m from the entrance of the west side of the tunnel. Figure 5.3 shows that the total volume of seepage water at the east side of the tunnel from November 1990 to September 1992 reached 1.8 million tons. The flow rate was 1.8 m^3 min^{-1} on the average and the maximum volume reached was 6.5 m^3 min^{-1} when the cutting face reached a point 600 m from the entrance of the east side of the tunnel.

The tunnel was being bored through both sides of the plateau, toward the center of the plateau, simultaneously. The tracer test borehole was sunk between the opposing cutting faces of the tunnels. Therefore there were two tunnels approaching each other during the construction process. We call these

the west and east tunnels. When the field tracer test was performed, it was 331 m between the borehole and the cutting face of the east tunnel and about 130 m between the borehole and the cutting face of the west tunnel. The cutting face of the west tunnel was advancing 3 ~ 4 m a day. Table 5.1 shows that the porosity values determined by the weight of samples in both water saturated and dry conditions were 7 ~ 15 %. The Lugeon tests results using three boreholes (tracer injection borehole and two boreholes near both entrances) indicated that hydraulic conductivity values ranged from $2.4 \times 10^{-4} \sim 6.4 \times 10^{-3}$ m hour^{-1}.

5.2 Tracer test

Figure 5.4 shows a cross section of the study area. A tracer solution was injected at the borehole. Tunnel seepage water was sampled for a month and the concentration of tracer was measured in a laboratory. There were 3 sampling points (130 m (No.1) and 265 m (No.2) from the borehole at the west tunnel and 331 m (No. 3) from the borehole at the east tunnel).

Br^- was selected as a tracer because Br^- was not adsorbed by the rock samples from the Matsumoto tunnel. The original volume of tracer solution which consisted of 30 kg NaBr and tunnel seepage water was 80000 cm^3. The tracer solution was injected into the borehole for 30 minutes. During the test, seepage water along the tunnel was sampled regularly to measure the concentration of Br^- by ion exchange chromatography. Figure 5.5 shows the relationship between elapsed time after the start of tracer injection and concentration of Br^- in the tunnel seepage. The concentration of Br^- at the No.3 sampling point of the east tunnel was below the detection limit (0.01

ppm). The concentration peak of Br^- at the No.1 sampling point of the west tunnel was about 180 hours. The concentration of Br^- at the No.2 sampling point of the west tunnel was detected but the peak could not be found. Therefore, we used the breakthrough curve at the No.1 sampling point for analysis.

5.3 Analysis

We used three-dimensional coupled groundwater flow and an advection-dispersion code using FEM (MIGR3D) made by Kawamura (1987). The detail and results of bench mark test of the code were referred by Kawamura. This code can't be applied to unsaturated zones. In this area, there were unsaturated zones of unconfined groundwater. It is necessary to determine the position of groundwater level which is the boundary between the saturated zone and the unsaturated zone. Therefore, we estimated the position of groundwater level by seepage analysis using FEM. Using migration analysis, groundwater levels were coincided with the upper surface of a three dimensional analytical model and MIGR3D was applied for these field tracer test results.

1) Seepage analysis

Figure 5.6 shows the seepage and migration analysis area. The groundwater level in this area was determined by seepage analysis using known groundwater levels for the tunnel and springs and wells in the middle of the plateau. There was a drain at the base of the tunnel. The altitudes of the drain were assumed to be the same as groundwater levels which were 659 and 675 m at the entrance and the cutting face of the west tunnel and 718 and 690 m at the

entrance and the cutting face of the east tunnel. There were two groundwater levels observed in the borehole. The upper groundwater level was about 800 m. The lower groundwater level was below 693 m. Therefore, there was a impermeable layer which was probably weathered rock between both the groundwater levels. The groundwater of the lower level was in accordance with the tunnel seepage water because the chemical composition and stable isotopic ratios of hydrogen and oxygen in the lower groundwater was similar with those of in the tunnel seepage water. There were springs and wells in the middle of the plateau. The chemical composition of spring, well and tunnel seepage water were very similar and the aquifer for these waters were thought to be the same according to Ii and Misawa (1994a, 1994b). Using the spring and well groundwater levels, groundwater level was determined to be about 710～ 720 m at a point 1.5 km from the tunnel.

The injected tracer solution at the borehole was selectively gathered at the tunnel because tunnel seepage was drained. Therefore, as the spread of the tracer was small, a migration analysis needed only to be done in an area near the tunnel. However a seepage analysis needed to be conducted over a wide area because the springs and wells were far from the tunnel. During the tracer test a change in groundwater level was not found. Therefore, groundwater level was determined by seepage analysis in a steady-state groundwater flow condition. The groundwater level was low at the tunnel and high far from the tunnel. Therefore the analytical area was from the tunnel to points whose groundwater levels were 710 ～ 720 m where groundwater level and topographical features were almost same. As the groundwater level and topographical features outside the analytical area were lower than those of the boundary and the groundwater level inside the analytical area was lower than that of the boundary, groundwater flowed from the boundary to inside and

outside area. Therefore, the boundary was assumed to be impermeable.

There was little information about groundwater levels in the north part of the plateau and the plateau extended in a north-west direction. Therefore the area 1.5 km from the tunnel was assumed to be the boundary of the analytical model. We assumed the analytical area to be a uniform medium because we had detailed information about geological conditions and there was no remarkable change found under construction. Figure 5.7 shows the analytical model for the seepage analysis and the distribution of analyzed piezometric head values. Table 5.2 displays the parameters and boundary conditions used in the seepage analysis. When a piezometric head level was constant and flow rate condition was not given, a piezometric head distribution could be determined without hydraulic conductivity values.

The equation governing steady-state groundwater flow in a three-dimensional system is generally given as uniform medium,

$$\frac{\partial^2 \phi}{\partial x^2} + \frac{\partial^2 \phi}{\partial y^2} + \frac{\partial^2 \phi}{\partial z^2} = 0 \qquad (12)$$

where ϕ : piezometric head, and x, y, z : Cartesian coordinates

The system boundaries are impermeable excepting the tunnel and springs. Boundary conditions can be given as follows,

$$\phi = \phi_0 \qquad \text{at the the tunnel and springs} \qquad (13)$$

where ϕ_0 : steady-state piezometric head level

A seepage analysis was performed using FEM in equation (12). The analysis was simplified using the boundary conditions described by equation (13).

These values were used to make a migration analytical model. Groundwater flows mainly into the west tunnel.

2) Migration

Figure 5.8 shows the analytical model for migration analysis. Using the piezometric head level, the model was made near the tunnel. A coupled equation governing groundwater flow and advection-dispersion in a three-dimensional system is given as follows,

$$\frac{\partial C}{\partial t} = \frac{\partial}{\partial x}(D\frac{\partial C}{\partial x}) + \frac{\partial}{\partial y}(D\frac{\partial C}{\partial y}) + \frac{\partial}{\partial z}(D\frac{\partial C}{\partial z}) - \frac{\partial}{\partial x}(VxC) - \frac{\partial}{\partial y}(VyC) - \frac{\partial}{\partial z}(VzC) + \frac{F}{\varepsilon} \qquad (14)$$

$$Vx = vx/\varepsilon, Vy = vy/\varepsilon, Vz = vz/\varepsilon$$

$$D = \alpha \mid V \mid, \quad \mid V \mid = \sqrt{Vx^2 + Vy^2 + Vz^2}$$

where ε : effective porosity, C : concentration, D : dispersion coefficient, α : longitudinal dispersivity,

Vx, Vy, Vz : actual velocity in the x, y and z directions, and

vx, vy, vz : apparent velocity in the x, y and z directions.

The dispersion coefficient is isotropic. But in the Toki field tracer test, the dispersion coefficient is anisotropic. Equation (7) indicates two different dispersion coefficients (longitudinal and transverse dispersivity). Transverse dispersivity agrees with molecular diffusion coefficient is smaller than longitudinal dispersivity. Therefore, apparently longitudinal dispersivity analyzed by the MIGR3D code is smaller than that analyzed by the Toki FEM method. The difference of longitudinal dispersivities determined by two

methods depends on the velocity.

The system boundaries are impermeable except at the borehole.

$$F = F_0 \text{ at the borehole} \qquad (15)$$

Where F : flux of mass ($\Delta C / \Delta t$) , and F_0 : flux of mass at the borehole.

A migration analysis was performed using FEM and the boundary conditions described by (14). The computer code used was developed by Kawamura. Figure 5.9 shows an analytical model for the migration analysis and analyzed piezometric-head distribution. Groundwater levels were coincided with the upper surface of the model. Table 5.3 displays the parameters and boundary conditions used in the migration analysis.

The Lugeon tests results using three boreholes indicated hydraulic conductivity values ranged from $2.4 \times 10^{-4} \sim 6.4 \times 10^{-3}$ m hour^{-1}. Porosities of the core samples taken from the borehole were determined by weighing the sample in both water saturated and dry conditions. The porosity values ranged from 7 to 15 %. Therefore, we assumed the maximum effective porosity was 15 %. A tracer solution containing 23289.6 g of Br^- (NaBr : 30000 g) was injected at the borehole for 30 minutes.

5.4 Numerical results

Figures 5.10 to 5.22 show the correlation between the Br^- concentration in the tunnel seepage water, which was 130 m apart from the borehole, and the time elapsed from the start of tracer injection (Ii 1994b, Ii 1994c and Ii *et al*.

1994a). The relationship was obtained from a three-dimensional FEM migration analysis. We used the breakthrough curve at the No.1 sampling point because the concentration from other sampling points were very low.

In this tracer test, from the governing equation (14) and the initial and boundary conditions, effective porosity, longitudinal dispersivity and hydraulic conductivity were unknown parameters for this migration analysis. Figure 5.10 indicates the influence of longitudinal dispersivity upon a breakthrough curve under constant conditions where effective porosity was 0.08 % and hydraulic conductivity 8.0×10^{-3} m hour^{-1}. As longitudinal dispersivity increases, the maximum concentration of an analytical breakthrough curve and its elapsed time from a tracer injection when a maximum concentration is reached decrease, and the slope of the analytical breakthrough curve becomes gentle. Figure 5.11 indicates the influence of hydraulic conductivity upon a breakthrough curve under constant conditions where longitudinal dispersivity was 10 m and effective porosity 0.056 %. As hydraulic conductivity increases, maximum concentration remains unchanged and its elapsed time decreases. However, Figure 5.12 indicates that as effective porosity increases, maximum concentration decreases and its elapsed time increases. Accordingly these parameters have a different influence upon the breakthrough curve. It is difficult to determine three parameters at once by comparing the tracer test results and analytical results. Hydraulic conductivity could be inferred by the Lugeon test results. First hydraulic conductivity was constant and we determined effective porosity and longitudinal dispersivity.

1) K= 6.4×10^{-3} m hour^{-1}

First we chose 6.4×10^{-3} m hour^{-1}, the maximum hydraulic conductivity

value of the Lugeon test results because there were many cracks at the bottom of the borehole where the tracer solution was injected. When longitudinal dispersivity and effective porosity were fixed at 70 m and 0.1 % (Figure 5.13 : case 1), the maximum concentration and its elapsed time of the analysis were in accordance with the tracer test results. However the slope of the analytical breakthrough curve was gentler than that of the tracer test results. Next we decreased longitudinal dispersivity in order to cause the slope of the analytical breakthrough curve to steepen. When longitudinal dispersivity and effective porosity were fixed at 20 m and 0.1 % (Figure 5.14 : case 2), the maximum concentration was higher and its elapsed time was longer than those of the tracer results.

Next we decreased effective porosity in order to match the elapsed time of a maximum concentration. When longitudinal dispersivity and effective porosity were fixed at 20 m and 0.08 % (Figure 5.15: case 3), the elapsed time approached that of the tracer results. However the maximum concentration became larger than that of the tracer results.

First, if only effective porosity is increased, the maximum concentration decreases and its elapsed time increases. In order to match the elapsed time of maximum concentration, longitudinal dispersivity was increased, and maximum concentration became smaller. Therefore, if hydraulic conductivity is 8.0×10^{-3} m hour^{-1}, a maximum concentration and its elapsed time will match the tracer results but the analytical breakthrough curve will not match that of the tracer test results.

2) K= 2.4×10^{-4} m hour^{-1}

Next, we chose 2.4×10^{-4} m hour^{-1}, the minimum hydraulic conductivity value of the Lugeon test results. When longitudinal dispersivity and effective porosity were fixed at 190 m and 0.064 % (Figure 5.16: case 4), the maximum concentration and its elapsed time of the analysis were in accordance with the tracer test results. However the slope of the analytical breakthrough curve was gentler than those of the the tracer test results and case 1 (K = 6.4×10^{-3} m hour^{-1}). Therefore, if the hydraulic conductivity value is smaller than 6.4×10^{-3} m hour^{-1}, an analytical breakthrough curve will not match that of the tracer test results.

3) K= 4.1×10^{-2} and 6.8×10^{-2} m hour^{-1}

We chose 4.1×10^{-2} and 6.8×10^{-2} m hour^{-1}, the hydraulic conductivity values which were higher than the maximum hydraulic conductivity value of the Lugeon test results. When longitudinal dispersivities and effective porosities were fixed at 20 m and 0.27 % (Figure 5.17 : case 5) and at 14 m and 0.4 % (Figure 5.18 : case 6), the maximum concentration and its elapsed time of the analysis were in accordance with the tracer test results. The slope of the analytical breakthrough curve was gentle. However, as hydraulic conductivity increases and longitudinal dispersivity decreases, the analytical breakthrough curves became more similar to the tracer test results.

4) K= 8.6×10^{-2} and 1.1×10^{-1} m hour^{-1}

We chose 8.6×10^{-2} and 1.1×10^{-1} m hour^{-1}, the hydraulic conductivity value which was higher than those of other cases. When longitudinal dispersivity and effective porosity were fixed at 12 m and 0.48 % (Figure 5.19 : case 7) and at 10 m and 0.59 % (Figure 5.20 : case 8), the breakthrough curves of the analysis were almost in accordance with that of the

tracer test results.

5) K= 1.5×10^{-1} and 2.8×10^{-1} m $hour^{-1}$

We chose 1.5×10^{-1} and 2.8×10^{-1} m $hour^{-1}$, the hydraulic conductivity values which were higher than those of other cases. When longitudinal dispersivity and effective porosity were fixed at 8 m and 0.76 % (Figure 5.21 : case 9) and at 5 m and 1.4 % (Figure 5.22 : case 10), the maximum concentration and its elapsed time of the analysis were in accordance with the tracer test results. However the slope of the analytical breakthrough curve was steeper than that of the tracer test results. Therefore, if hydraulic conductivity is more than 1.5×10^{-1} m $hour^{-1}$, an analytical breakthrough curve will not match that of the tracer test results.

Using the breakthrough curve from the tracer test results, effective porosity was determined to be 0.48 $\sim$ 0.59 %, longitudinal dispersivity 10 $\sim$ 12m and hydraulic conductivity 8.6×10^{-2} $\sim$ 1.1×10^{-1} m $hour^{-1}$. If tunnel seepage is free water in the rocks unsaturated during tunnel construction, effective porosity is calculated to be 0.6 % by the equation ε = Qt Vr^{-1}. The concentration of tritium indicated tunnel seepage was not surface water but groundwater stored in the rocks for more than 60 years (Ii and Misawa 1994a, 1994b). Qt represents the total volume of the tunnel seepage, 2.8 million ton. Vr represents the total volume of the rock unsaturated during tunnel construction. The calculated effective porosity coincides with the analyzed effective porosity. The effective porosity value is smaller than the porosity value (7$\sim$10 %) and is useful for an estimation of storage volume.

Figure 5.23, 5.24 and 5.25 show Br^- concentration distributions analyzed

by FEM using 12 m longitudinal dispersivity and 0.48 % effective porosity, 40, 100 and 300 hours after the start of tracer injection. The Br^- concentration peak moves towards the cutting face at the west side of the tunnel and the Br^- concentration peak reduces in progression.

6. BENTONITE AND QUARTZ-SAND MIXTURE LABORATORY TRACER TESTS

In the laboratory tests no cracks appeared in the samples because latent cracks in the core sample separated during boring. However selective flow paths, such as cracks, may have existed during the field tests. Therefore, we performed laboratory tracer tests using bentonite and quartz sand mixtures with the same conditions of porosity but different pore geometry in order to estimate the influence of selective flow paths on hydraulic conductivity, effective porosity and dispersion.

6.1 Material

Samples used in this test were composed of Kunigel bentonite, marketed in Japan by Kunimine Industries Co., LTD., and Flattery quartz-sand, from Australia. The samples used had bentonite to quartz ratios of 1 : 9. Mineralogical analysis, using an X-ray diffractometer determined that the bentonite was composed of approximately 60 % montmorillonite, 30 % quartz, and 5 % feldspar. Flattery sand is 99 % quartz.

Figure 6.1 shows the grain size distribution curves for bentonite and quartz-sand. Grain sizes smaller than 0.044 mm were measured using the Andreasen pipette method. Grain sizes greater than 0.044 mm were measured with a sieve under dry conditions. The bentonite consisted of very fine grains, with an accumulation content of more than 50 % for grains smaller than 0.002 mm. Large grains, 0.1 to 0.3 mm, are characteristic of the quartz-sand.

The porosity of the sample must be determined initially in order to compare effective porosity with porosity. Porosity can be calculated using true gravity density and dry density values. As the true gravity density values for bentonite

and quartz sand, and therefore for all of the mixture samples, were very similar, the porosity for all three samples was established from the density values of one representative sample. For the sample with a 10 % bentonite to 90 % quartz sand ratio, the true gravity density is 2.61 g cm^{-3}. The porosity of the bentonite and sand mixture was calculated to be 43 %, using the following formula:

$$\text{Porosity } (\%) = (1\text{-}Pd \div G) \times 100 \qquad (16)$$

Where Pd : dry density, and G : true gravity density

6.2 Method

Bentonite and quartz sand mixtures were placed in a metallic or acrylic resin cylinder with an inner diameter of 5 cm. The samples were compacted by an unconfined pressure apparatus. The sample material had a dry density of 1.5 g cm^{-3}, a water content of 5 %, and a mixture ratio of bentonite to quartz-sand of 1 : 9. The height of the compacted samples was adjusted to achieve a fixed porosity. A tracer solution was pumped into the column under a constant flow rate. The tracer concentration in the effluent solution was analyzed with ion exchange chromatography. The Toki laboratory tracer tests and the bentonite and quartz-sand mixture laboratory tracer tests used the same method of analysis.

6.3 Results

Table 6.1 gives the conditions and results of the bentonite and quartz-sand mixture laboratory tracer tests (Ii and Sugiyama 1991). Figure 6.2 to 6.8 show breakthrough curves obtained from the laboratory tracer test data. Effective porosities ranged from 13 to 44 %. In some cases, the maximum effective porosity value corresponded to the porosity. Figure 6.9 shows the relationship between effective porosity and hydraulic conductivity. Despite a constant porosity value, the hydraulic conductivity values changed from 1.0×10^{-8} to 1.4×10^{-7} cm sec^{-1}. However, samples varied with respect to pore geometry. As the hydraulic conductivity increased, the effective porosity decreased. This was seen strange because as the areas that water can flow through increase, generally the flow rate and hydraulic conductivity increase. When using the same porosity conditions, only pore geometry and pore size distribution can differ between samples. Next, a relationship between pore size and accumulation porosity for the samples was investigated to clear up the inconsistency.

7. PORE SIZE MEASUREMENT OF BENTONITE QUARTZ-SAND MIXTURE

When a dye solution was pumped into the soil column, dyed areas indicated flow paths. The flow path variation between samples depended on pore geometry. Therefore, pore size distribution for dyed areas and undyed areas was measured.

7.1 Method

After the effective porosity test was completed, the tracer solution in the laboratory feed tank was replaced with a solution containing dye. This solution was pumped into the soil column. When the dye appeared in the effluent solution, indicating that it had passed through the sample, the cylinder was dismantled. The sample was then quick frozen in liquid nitrogen and dried using a vacuum pump. The quick-freezing process fixed the texture of the sample, and worked to avoid the shrinkage that occurs when bentonite is dried at normal temperatures. The dried sample was cut into rectangular sections with sides less than 1 cm long. Two types of rectangular sections were cut: one containing dyed areas indicating the flow path of the colored solution, and the other containing areas where no dye was present. The porosity of the dried sample sections was measured using a mercury pressure porosimeter which determines porosity for pores smaller than 0.1 mm. This porosity measurement assumes that pores are cylindrical in shape. The porosity and the accumulation porosity were determined from the pressure and volume of the mercury forced into the sample. The relationship between pore diameter and pressure is as follows:

$$r = 2 \times T \times \cos O \div P \qquad (17)$$

where r : diameter of pore, T : surface tension of mercury, O : contact angle, and P : pressure

7.2 Results and discussion

Figure 7.1 presents the relationship between pore size and accumulation porosity for the two types of rectangular sections. Pores smaller than 0.001 mm in size were seen to characterize the medium accounting for 70 % of all pores. The accumulation porosity for this pore size was found to be about 30 %. A comparison of Figure 7.1 and Figure 6.1 reveals that a pore size smaller than 0.1 mm, which corresponds to the grain size of bentonite, makes up more than 90% of all void areas. However, a pore size greater than 0.1 mm, the grain size of quartz sand, is very rare. The gaps between the large grains of quartz-sand seem therefore to be closed by bentonite. The flow sections, or dyed areas, had a larger proportion of pores between 0.001 mm and 0.1 mm (the grain size of bentonite) than the section with no evidence of a flow path. The flow paths seemed to result from an irregular distribution of bentonite in the sample.

As seen in Figure 7.1, the results revealed differences between the two types of rectangular sections. Five percent of the sections containing dyed areas had pore sizes greater than 0.001 mm contrasted with only 1 % of the undyed sections. However, the accumulation porosity for pore sizes smaller than 0.1 mm in the section without dyed areas varied little from that in the section with dyed areas. Therefore, even at the same porosity condition, the pore size in flow path areas was larger than in no-flow path areas.

If the shape of the pores is regarded as cylindrical, the flow rate is given as follows (Marsily 1986),

$$Q = \frac{\pi r^4}{8\mu} \rho g i$$

$$\frac{Q}{\pi r^2} = \frac{r^2}{8\mu} \rho g i \qquad (18)$$

where r : radius, μ : coefficient of viscosity, and ρ : water gravity density.

If the shape of the pores is regarded as rectangular, the flow rate is given as follows (Marsily 1986),

$$Q = \frac{w^3 L}{12\mu} \rho g i$$

$$\frac{Q}{wL} = \frac{w^2}{12\mu} \rho g i \qquad (19)$$

where L: length, and w : width.

The flow rate per unit pore area is in proportion to the square of r or w. Therefore, as pore dimensions increase, with porosity held constant, the flow rate becomes larger. Even under the same porosity conditions, hydraulic

conductivity changes depending on pore size distribution. As the contrast between pore sizes, within a sample, increases, the total flow through the sample approaches the amount of flow through the large pores only and the flow through the small pores becomes negligible. As a result, effective porosity become smaller. Therefore, under constant porosity conditions, as the large pores increase in size, hydraulic conductivity increases and effective porosity decreases.

8. DISCUSSION

The effect of test scale on effective porosity was considered by comparing field tracer and laboratory tracer tests results. Figure 8.1 shows the relationship between effective porosity relative to porosity, and test scale. Test scale was defined as the length of the sample in the laboratory tests and the distance between the tracer injection point and the sampling point in the field test. The ratio of effective porosity to porosity indicates the proportion of pore volume through which solution actually flows to total pore volume. As the test scale increased from 1.0 cm to 130 m, effective porosity relative to porosity decreased from 100 to less than 5 %.

At the Toki site the results of the field permeability test between the two boreholes used for the field tracer test showed that the hydraulic conductivity of the permeable layer was 2×10^{-5} cm sec^{-1}. This value was larger than those estimated in the laboratory tests, which were $2\times10^{-8}\sim4\times10^{-7}$ cm sec^{-1}. In the laboratory tests, borehole core samples with no cracks were used. If a crack had existed in the core sample, the sample would have separated at the crack. If a fracture with a width of $0.1\sim0.2$ mm existed at the field scale, the mean hydraulic conductivity of a 10 m zone would be 2×10^{-5} cm sec^{-1} based upon the Hele-Shaw model. The occurrence of fractures do not greatly influence the porosity of the zone. Therefore, it is possible that permeable cracks or fissures existed at the Toki field site. The number of permeable cracks or fissures are thought to increases as test scale increases. From the laboratory scale to the field scale, the decrease in effective porosity and increase in hydraulic conductivity was due to the increase of cracks or fissures according to the bentonite and quartz sand mixture laboratory tests results. On the laboratory scale, the decrease in effective porosity was probably due to a

loss of connectivity of continuous pores as neither cracks nor fissures were present in the samples.

Figure 8.2 shows the relationship, estimated in laboratory tests, between the dispersion coefficient and actual velocity. As the actual velocity increases, the dispersion coefficient increases (Klotz *et al.*1980). Figure 8.3 shows the relationship between the test scale and longitudinal dispersivity in sedimentary rocks. Longitudinal dispersivity is the dispersion coefficient divided by actual velocity. Originally Leonhart *et al.* (1985) showed that as the scale of field tests increased, longitudinal dispersivity increased. Our results at the Toki and the Matsumoto tracer test site and the Leonhart *et al.* results indicate that as the test scale increases from laboratory scale, several centimeters, to field scale, several thousand meters, longitudinal dispersivity increases proportionally. The following empirical relationship has been found from these results: longitudinal dispersivity equals one tenth of test scale for the sedimentary formation. This is in agreement with the relationship presented in the paper by Pickens and Grisak (1981a, 1981b).

Figure 8.4 shows schematic representation of the dilution process caused by mechanical dispersion in homogeneous media and heterogeneous media (Freeze and Cherrry 1979). At smaller scales, water flows through homogeneous media in case of the Toki laboratory tracer tests. At larger scales, water flows through heterogeneous media in case of the Toki and the Matsumoto field tracer tests.

According to Harleman and Rumer (1963), Day (1975), Schwartz (1977) and Domenico and Robbins (1984), several reasons were offered to explain scale effects of longitudinal dispersivity, most of which relied on heterogeneity and modeling. The heterogeneity argument relates to the number, size, and arrangement of heterogeneities in the porous medium. Gelhar

et al. (1992) stated also the variations in dispersivity reflected the influence of differing degrees of aquifer heterogeneity at different sites. At larger scales, a great number of heterogeneities may be encountered, and a higher dispersivity would be expected. The existence of cracks on a scale of more than several meters explain also scale effects of longitudinal dispersivity.

9. CONCLUSION

We performed both laboratory and field tracer tests using conservative tracers in order to estimate the effective porosity and longitudinal dispersivity of a sedimentary rock. Both the laboratory and field tracer test results indicate that as test scale increases from 1.0 cm to 130 m, effective porosity decreases and longitudinal dispersivity increases. The following empirical relationship has been found for the sedimentary formation : longitudinal dispersivity equals one tenth of scale. The relationship is useful for estimating mass transport in groundwater.

The decrease in effective porosity may be attributed to the loss of continuous pore connectivity at the laboratory scale and the increase of selective flow path such as cracks and fissures from laboratory scale to field scale. The existence of selective flow paths such as cracks and fissures has been suggested based on the results of field permeability tests. The lower effective porosity encountered at the field scale may be attributed to the existence of selective flow paths not present in the laboratory samples. The existence of cracks at the field scale explain also effects of longitudinal dispersivity because heterogeneities may be encountered and a higher longitudinal dispersivity would be expected.

10. ACKNOWLEDGMENT

The author is sincerely grateful to Professor Dr. Shindo, S. and Associate Professor Dr. Sakura, Y., Department Earth Science of Chiba University for useful suggestions and cooperation throughout the study, to Professor Dr. Shirai, T., Department of Education, Professor Dr. Furuya, T., and Associate Professor Dr. Inoue, A., Department Earth Science of Chiba University for useful suggestions, to Ohtsuka, Y. and Mori, N. of Shimizu Corporation for supporting the Matsumoto tracer test, to Sugiyama, H. of Kunimine Industries Co., Ltd., for supporting the bentonite and quartz-sand mixture tests and to .Ishikawa, Y. and Sugihara, K. of Power Reactor and Nuclear Fuel Development Corporation and Utsugida, Y. of Shimizu Corporation for supporting the Toki tracer tests.

11. REFERENCE

Anderson, M.P. 1979. Using models to simulate the movement of contaminants through groundwater flow systems, *CRC Crit. Rev.Environ. Control, 9*, 97-156.

Day, T.J. 1975. Longitudinal dispersion in natural channels. Water Resource research, 11, 6 ; 909-918.

Domenico, P.A. & Robbins, G.A. 1984. A dispersion scale effect in model calibrations and field tracer experiments. J. Hydrology, 70 ; 123 -132.

Eckis, R. 1934. South Coastal Basin investigation, geology and groundwater storage capacity of valley fill, *Bull.* 45, Calif. Div. Water Resources, Sacramento, pp279.

Davis, S.N. & DeWiest, R.J.M. 1966. *Hydrology.* John & Sons.

Freeze, R.A. & Cherry, J.A. 1979. *Groundwater.* New Jersey : Prentice-Hall Inc. pp604.

Fukui, M. & Katsurayama, K. 1975. Fundamental study on longitudinal dispersion of tritiated water through saturated porous media. J. Health Phys. 28 ; 717 -725.

Gelhar, L.W. 1982. Analysis of two-well tracer tests with a pulse input, RHO-B W-CR, 131P.

Gelhar, L.W., Mantaglou, C.W. & Rehfeldt, K.R. 1985. A review of field-scale physical solute transport processes in saturated and unsaturated porous media, *EPRI Rep. EA-4190,*. Elec. Power Res. Inst., Palo Alto, Calif., Aug.

Gelhar, L.W., Welty, C. & Rehfeldt, K.R. 1992. A Critical Review of Data on Field-Scale Dispersion in Aquifers. Water Resource research, 28. 7 ;

1955-1974.

Harleman, D.R.F. & Rumer, R.R. 1963. Longitudinal and lateral dispersion in an isotropic porous media. J. Fluid Mechanics, 16 ; p391.

Ii, H. & Sugiyama, H. 1991. Physical properties, especially effective porosity, of a bentonite and quartz sand mixture as backfill and buffer material for disposal of high-level radioactive waste. Proceeding of the 1991 Joint International Waste Management Conference, 2 ; 243-248.

Ii, H., Ishikawa, Y., Sugihara, K. & Utsugida, Y. 1993a. Dispersion coefficient and effective porosity of a sedimentary rock by a field tracer test. J. Groundwater Hydrology., 35,1;23-36. (in Japanese).

Ii, H., Ishikawa, Y., Sugihara, K. & Utsugida, Y. 1993b. Estimation of scale effect on effective porosity and longitudinal dispersivity of a Tertiary sedimentary rock by laboratory tracer tests and a field tracer test. International Association of Hydrogeologists., 4 ; 153-162.

Ii, H. 1994a. Effective porosity, longitudinal dispersivity and hydraulic conductivity of a sedimentary formation by laboratory tracer tests and a field tracer test. Shimizu. Tech. Res. Bull., 13 ; 1-10.

Ii, H. 1994b. Groundwater tracer test of a sedimentary formation by three-dimensional analysis using FEM at the Matsumoto tunnel. RIKEN Review., 5 ; 17-18.

Ii, H. 1994c. Effective Porosity and Longitudinal Dispersivity of Sedimentary Rocks Determined by Laboratory and Field Tracer Tests. J. Environmental Geology.(in press)

Ii, H. & Misawa, S. 1994a. The groundwater chemistry of the Matsumoto tunnel and surrounding area. J. Groundwater Hydrology., 36, 1 ; 13-29.(in Japanese).

Ii, H. & Misawa, S. 1994b. The groundwater chemistry within a plateau

neighboring Matsumoto city, Japan. J. Environmental Geology.(in press).

Ii, H., Misawa, S. & Kawamura, R. 1994a. Effective porosity, longitudinal dispersivity and hydraulic conductivity of a sedimentary formation determined by field tracer testing, three-dimensional groundwater flow and advection-dispersion FEM. Proceeding of the 7th Congress of the International Association of Engineering Geology.6 : 4213-4221.

Ishikawa, Y. & Sugihara, K. 1991. Data acquisition in order to estimate the operating conditions of uranium mine developed by the in-place leaching method. PNC TN, 78; 59 -66. (in Japanese).

Kawamura, R. 1987. Three-dimensional groundwater flow and advection diffusion code for treating decay chain of radioactive materials by finite element method. J. Nuclear. Sci. Tech. 24, 11; 937-950.

Klotz, D., Seiler, K.-P., Moser, H. & Neumaier, F. 1980. Dispersivity and velocity relationship from laboratory and field experiments. J. Hydrology, 45 ; 169-184.

Lallemand-Barres,A. & Peaudecerf, P. 1978. Recherhe des relations entre la valeur de la dispersivite macroscopique d`un milieu aquifere, ses autres caracteristiques et les conditions de mesure, *Bull. Bur. Rech. Geol. Min., Sect. 3, Ser. 2, 4.*

Leonhart, L.S., Jackson, R.L., Graham, D.L., Gelhar, L.W., Thompson, G.M., Kanehiro, B.Y. & Wilson, C.R. 1985. Analysis and interpretation of a recirculating tracer experiment performed on a deep basalt flow top, Bulletin of the Association of Engineering Geologists, Vol.XXII, 3; 259-274.

Linsley,R.K., Kohler, M.A. & Pauthus, J.L.H. 1958. *Hydrology for*

Engineers. Mcgraw-Hill.

Marsily, G. 1986. *Quantitative Hydrogeology*. Florida : Academic press Inc. pp440.

Neretnieks, I. 1985. Transport in fractured rocks, paper presented at the 17 International Congress on the Hydrology of Rock of Low Permeability, Intl. Asscoc. of Hydrogeol., Tucson, Ariz., Jan. 7-12.

Ogata, A. 1970. Theory of dispersion in a granular medium. U.S.Geol.Sarv.Prof.Paper 411-I.

Pickens, J.F. & Grisak, G.E. 1981a. Scale-dependent dispersion in a saturated granular aquifer. Water Resource research, 17, 4 ; 1191-1211.

Pickens, J.F. & Grisak, G.E. 1981b. Modeling of scale-dependent dispersion in hydrogeologic systems. Water Resource research, 17, 6 ; 1701-1711.

Saffman, P.G. 1959. A theory of dispersion in a porous media. J. Fluid Mechanics, 6 ; p321.

Schwartz, F.W. 1977. Macroscopic dispersion in porous media : The controlling factors.. Water Resource research, 13, 4 ; 743-752.

Shimooka, K., Takebe, S., Ii, H., Hirosue, F., Yamada, K., Miyahara, H.,Wadachi, Y. and Hirano, K. 1989. Performance experiment of LLRW disposal concrete vault -migration behavior of radionuclides in backfill and concrete.Proceeding of the 1989 Joint International Waste Management Conference, 1; 581-586.

Utsugida, Y., Tanaka, S. & Ishii, T. 1984.The solution of migration problems by finite element method. Proceedings of the 6th Japan symposium on rock mechanics.(in Japanese).

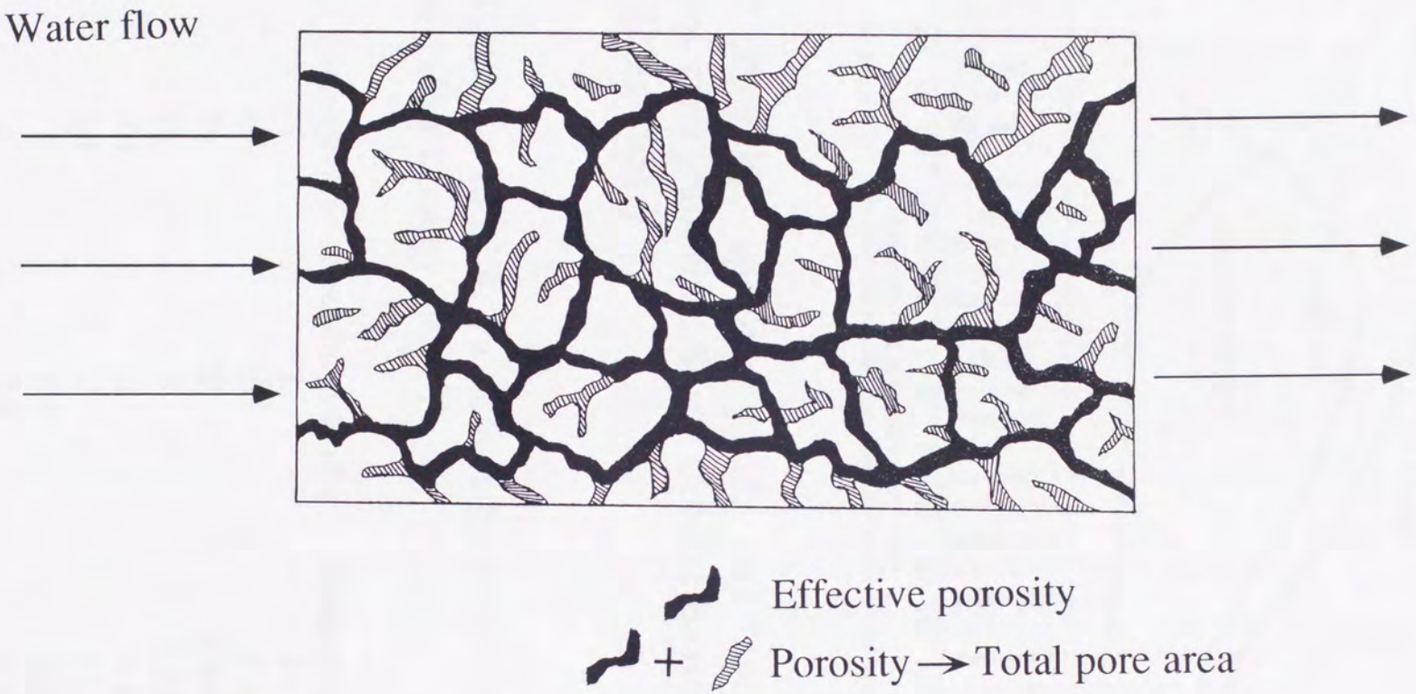


Figure 1.1 Schematics of effective porosity and porosity

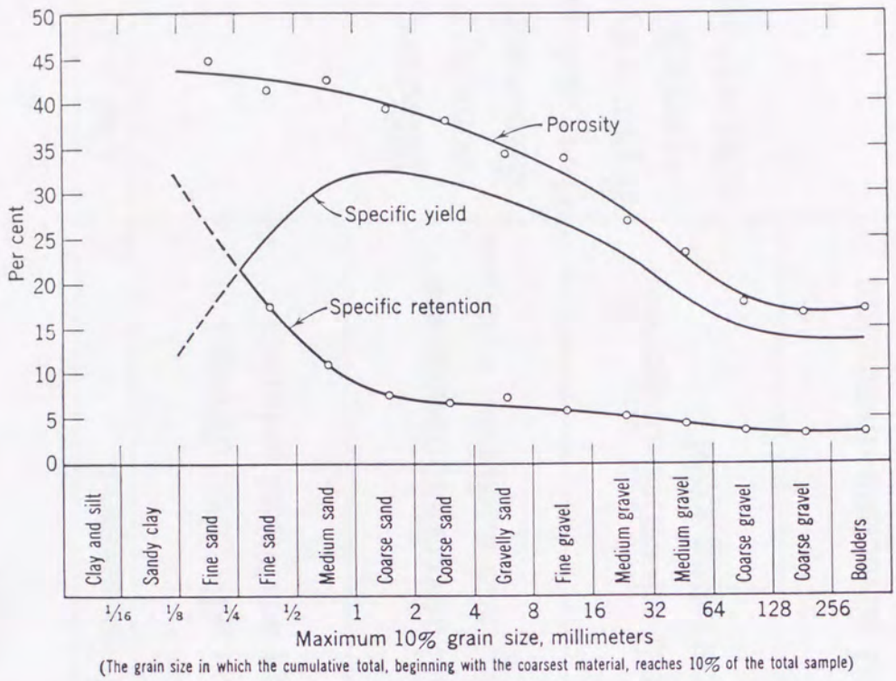


Figure 1.2 Porosity, specific yield, and specific retention variations with grain size, South Coastal Basin, Calif. (after Eckis 1934)

Table 1.1 Porosity, specific yield, and hydraulic conductivity for aquifers (after Linsley 1958)

Material	Porosity (%)	Specific yield (%)	Hydraulic conductivity (m/s)
Clay	45	3	5×10^{-7}
Sand	45	25	4×10^{-4}
Gravel	25	22	2.5×10^{-3}
Sandstone	15	8	3.5×10^{-4}
Limestone	10	2	5×10^{-7}
Shale	10	2	5×10^{-7}
Chert	5	0.5	5×10^{-8}
Granite	5	0.5	5×10^{-8}

Table 1.2 Tracer tests

Site	Material	Scale	Analysis method	Out put
Toki	Neogene Sedimentary rock	Laboratory 1～6 cm	One-dimensional advection-dispersion equation using analytical solution	Effective porosity, dispersion (longitudinal dispersivity), hydraulic conductivity
		Field 7 m	Two-dimensional advection-dispersion equation using FEM and analytical solution	
Matsumoto	Miocene Sedimentary rock	Field 130 m	Three-dimensional advection-dispersion equation using FEM	
Artificial	Bentonite and quartz-sand mixture	Laboratory 2 cm	One-dimensional advection-dispersion equation using analytical solution	

Table 2.1 Distribution coefficients of Cl^- and Br^-

T-1,T-2,T-3 samples are derived from the recovery borehole, 79～80m in depth at the Toki site, M-1 and M-2 are derived from the Matsumoto tunnel.

No.	Rock type	Sample to solution	Kd (ml g^{-1})	
			Cl^-	Br^-
T-1	Sandstone	3.8/100	0	0
T-2		4.4/100	0	0
T-3		3.1/100	0	0
M-1	Clay (originally Tuff breccia)	1.0/100	0	0
		4.8/100	0	0
M-2	Tuff breccia	1.0/100	0	0
		4.6/100	0	0
B-1	Bentonite and quartz sand mixture	1/20	0	—
		1/40	0	0
		1/100	0	0
		1/200	0	—

Table 3.1 Maximum concentration and the time at the recovery borehole, if the mass of tracer is 1g

Flow rate ($cm^3 min^{-1}$)		2000		4000		8000	
Longitudinal dispersivity (m)	Effective porosity (%)	Time (day)	Maximum concentration (ppm)	Time (day)	Maximum concentration (ppm)	Time (day)	Maximum concentration (ppm)
1.4	30	95.9	0.0014	47.9	0.0014	24.0	0.0014
	10	32.0	0.0042	16.0	0.0042	8.0	0.0042
	5	16.0	0.0084	8.0	0.0084	4.0	0.0084
0.7	30	66.4	0.0018	33.2	0.0018	16.6	0.0018
	10	22.1	0.0054	11.1	0.0054	5.5	0.0054
	5	11.1	0.0108	5.5	0.0108	2.8	0.0108
0.07	30	58.7	0.0038	29.4	0.0038	14.7	0.0038
	10	19.6	0.0114	9.8	0.0114	4.9	0.0114
	5	9.8	0.0228	4.9	0.0228	2.4	0.0228

Table 3.2 Parameters used in the two dimensional analysis of the Toki field tracer test

Distance (m)	7
Flow rate ($cm^3\ min^{-1}$)	7800
Thickness of permeable layer (m)	10
Mass of tracer (g)	1920 (Br^-)
Effective porosity (%)	2～30
Longitudinal dispersivity (m)	0.014～7

Table 3.3 Parameters and boundary conditions used in the seepage analysis at the Toki field tracer test

Thickness of permeable layer	10m
Hydraulic conductivity	$5\times10^{-6}\sim1\times10^{-4}$cm/sec
Boundary conditions	Impermeable boundary (Except the boreholes)
Injection borehole	Constant flow rate: 3900cm^3/min (half area)
Recovery borehole	Steady-state piezometric head level (-15m from natural water table)

Table 3.4 Parameters and boundary condition used in the migration analysis at the Toki field tracer test

Initial concentration	1700ppm (112.8min)
Hydraulic conductivity	2.2×10^{-5}cm/sec
Flow velocity distribution	Seepage analysis used
Effective porosity	Maximum 30%
Longitudinal dispersivity	0.014～7.0m
Thickness of permeable layer	10m
Boundary condition	Impermeable

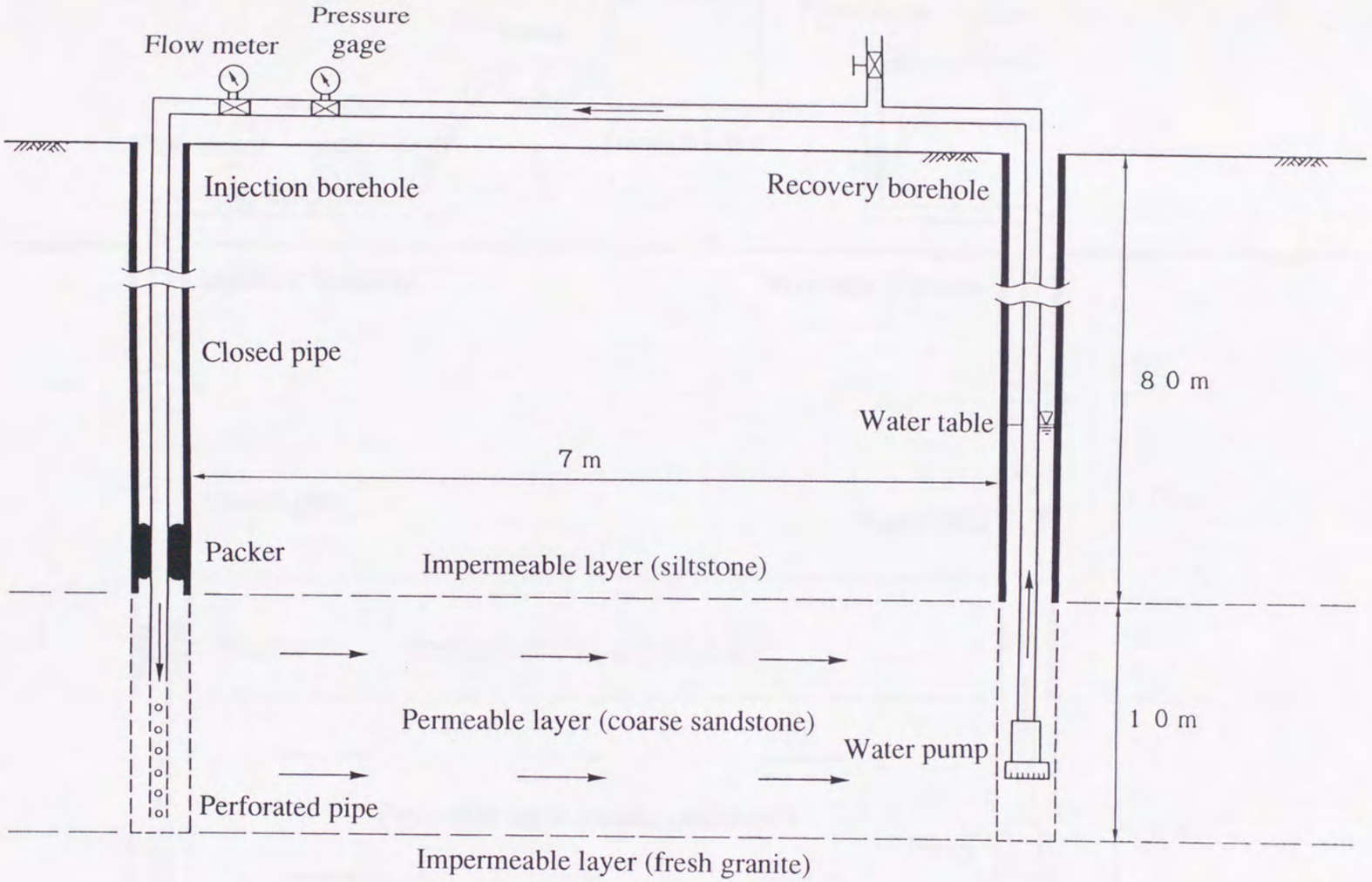


Figure 3.1 Schematic figure of the Toki field tracer test (before tracer injection)

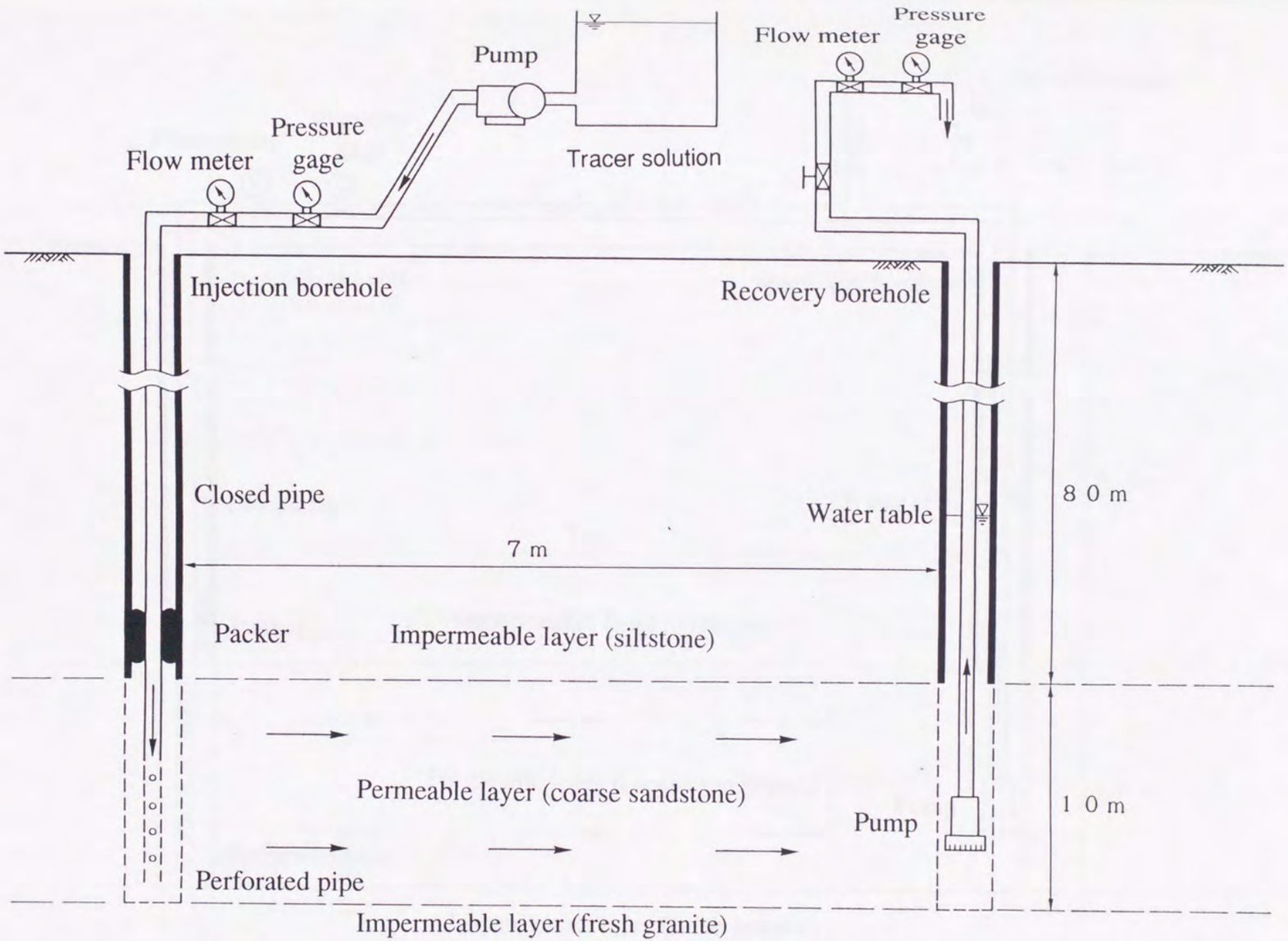


Figure 3.2 Schematic figure of the Toki field tracer test (during tracer injection)

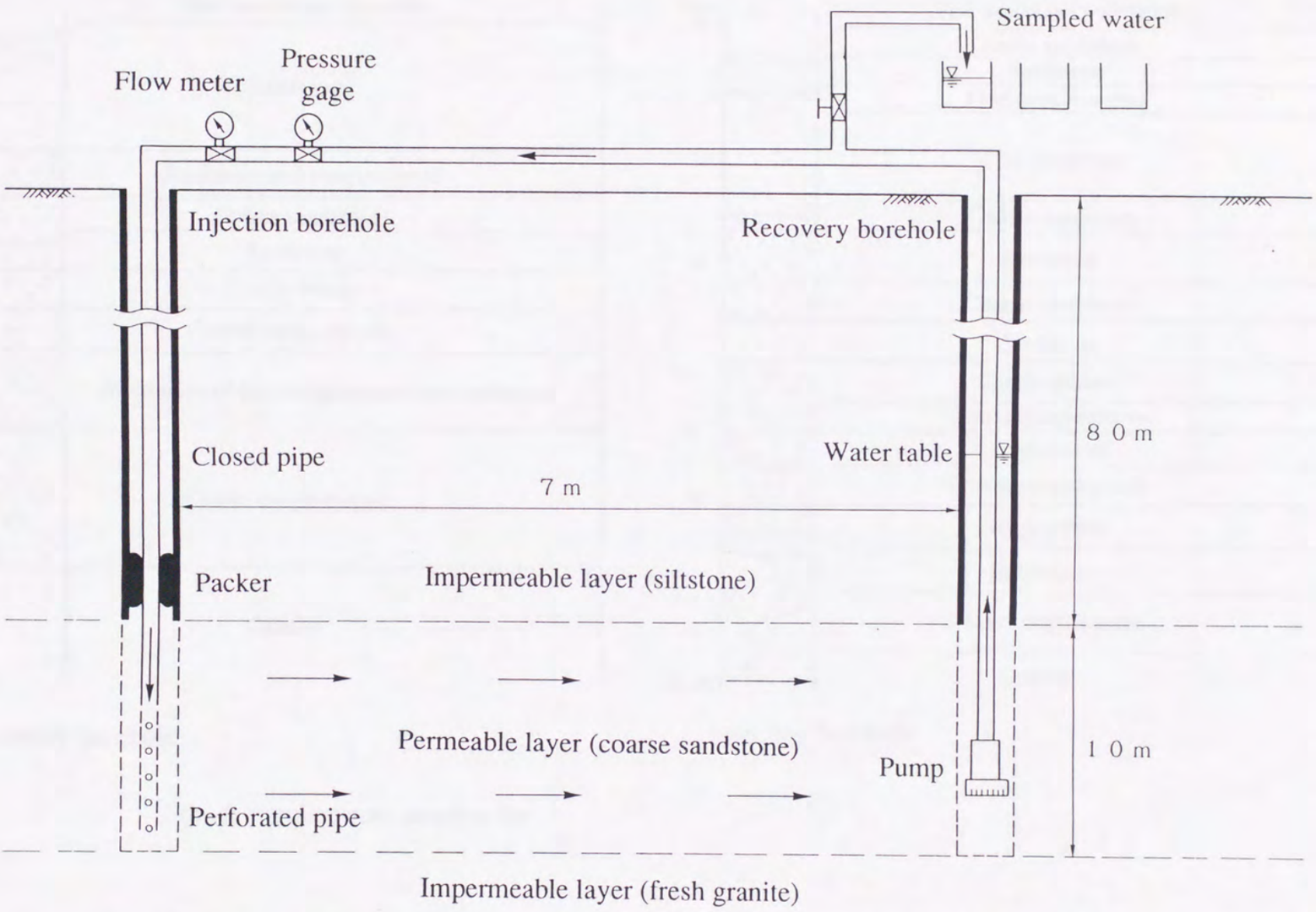
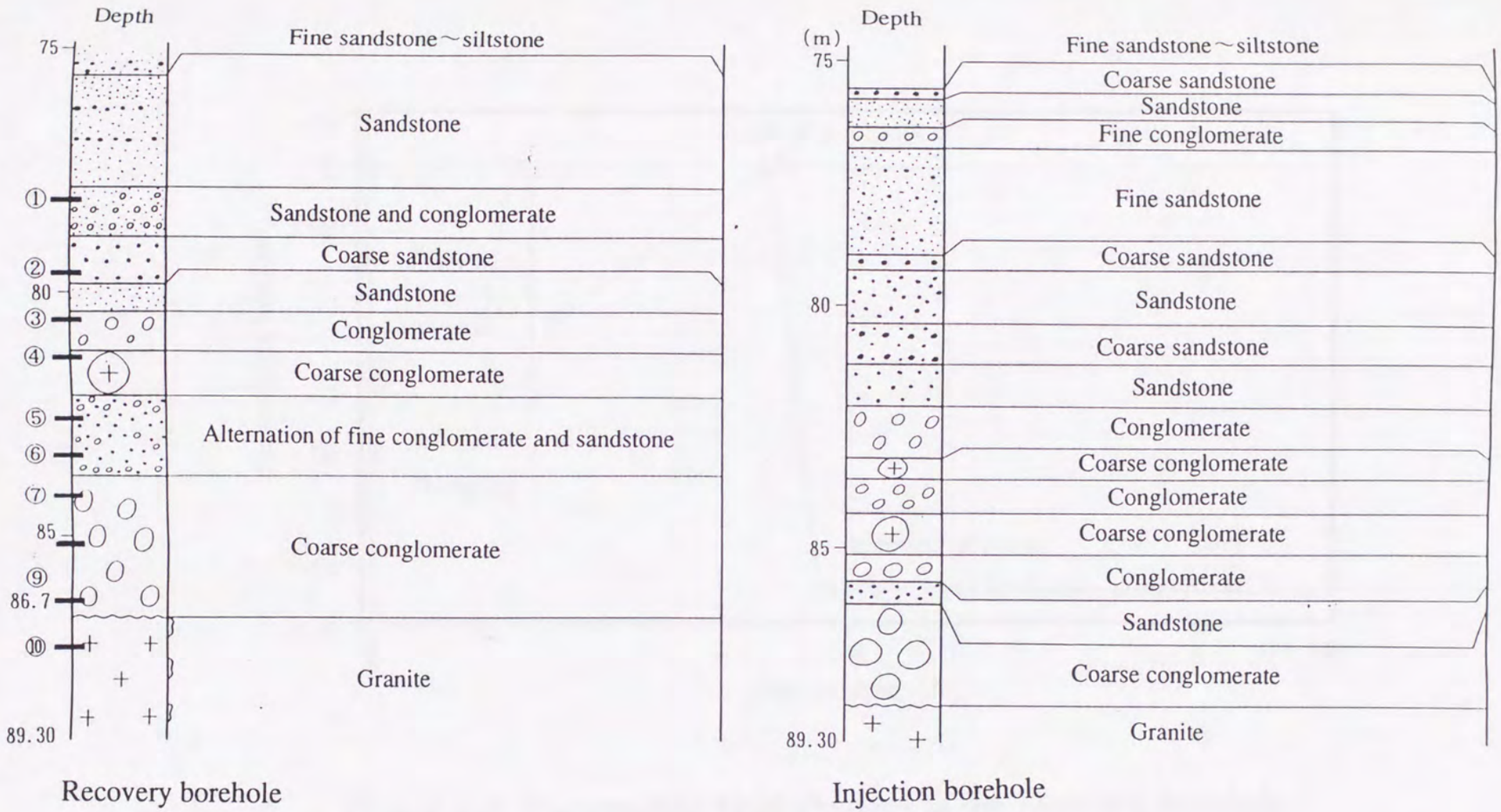


Figure 3.3 Schematic figure of the Toki field tracer test (after tracer injection)



①～⑩ sampled core position for

Figure 3.4 Geological column of the boreholes at the Toki site

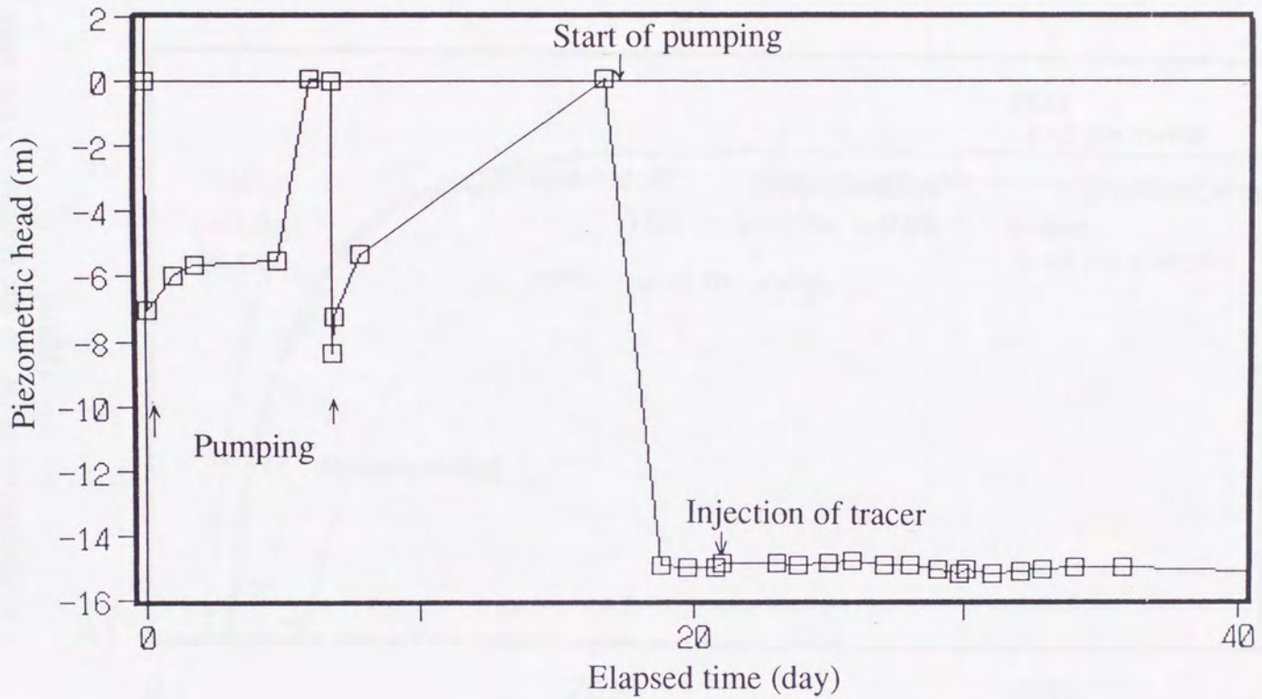


Figure 3.5 Piezometric head changes at the recovery borehole

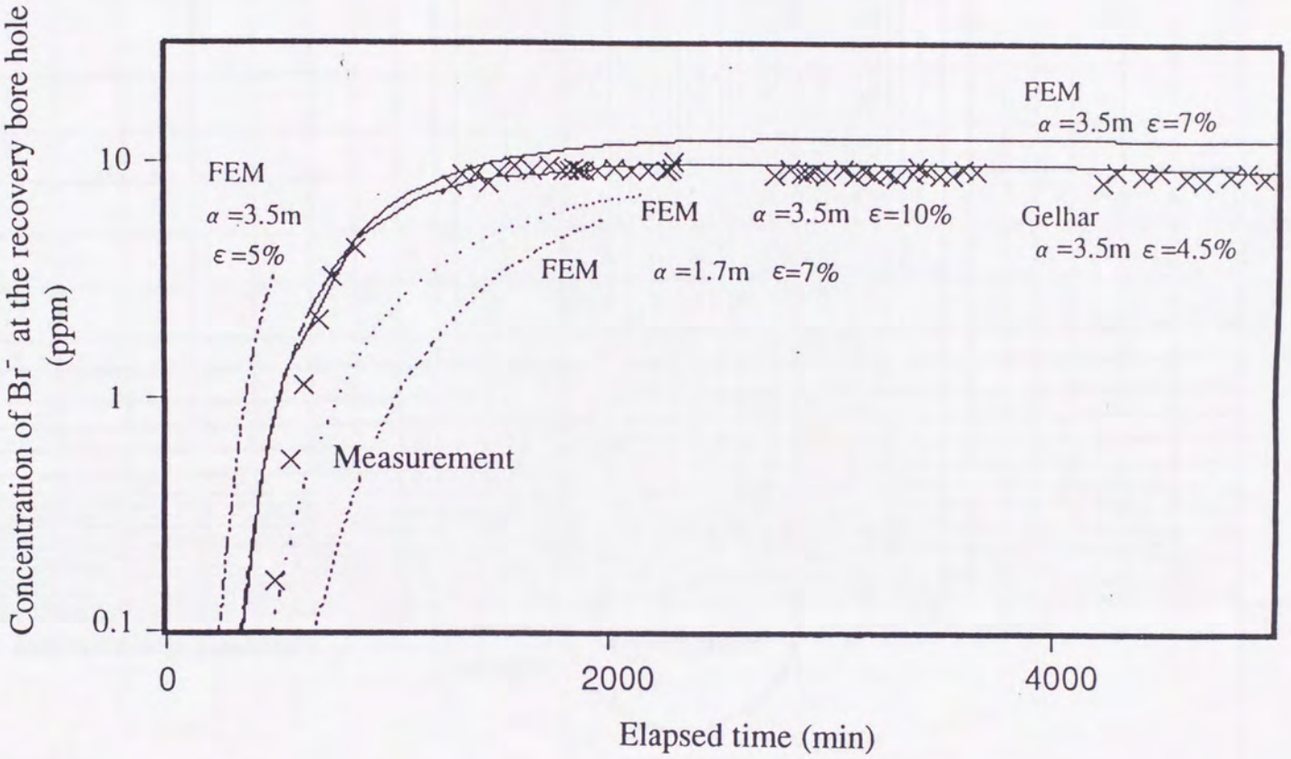


Figure 3.6 Relationship between elapsed time after the stat of tracer injection and concentration of Br^- at the recovery borehole at the Toki site

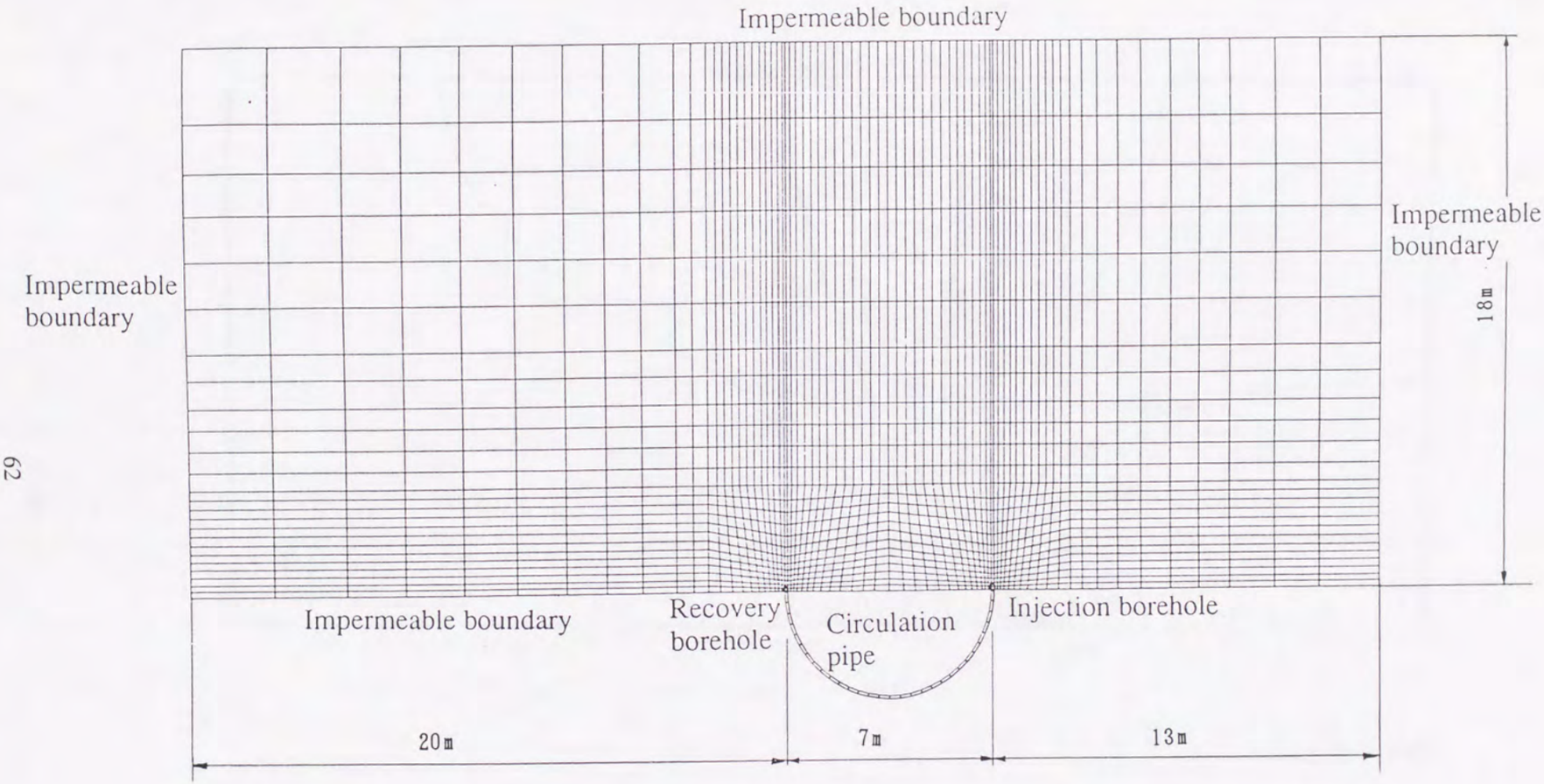


Figure 3.7 Analytical model (horizontal section) at the Toki site

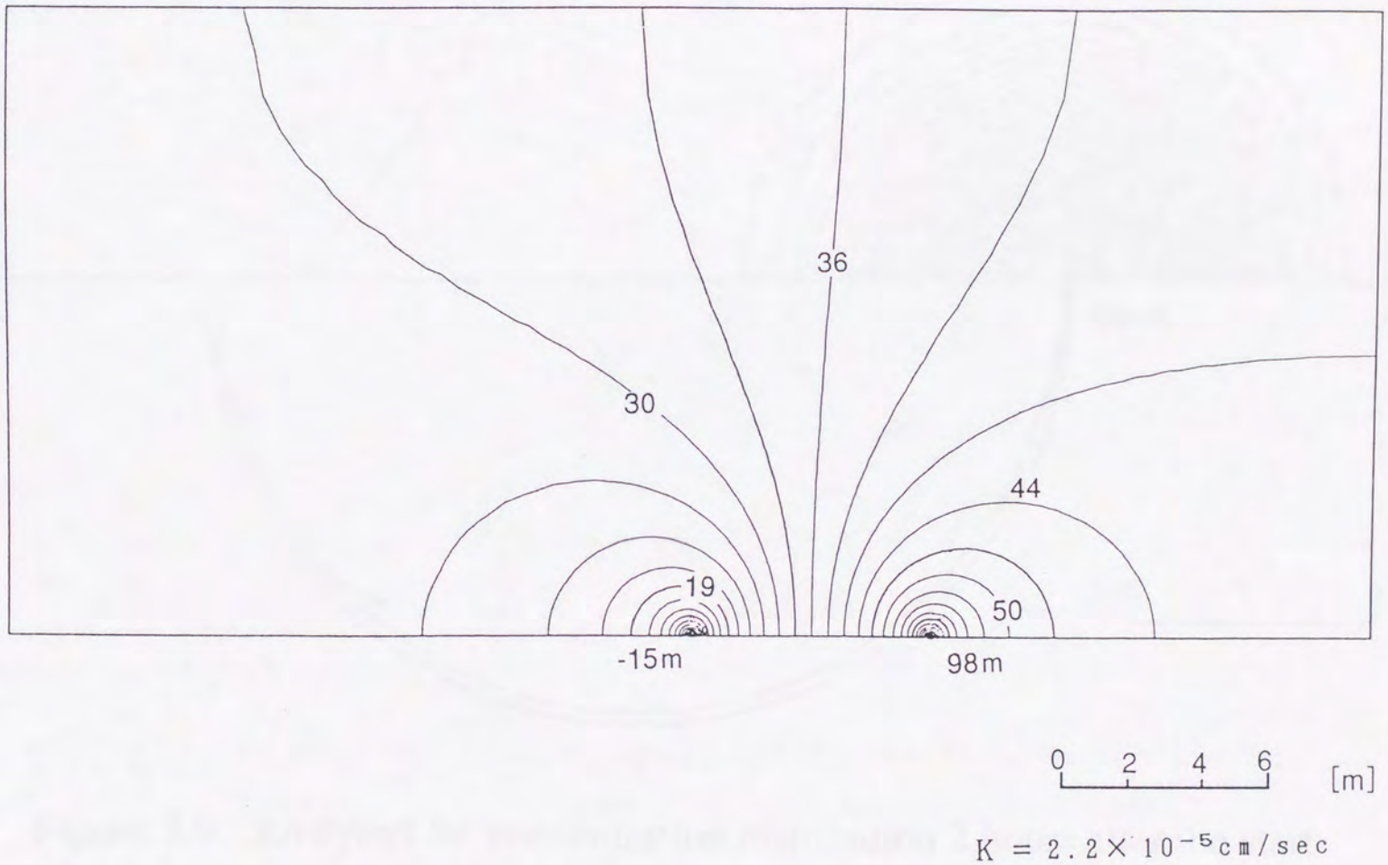


Figure 3.8 Analyzed piezometric-head distribution at the Toki site (horizontal section)

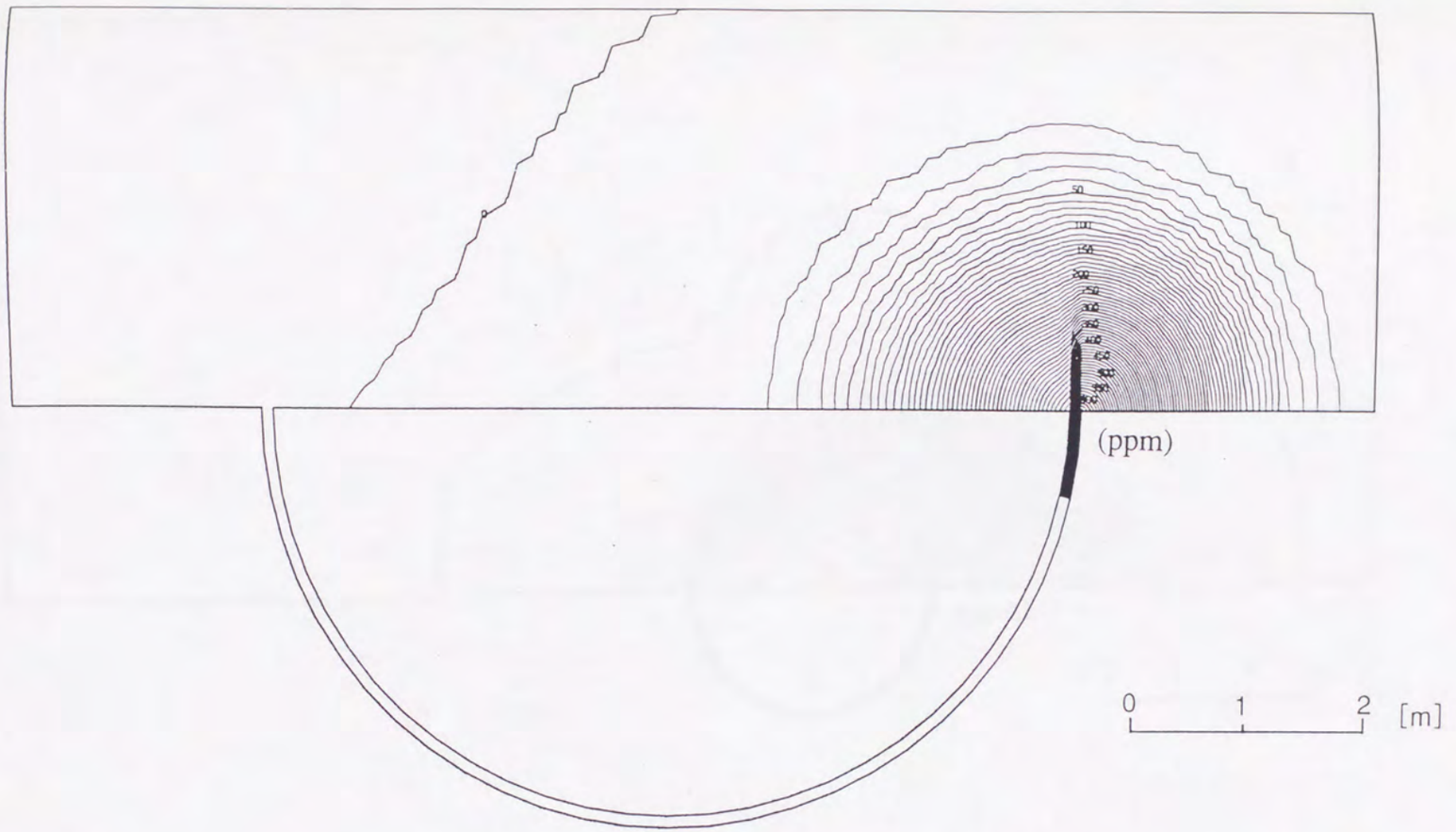


Figure 3.9 Analyzed Br^- concentration distribution 2 hours after the start of tracer injection at the Toki site (horizontal section)

(α=3.5m ε=7%)

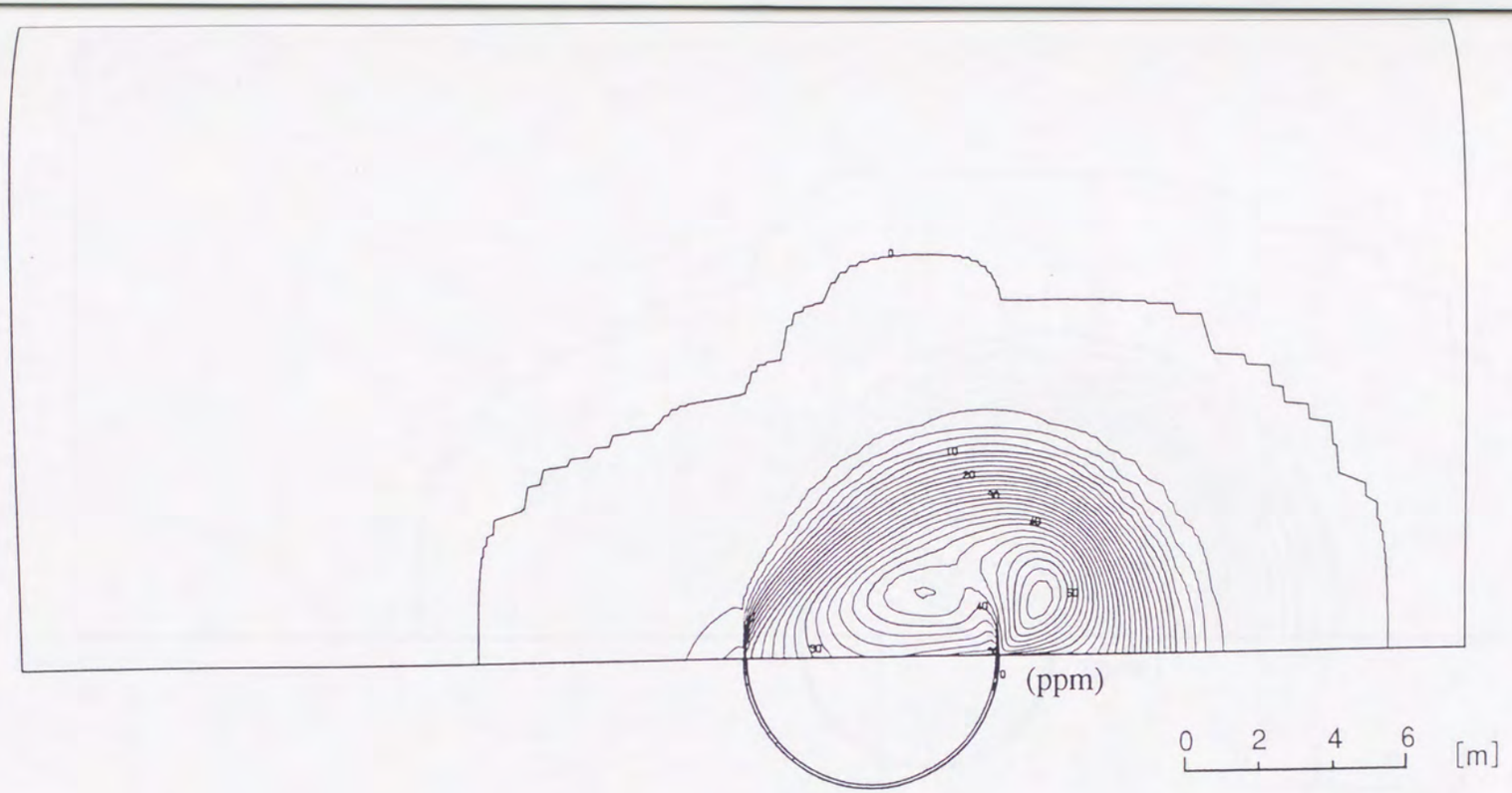


Figure 3.10 Analyzed Br^- concentration distribution 36 hours after the start of tracer injection at the Toki site (horizontal section)

(α=3.5m ε=7%)

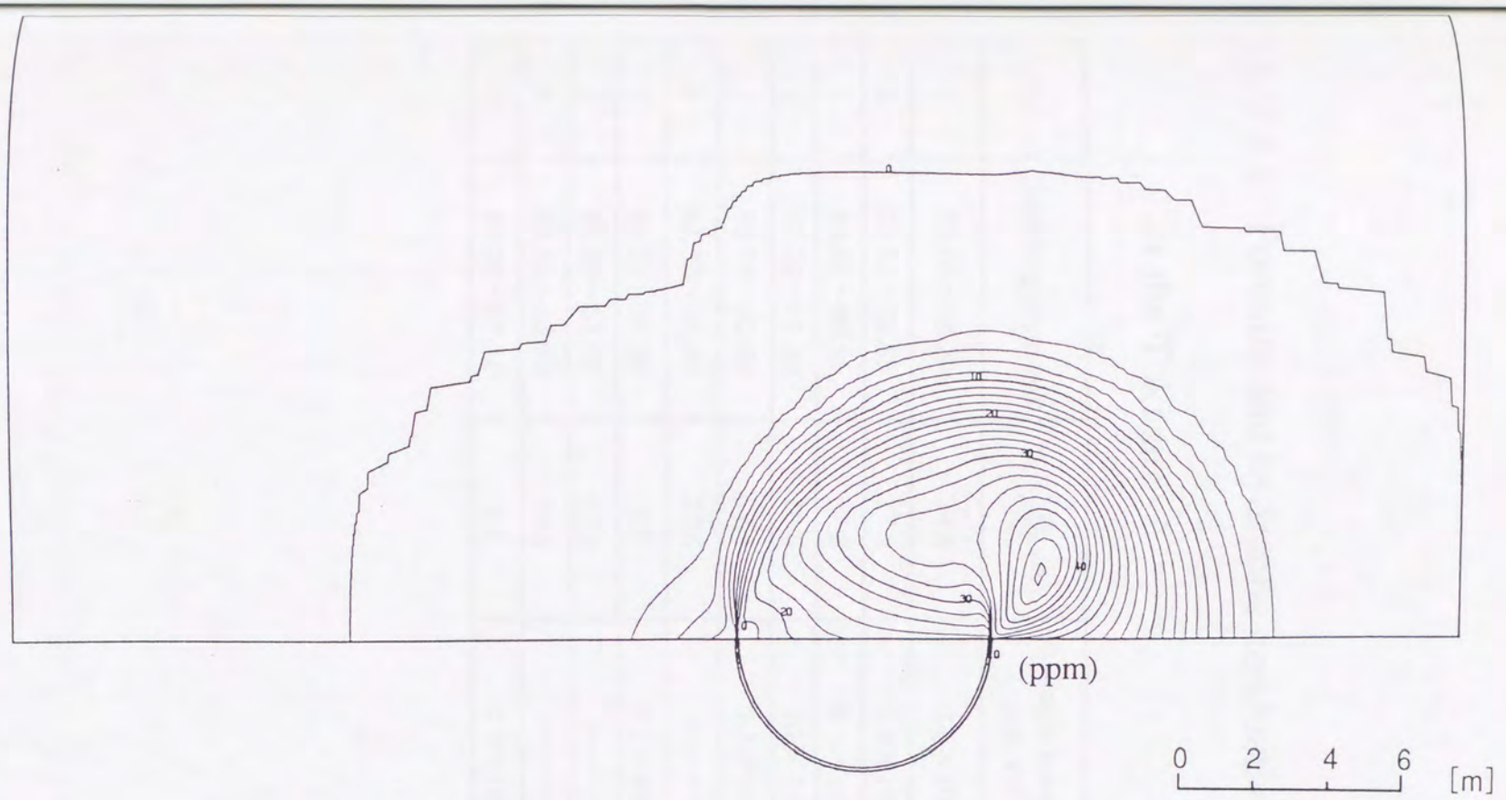


Figure 3.11 Analyzed Br^- concentration distribution 100 hours after the start of tracer injection at the Toki site (horizontal section)

(α=3.5m ε=7%)

Table 4.1 Porosity and hydraulic conductivity of laboratory tests at the Toki site

No.	Sampling depth (m)	Porosity (%)	Hydraulic conductivity (cm sec^{-1})	Rock type
1	78.10～78.20	24.8	2.6×10^{-7}	Sandstone and conglomerate
2	79.55～79.65	27.9	2.4×10^{-7}	Coarse sandstone
3	80.45～80.55	27.3	9.4×10^{-8}	Conglomerate
4	81.20～81.30	26.8	1.2×10^{-7}	Coarse conglomerate
5	82.70～82.80	31.1	3.7×10^{-8}	Alternation of fine conglomerate and sandstone
6	83.30～83.40	27.6	———	
7	84.10～84.20	5.5	2.7×10^{-8}	Coarse conglomerate
8	85.00～85.10	47.3	———	
9	86.30～86.40	30.8	———	
10	87.20～87.30	5.8	2.9×10^{-6}	Granite

Table 4.2 Conditions and results of laboratory tests at the Toki site

Rock Type	Porosity (%)	No	Hydraulic conductivity (cm sec^{-1})	Length of sample (cm)	Actual velocity (cm sec^{-1})	Flow rate (cm^3 sec^{-1})	Dispersion coefficient (cm^2 sec^{-1})	Effective porosity (%)
Sandstone	27	T1-1	2.6×10^{-7}	1.10	5.2×10^{-4}	1.9×10^{-3}	9.2×10^{-5}	24
					1.4×10^{-4}	5.5×10^{-4}	3.5×10^{-5}	27
					2.9×10^{-4}	1.2×10^{-3}	8.5×10^{-5}	28
		T1-2	4.2×10^{-7}	2.01	9.5×10^{-4}	3.2×10^{-3}	2.5×10^{-4}	22
					1.2×10^{-4}	4.6×10^{-4}	3.8×10^{-5}	24
					2.0×10^{-3}	7.4×10^{-3}	9.4×10^{-4}	25
	31	T2-1	2.4×10^{-8}	1.99	2.9×10^{-4}	1.1×10^{-3}	4.5×10^{-5}	25
					6.5×10^{-5}	2.6×10^{-4}	8.8×10^{-6}	26
					1.7×10^{-4}	7.1×10^{-4}	2.3×10^{-5}	27
					3.7×10^{-4}	1.5×10^{-3}	3.8×10^{-5}	27
					6.8×10^{-5}	2.8×10^{-4}	8.2×10^{-6}	27
		T2-2	3.1×10^{-8}	5.01	8.5×10^{-5}	2.7×10^{-4}	1.4×10^{-5}	21
					4.5×10^{-5}	1.5×10^{-4}	7.6×10^{-6}	21
					2.2×10^{-4}	7.3×10^{-4}	3.5×10^{-5}	22
					2.0×10^{-4}	6.8×10^{-4}	2.7×10^{-5}	23
					1.7×10^{-4}	6.1×10^{-4}	2.5×10^{-5}	24
		T2-3	4.7×10^{-8}	6.05	4.3×10^{-4}	1.4×10^{-3}	6.9×10^{-5}	22
					2.3×10^{-4}	8.1×10^{-4}	3.2×10^{-5}	24
	29	T3-1	8.3×10^{-8}	2.37	5.5×10^{-4}	1.7×10^{-3}	2.3×10^{-4}	21
		T3-2	4.2×10^{-8}	6.14	3.4×10^{-4}	9.8×10^{-4}	7.5×10^{-5}	19

T1, T2, T3 samples are derived from the recovery borehole 79～80m in depth.

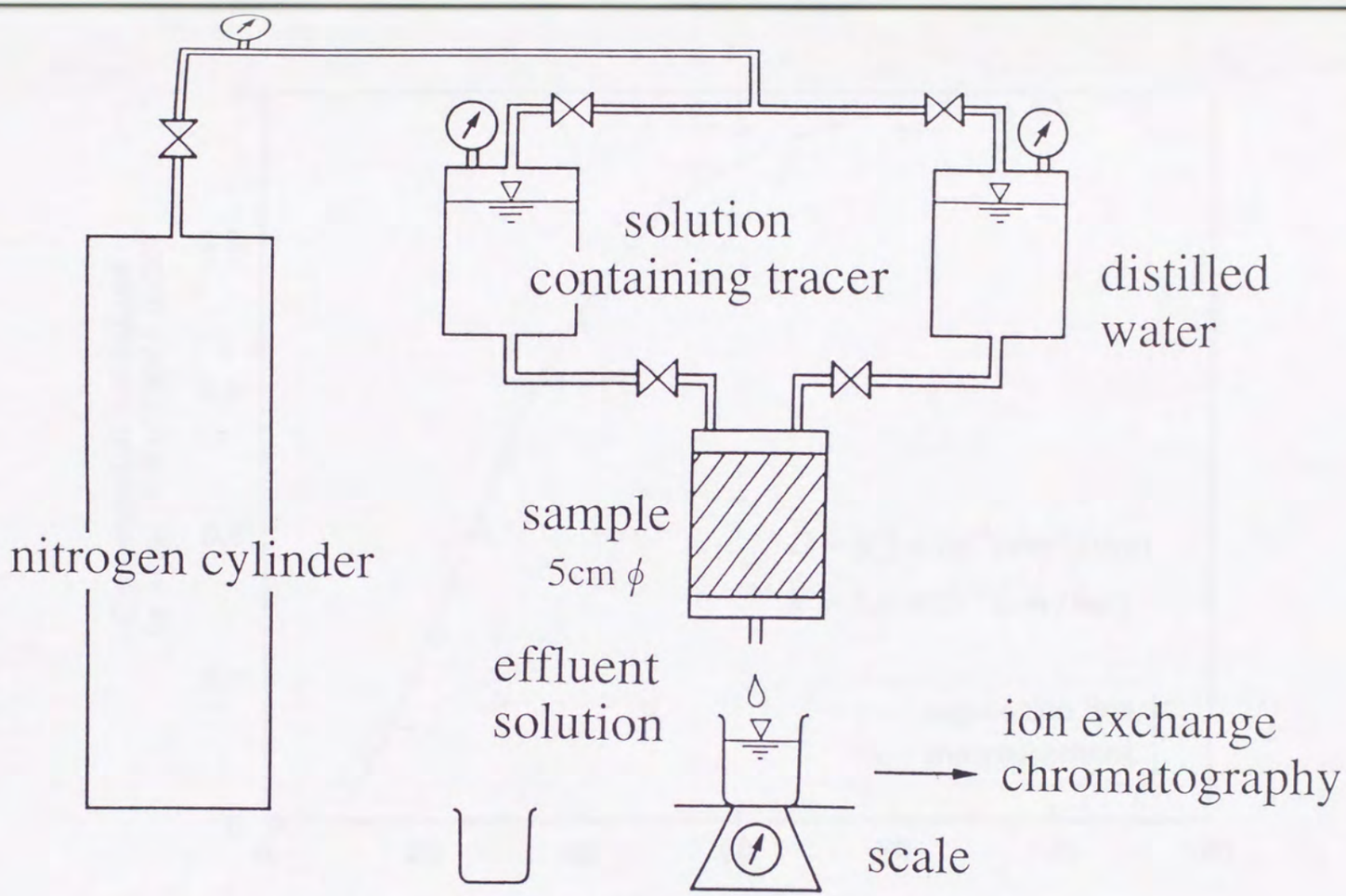


Figure 4.1 Apparatus for laboratory tracer test

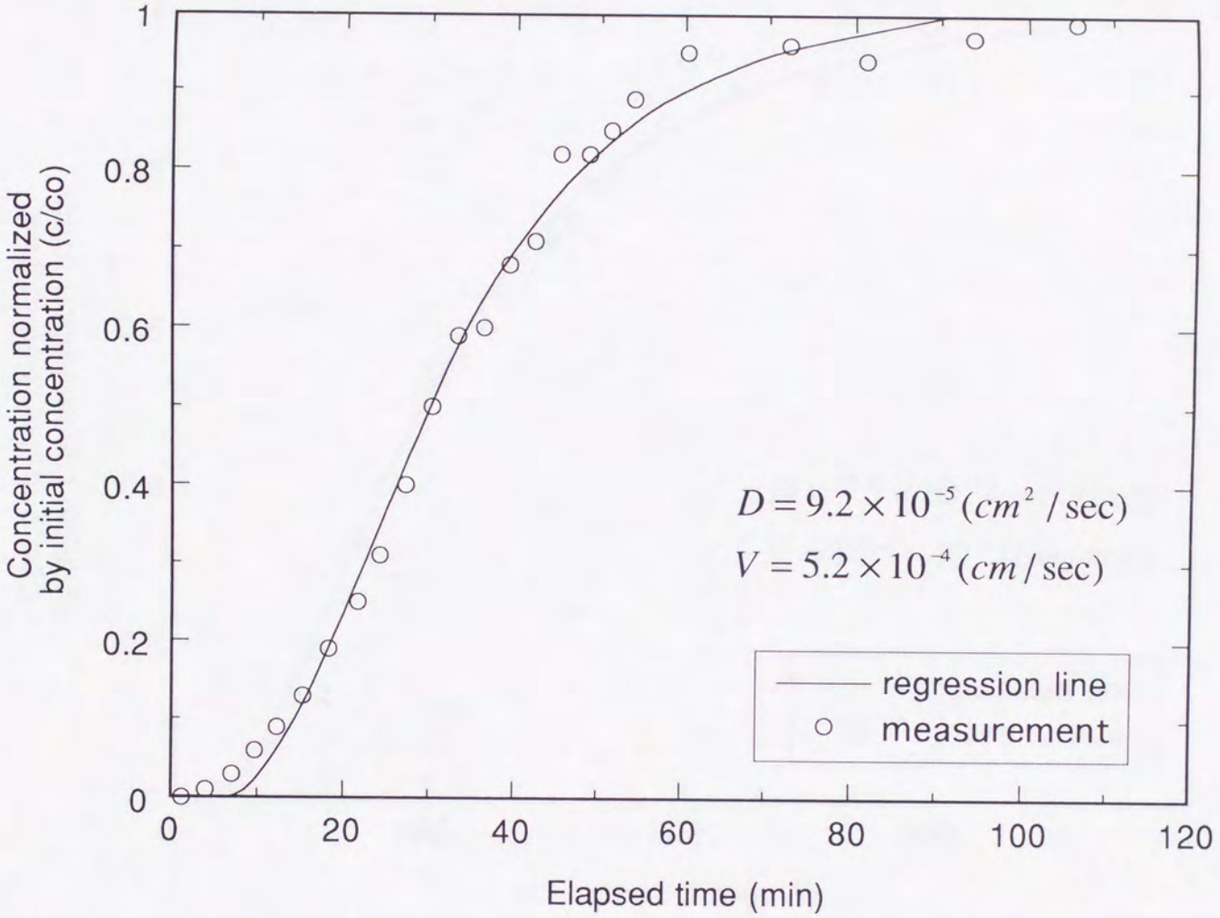


Figure 4.2 Breakthrough curve in Toki laboratory tracer tests (T1-1)

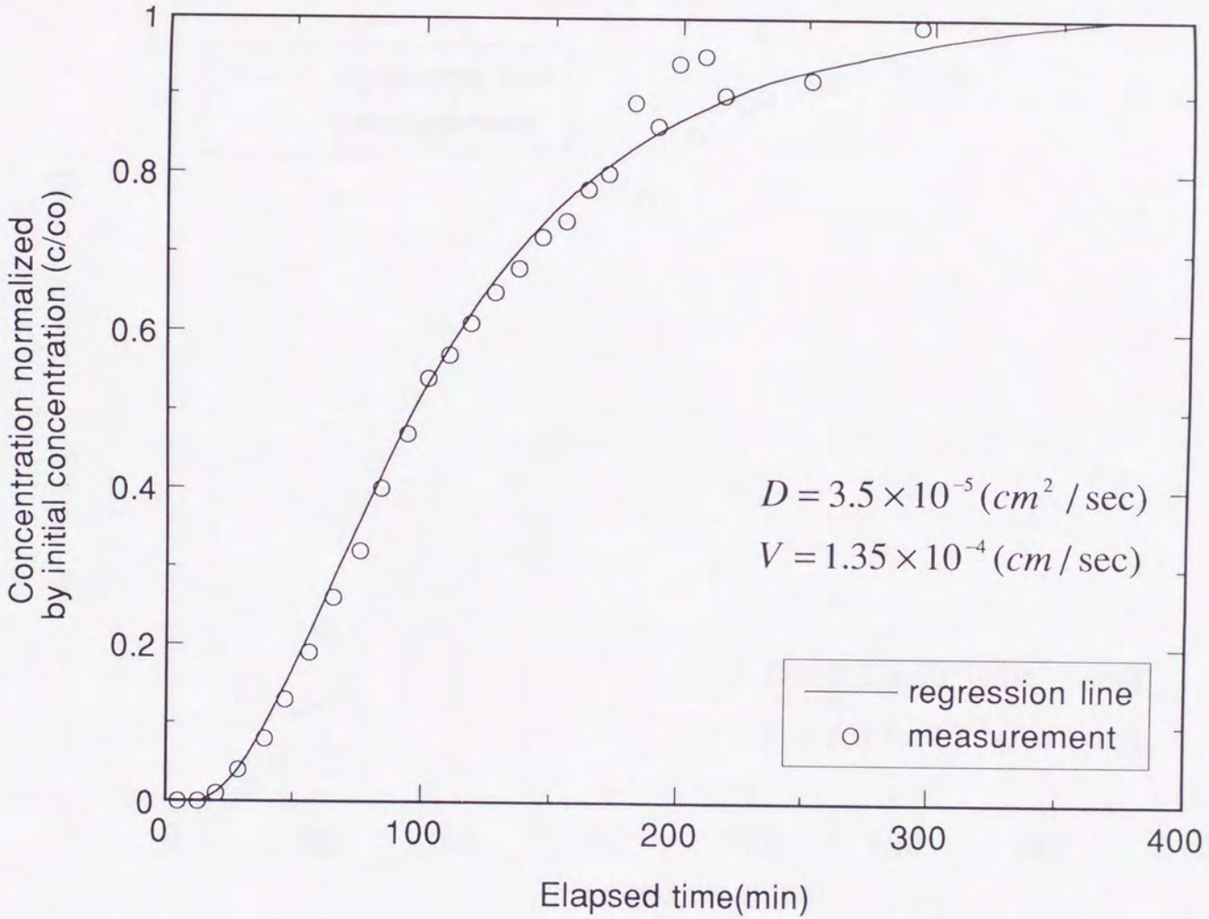


Figure 4.3 Breakthrough curve in Toki laboratory tracer tests (T1-1)

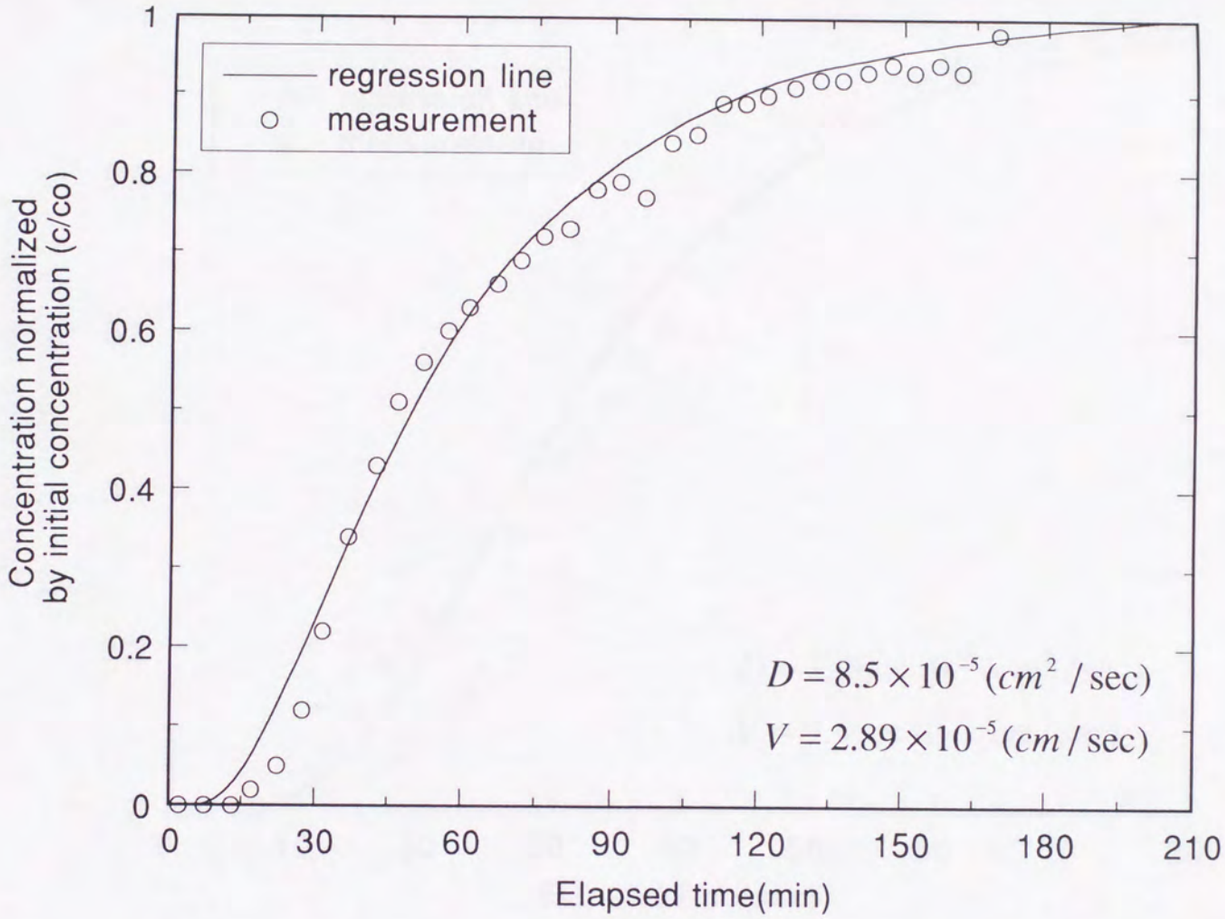


Figure 4.4 Breakthrough curve in Toki laboratory tracer tests (T1-1)

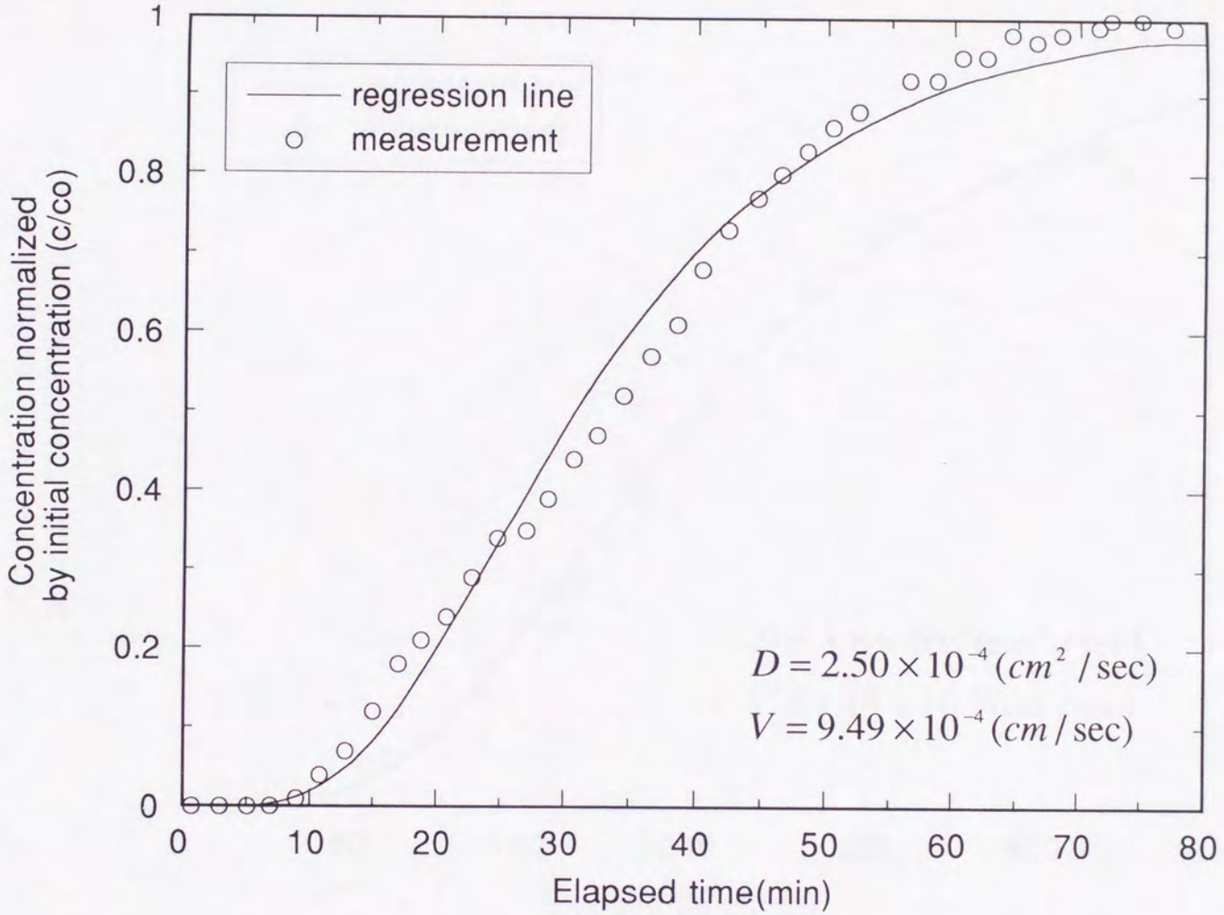


Figure 4.5 Breakthrough curve in Toki laboratory tracer tests (T1-2)

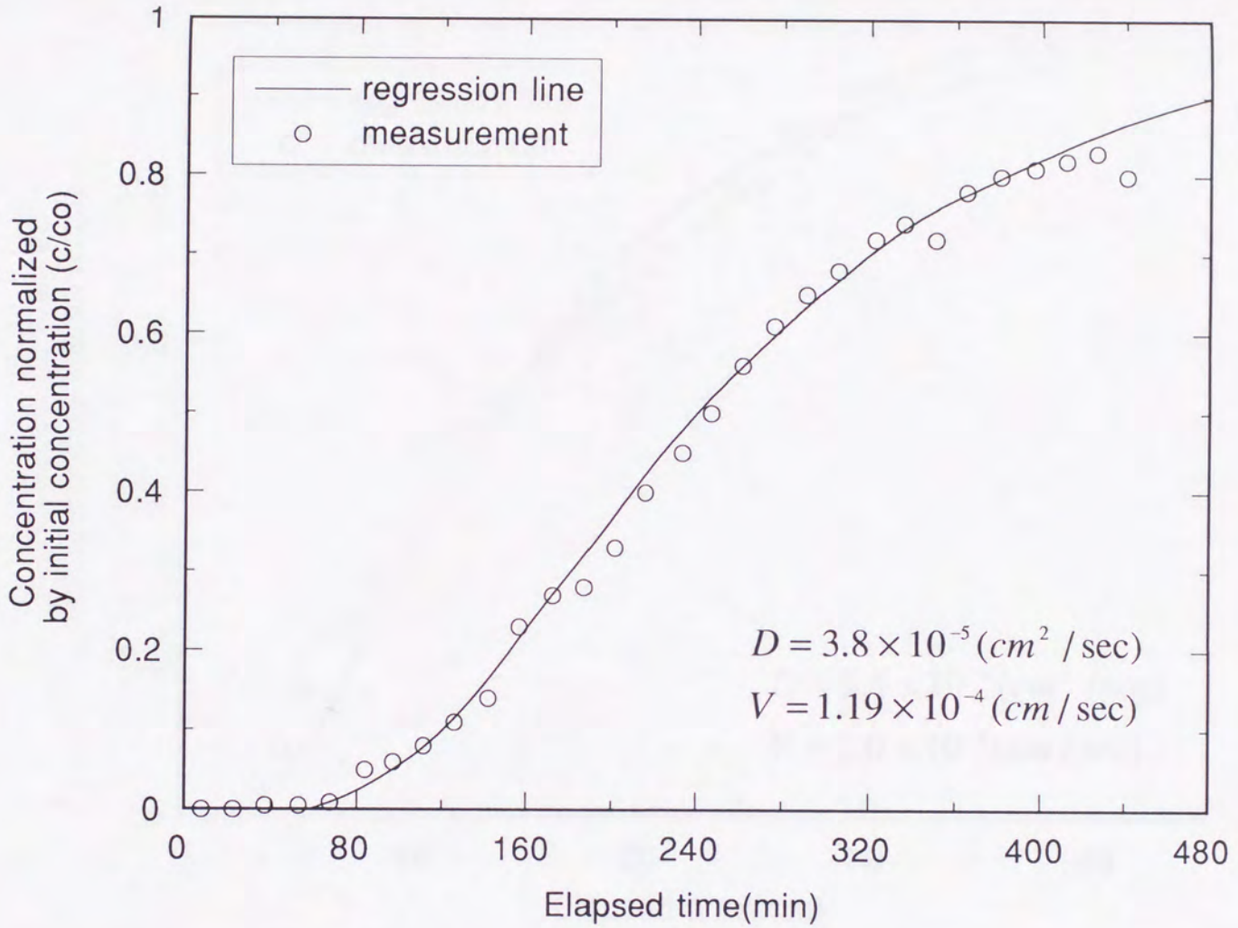


Figure 4.6 Breakthrough curve in Toki laboratory tracer tests (T1-2)

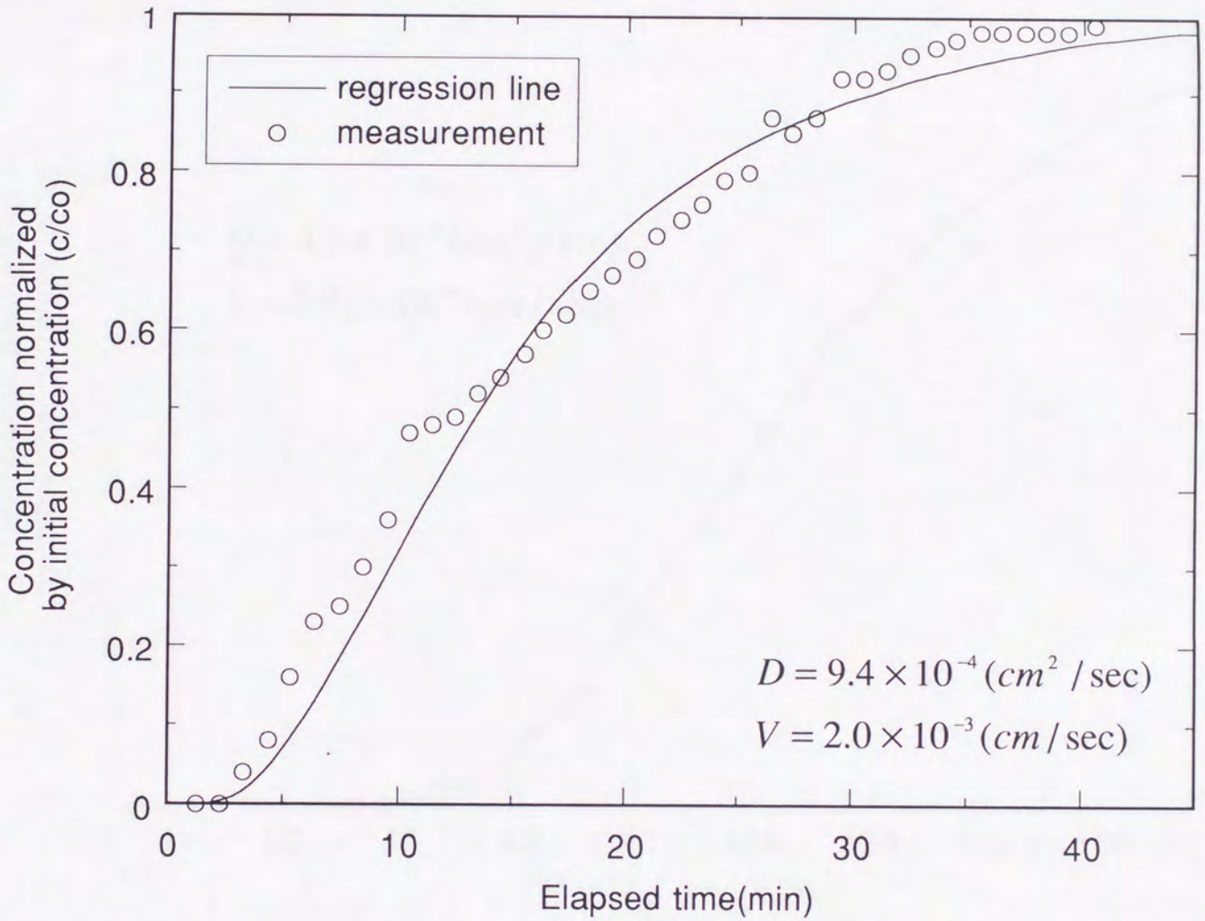


Figure 4.7 Breakthrough curve in Toki laboratory tracer tests (T1-2)

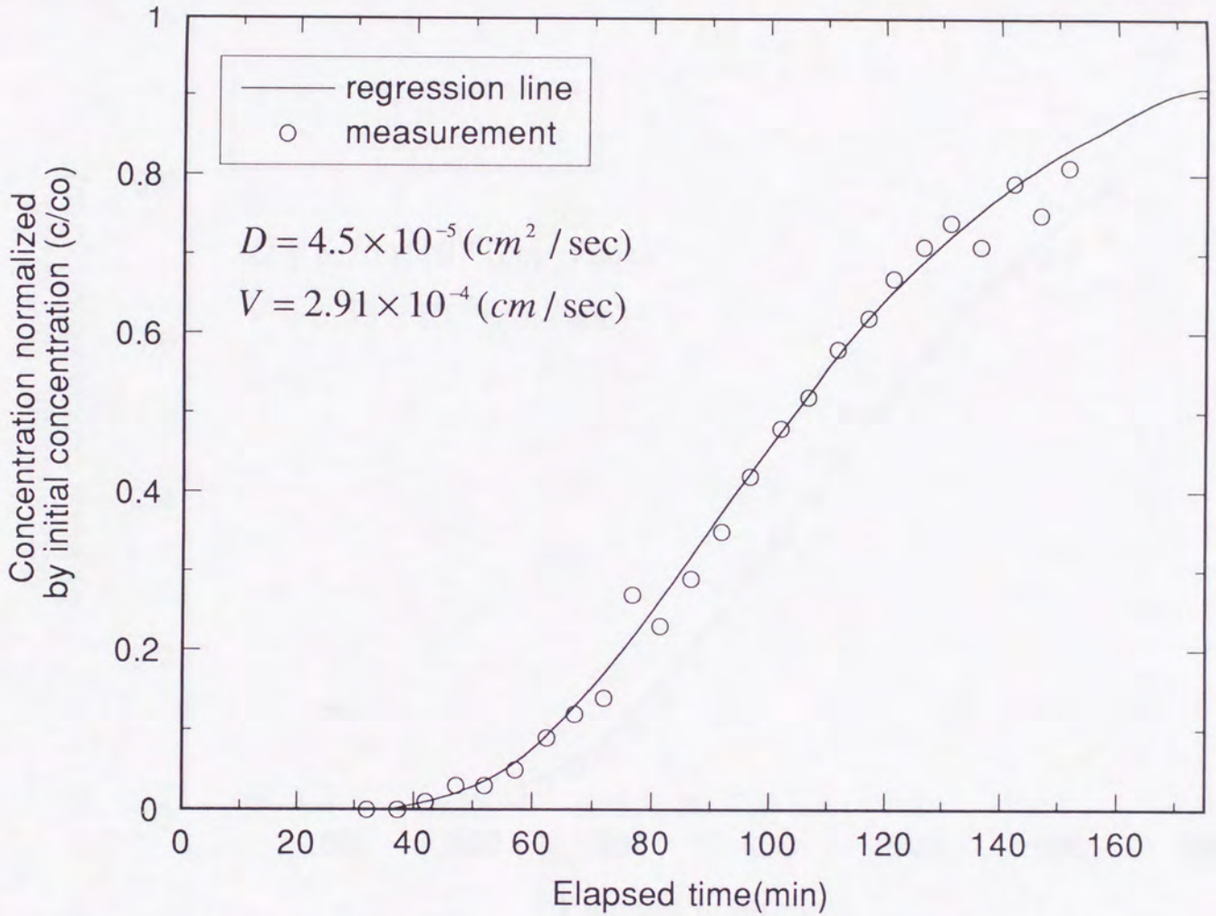


Figure 4.8 Breakthrough curve in Toki laboratory tracer tests (T2-1)

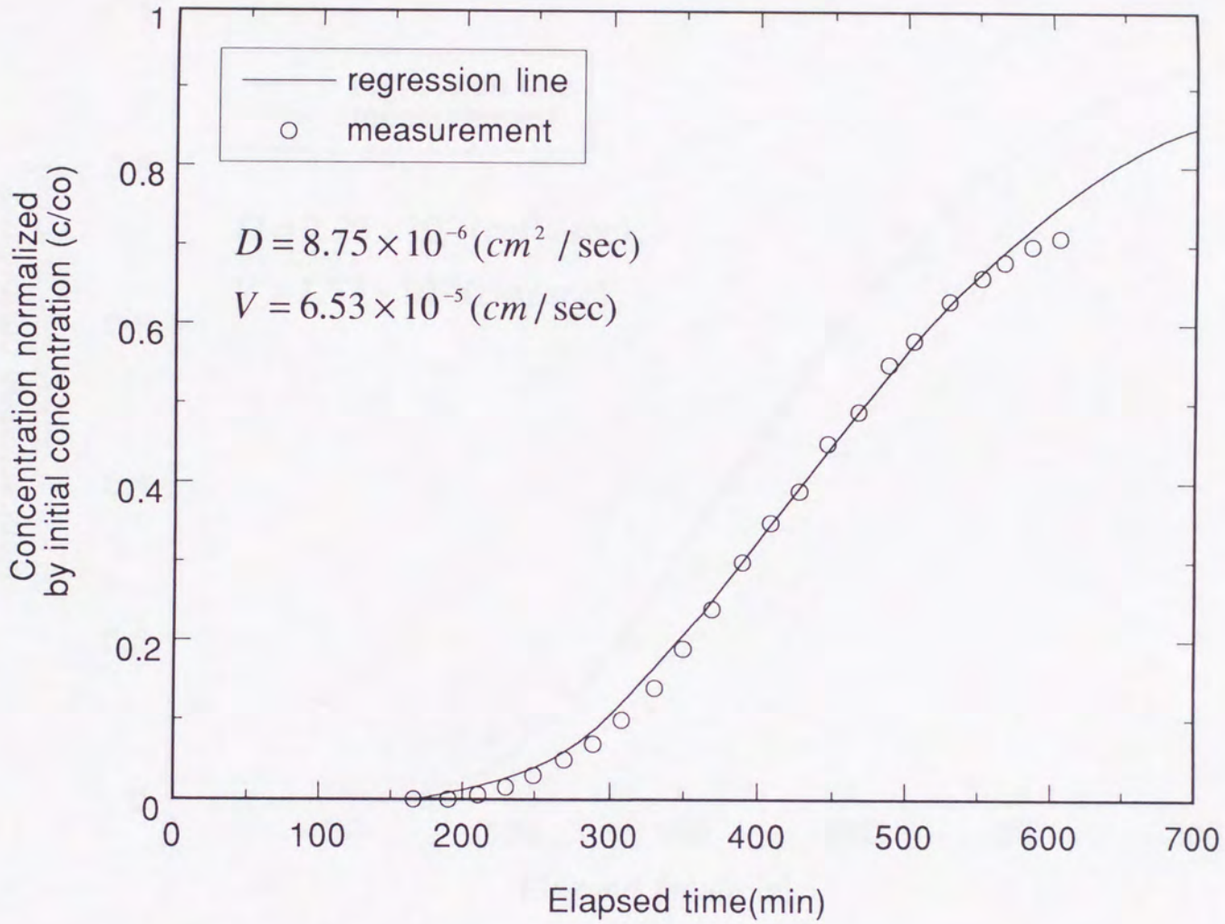


Figure 4.9 Breakthrough curve in Toki laboratory tracer tests (T2-1)

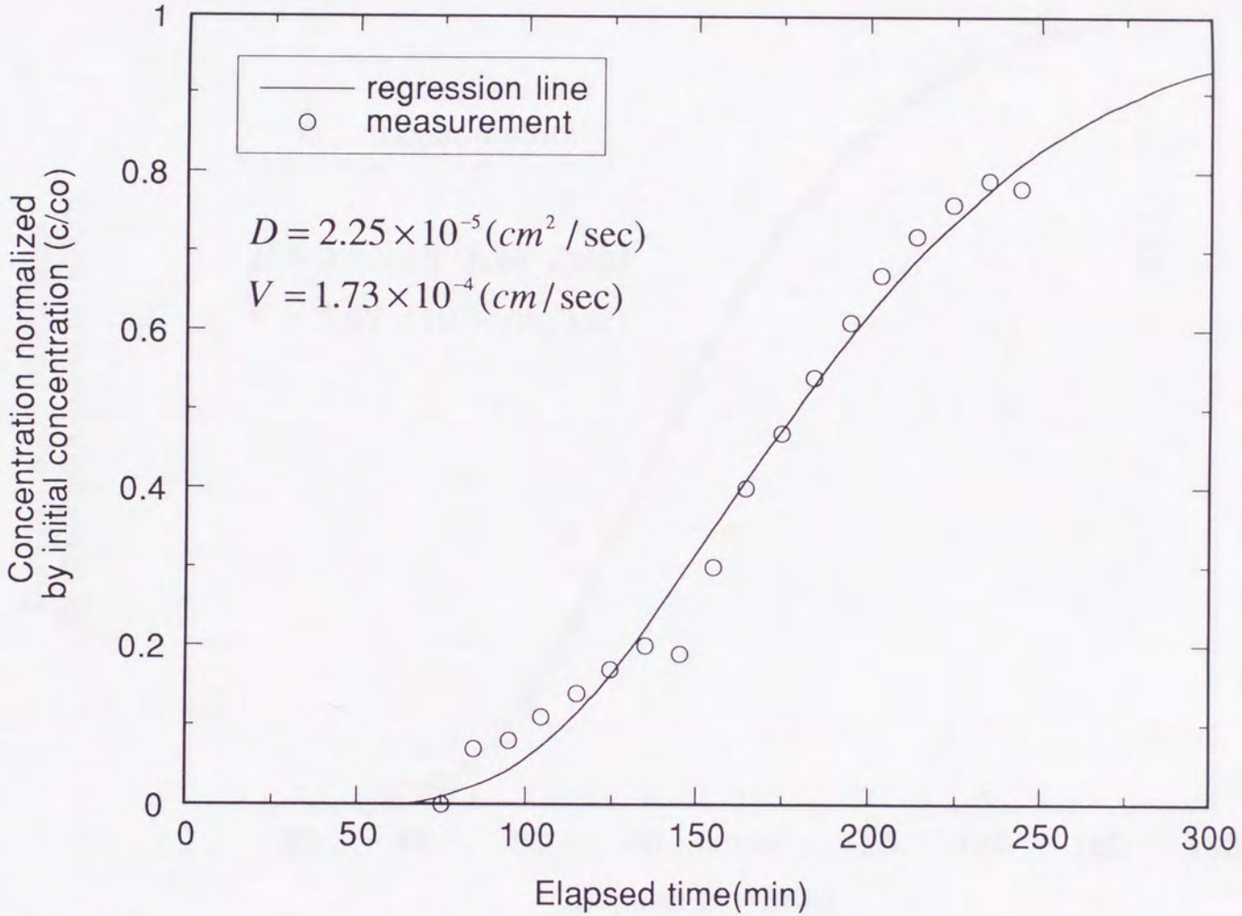


Figure 4.10 Breakthrough curve in Toki laboratory tracer tests (T2-1)

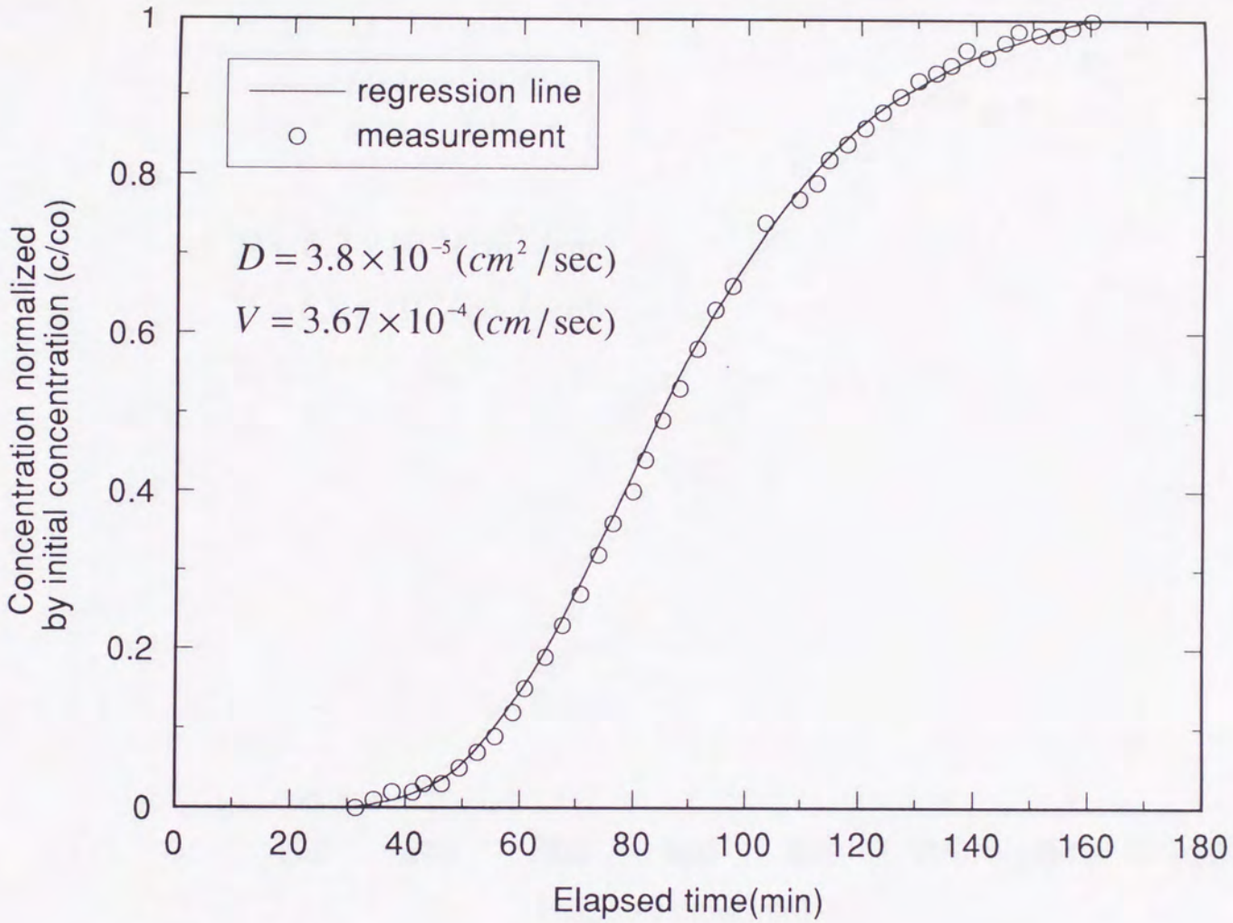


Figure 4.11 Breakthrough curve in Toki laboratory tracer tests (T2-1)

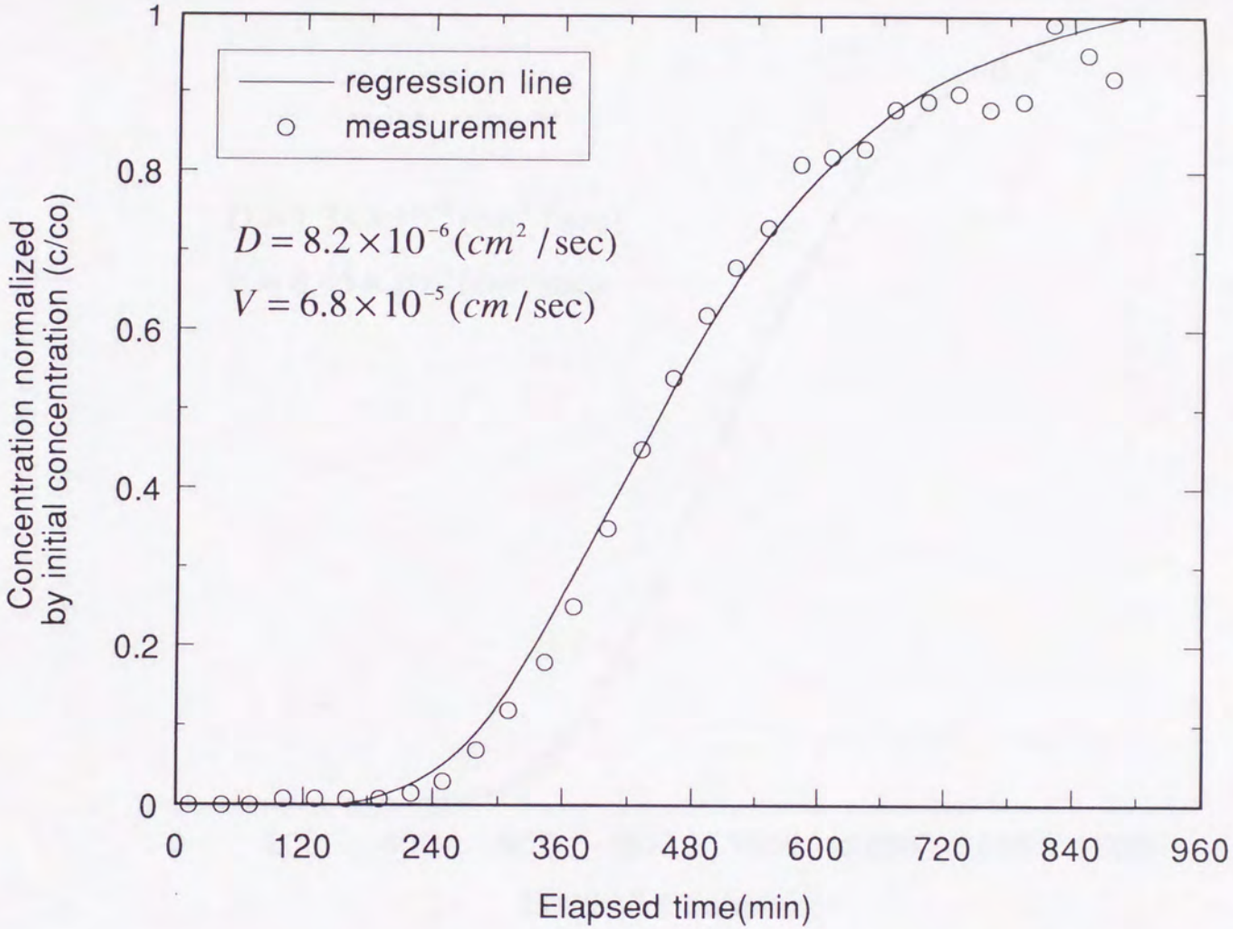


Figure 4.12 Breakthrough curve in Toki laboratory tracer tests (T2-1)

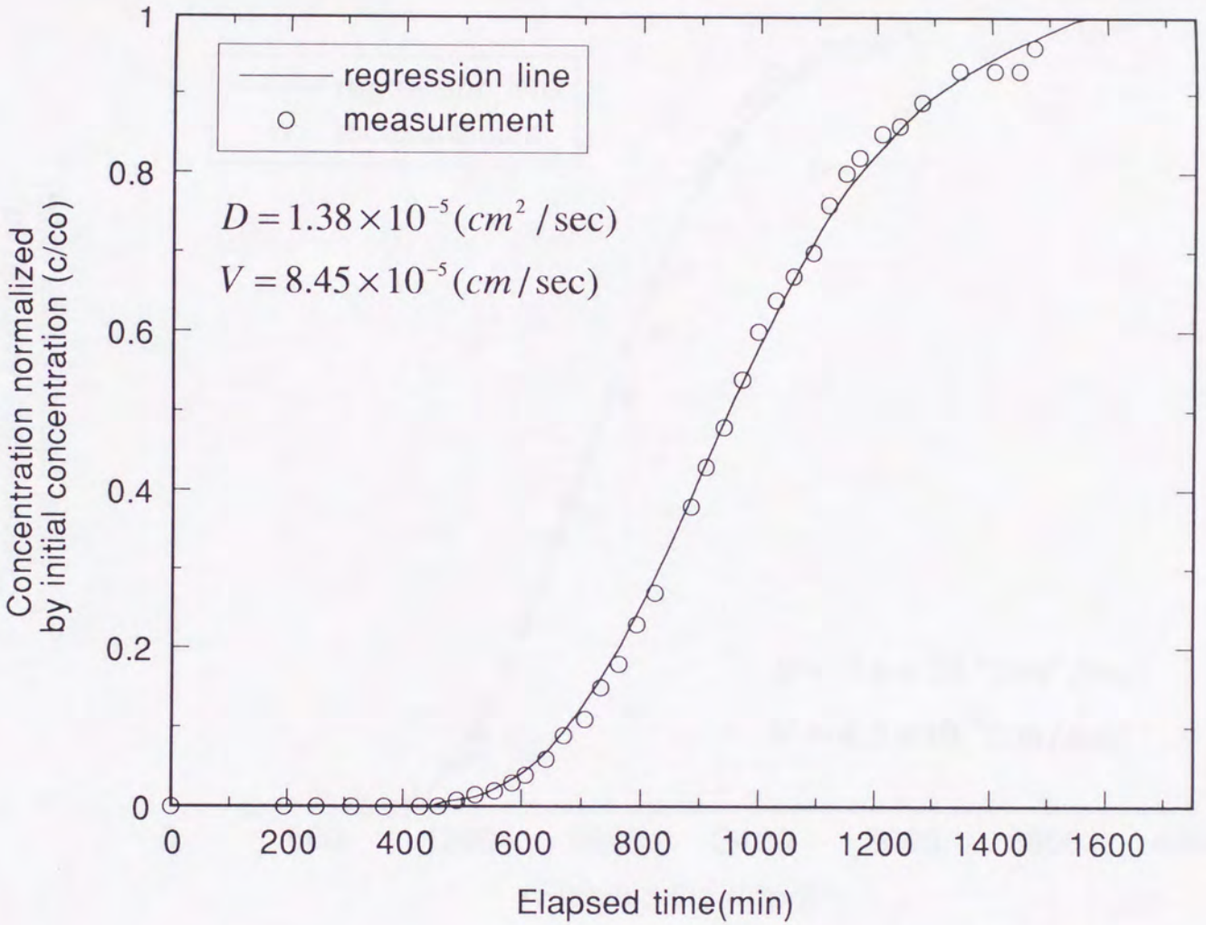


Figure 4.13 Breakthrough curve in Toki laboratory tracer tests (T2-2)

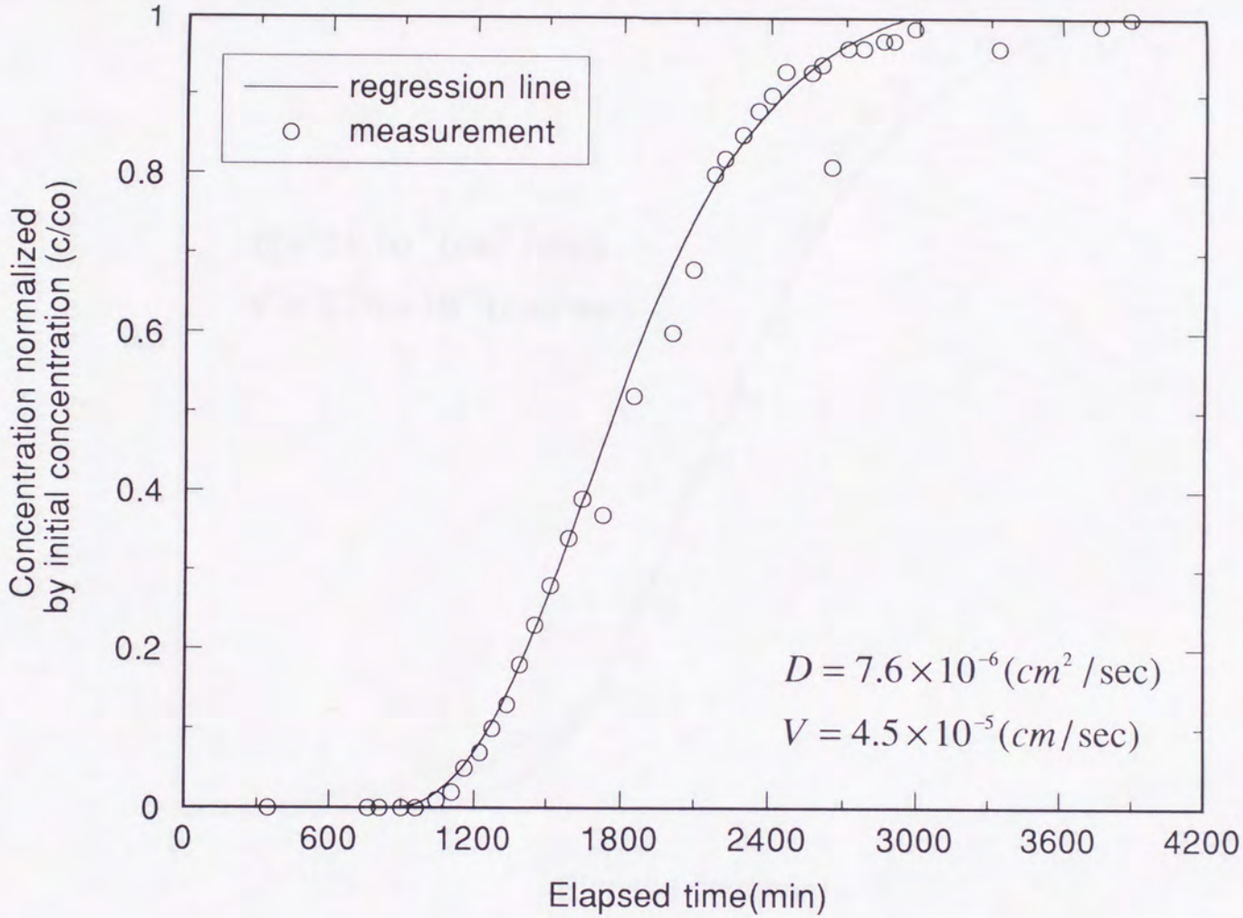


Figure 4.14 Breakthrough curve in Toki laboratory tracer tests (T2-2)

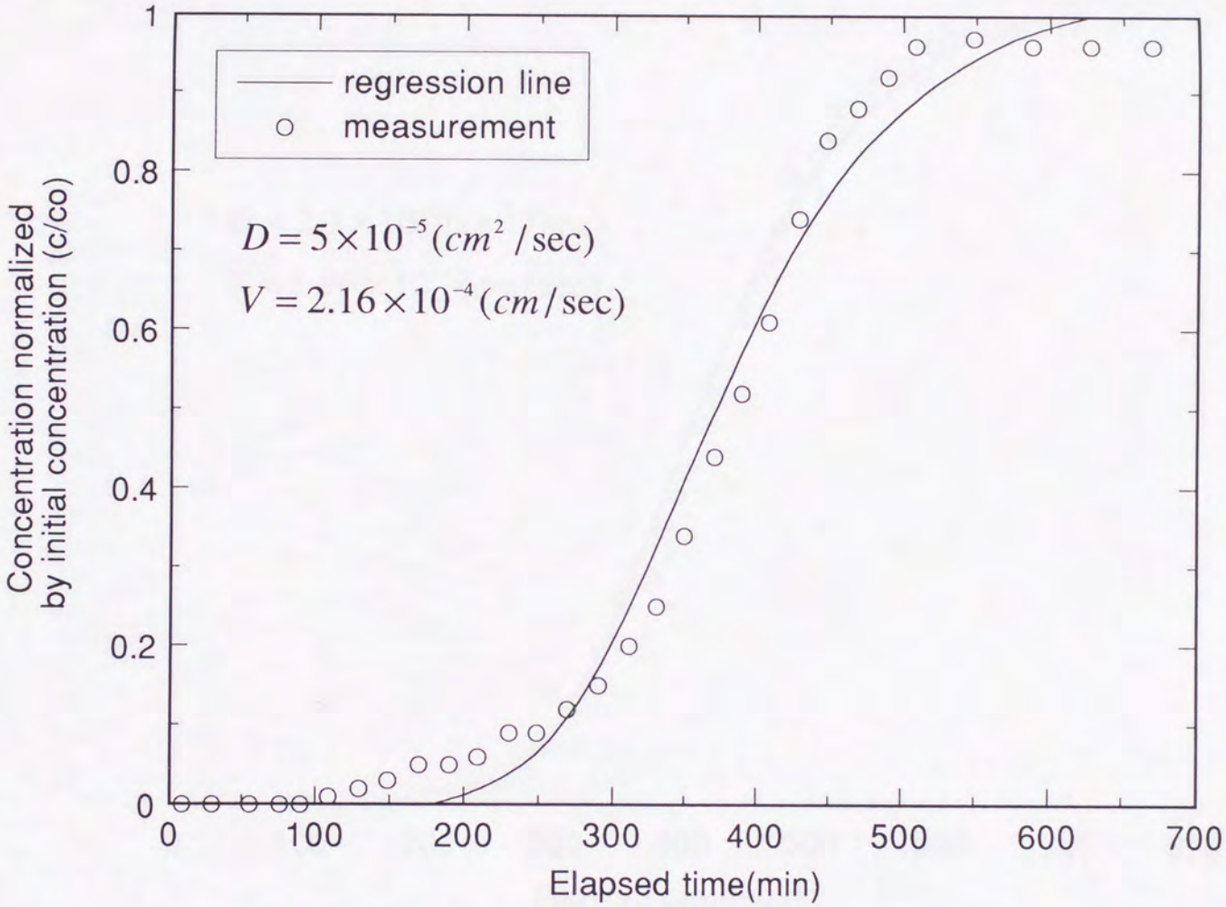


Figure 4.15 Breakthrough curve in Toki laboratory tracer tests (T2-2)

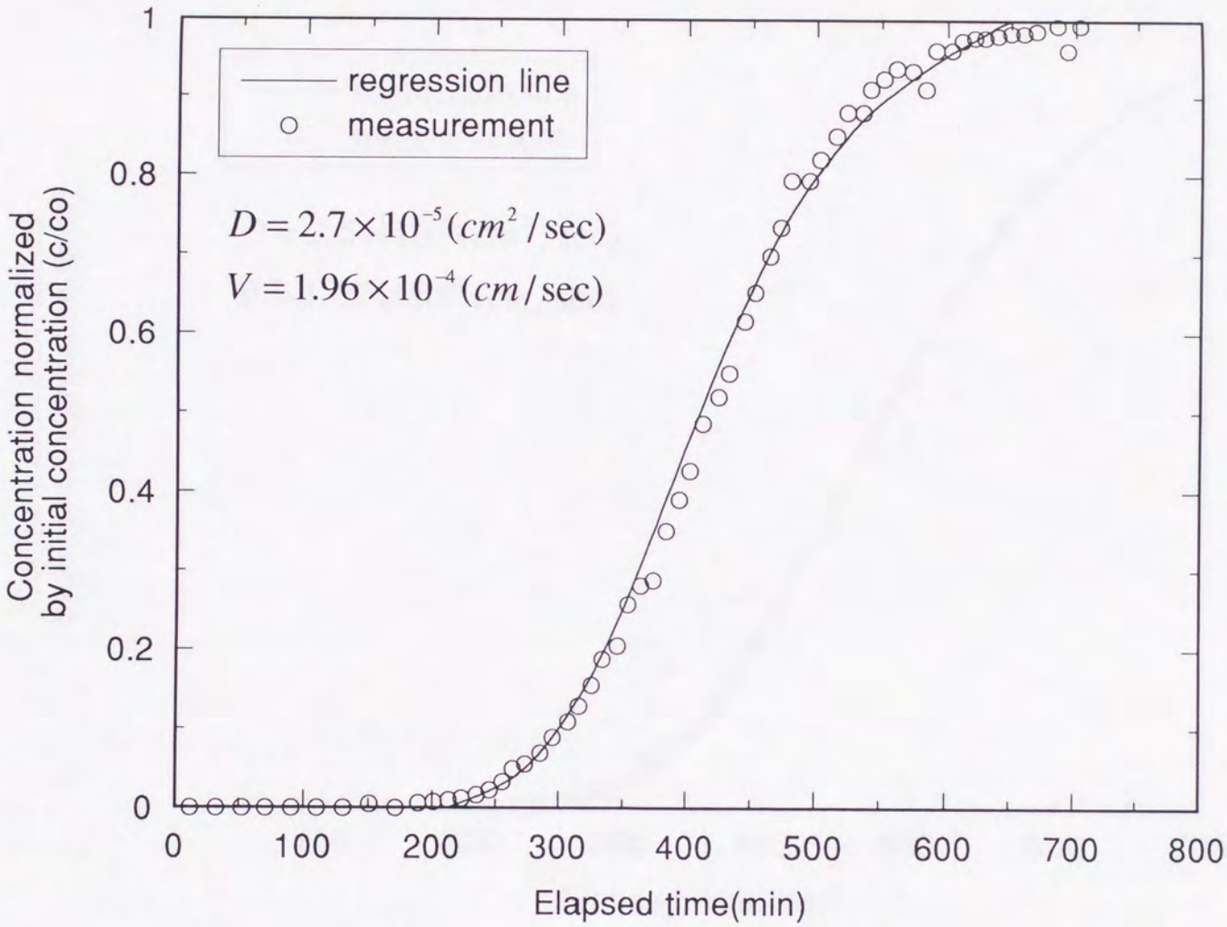


Figure 4.16 Breakthrough curve in Toki laboratory tracer tests (T2-2)

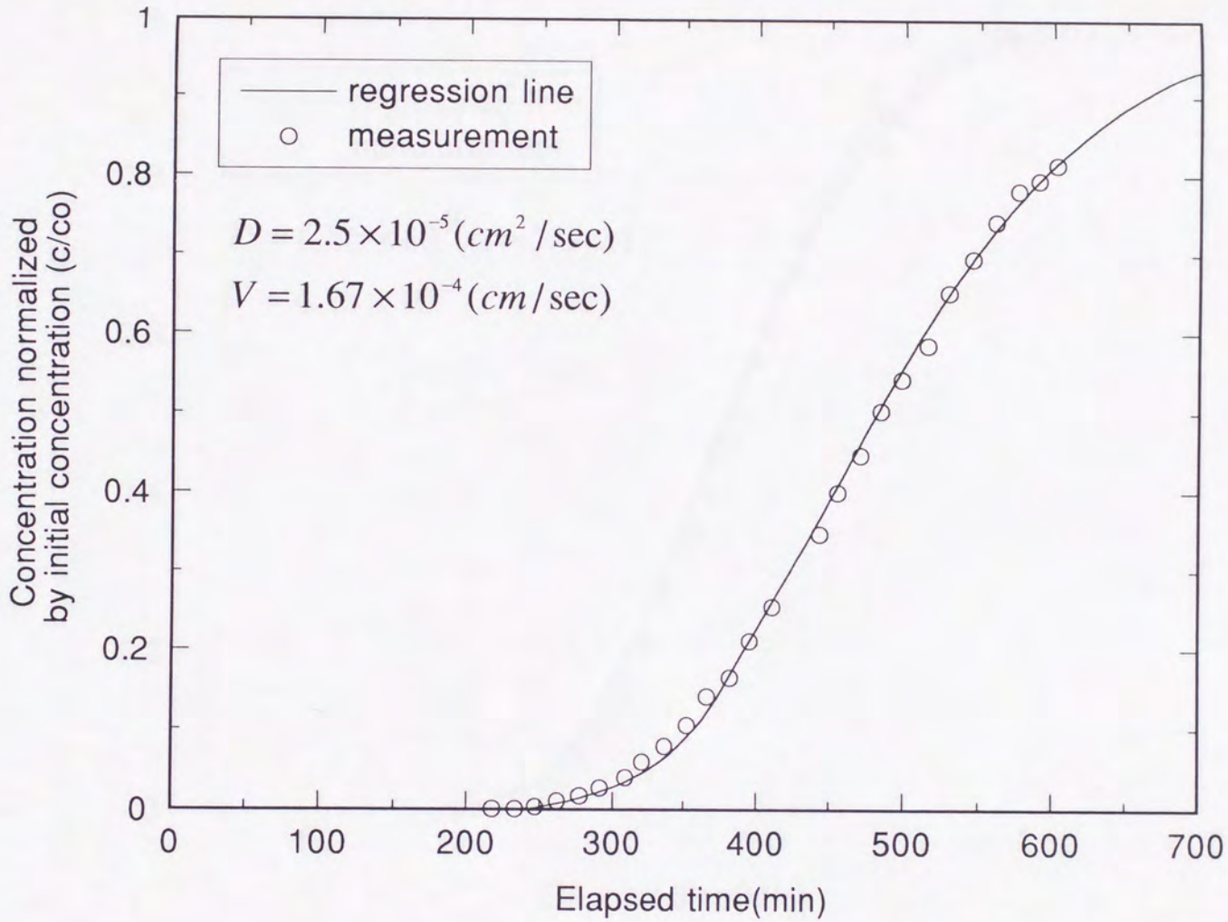


Figure 4.17 Breakthrough curve in Toki laboratory tracer tests (T2-2)

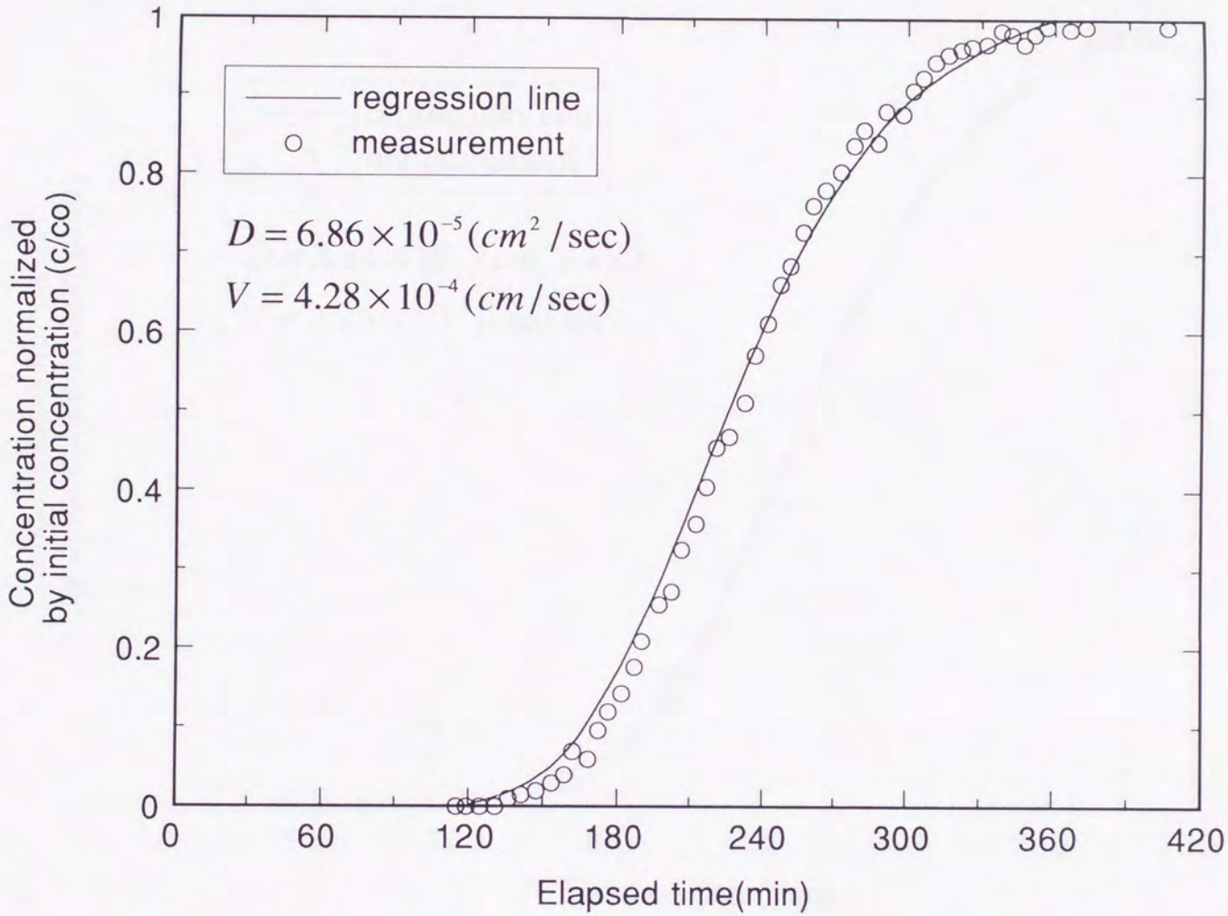


Figure 4.18 Breakthrough curve in Toki laboratory tracer tests (T2-3)

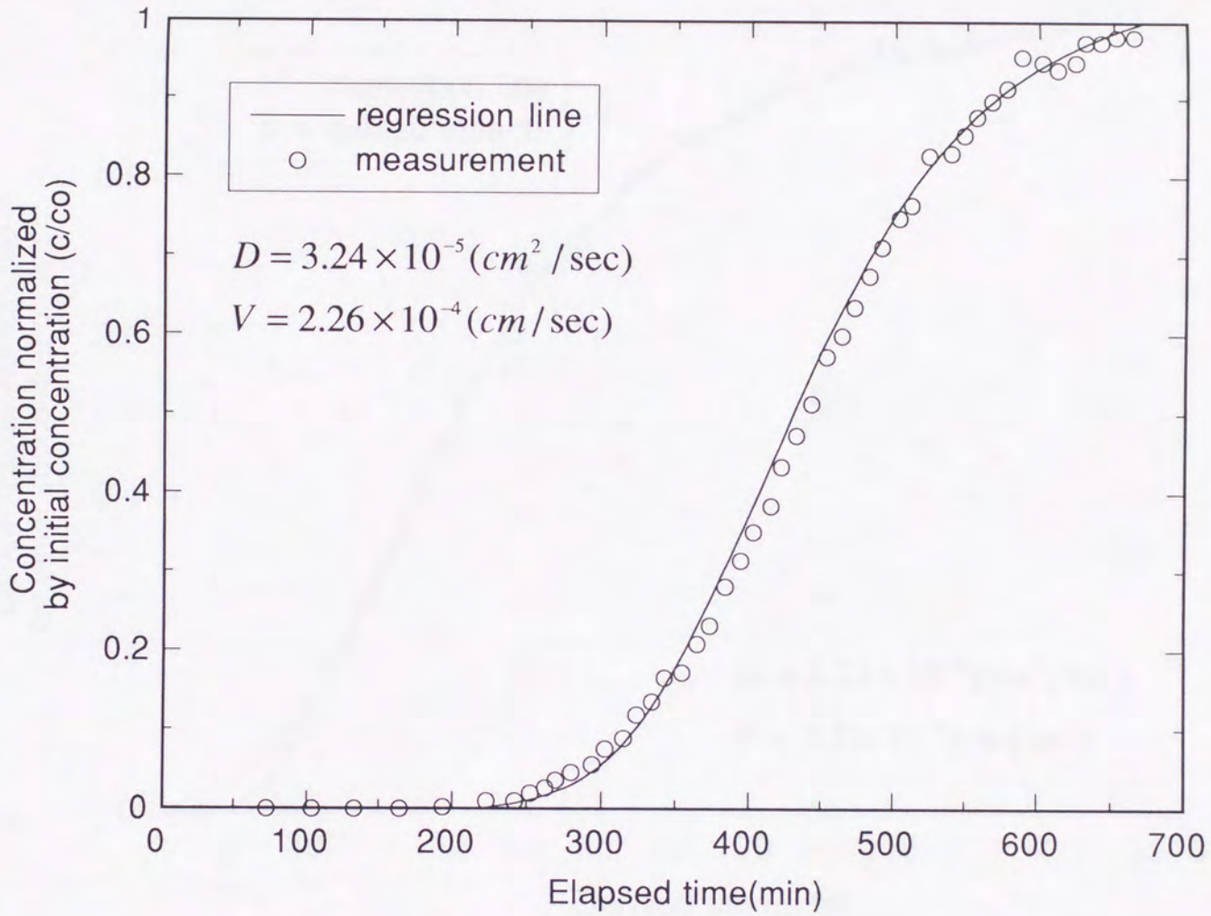


Figure 4.19 Breakthrough curve in Toki laboratory tracer tests (T2-3)

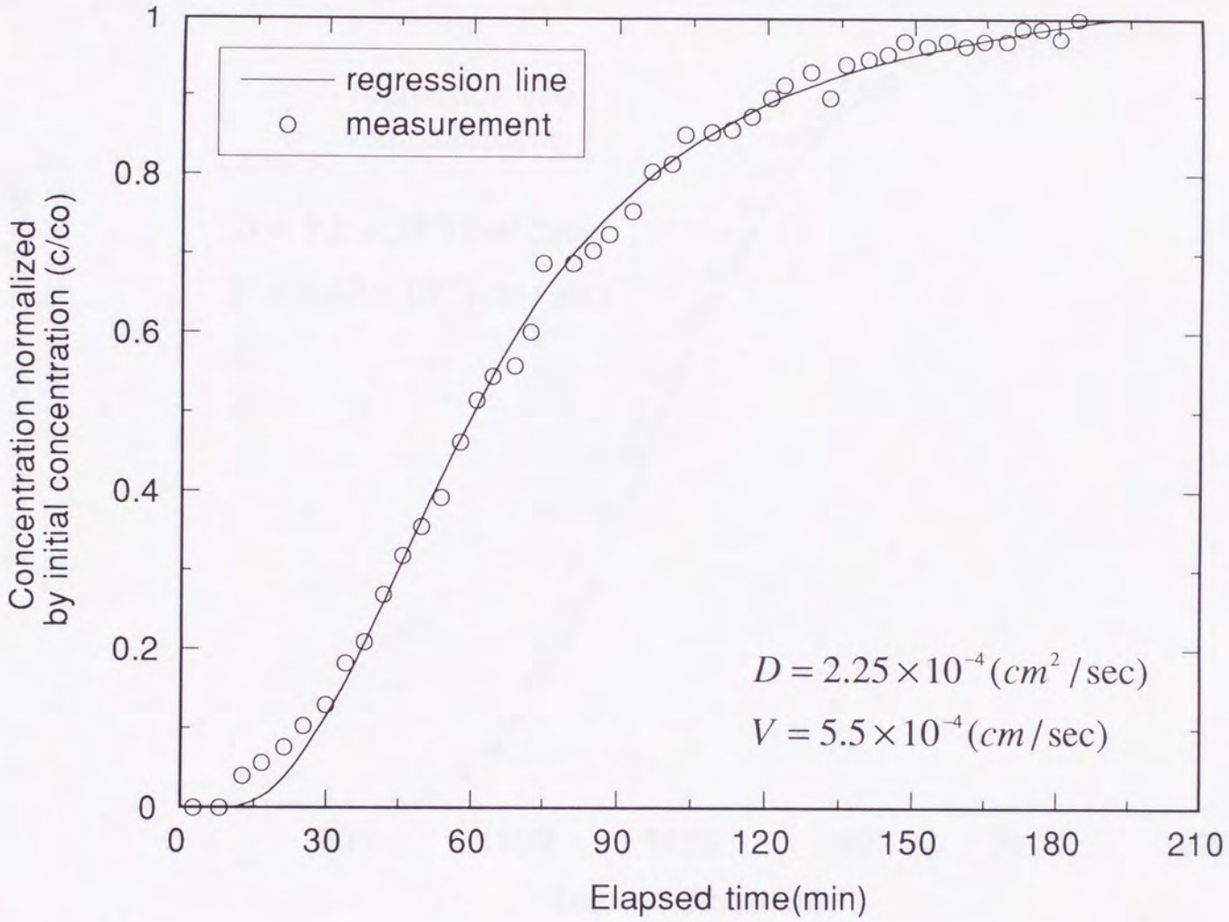


Figure 4.20 Breakthrough curve in Toki laboratory tracer tests (T3-1)

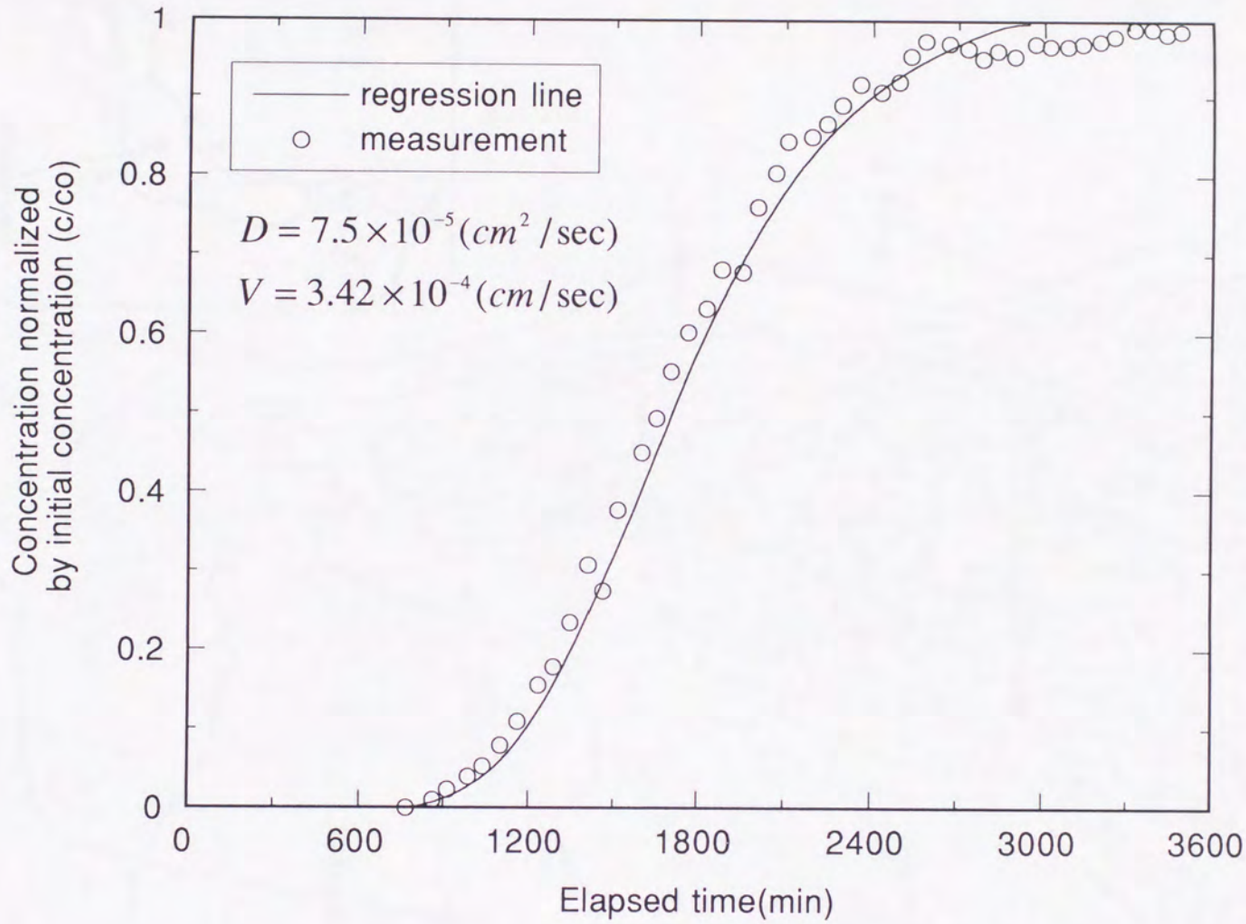


Figure 4.21 Breakthrough curve in Toki laboratory tracer tests (T3-2)

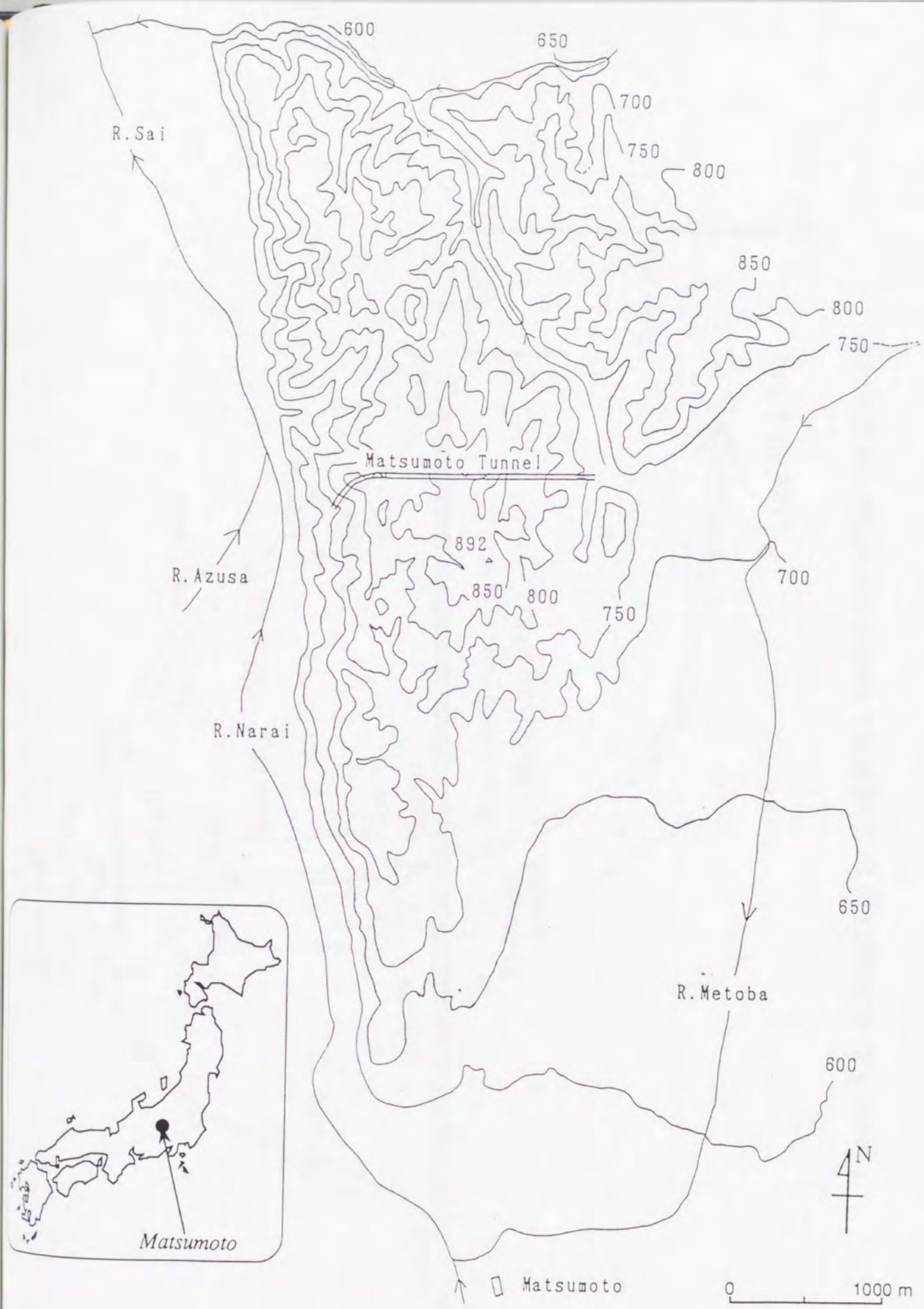


Figure 5.1 Location of study area

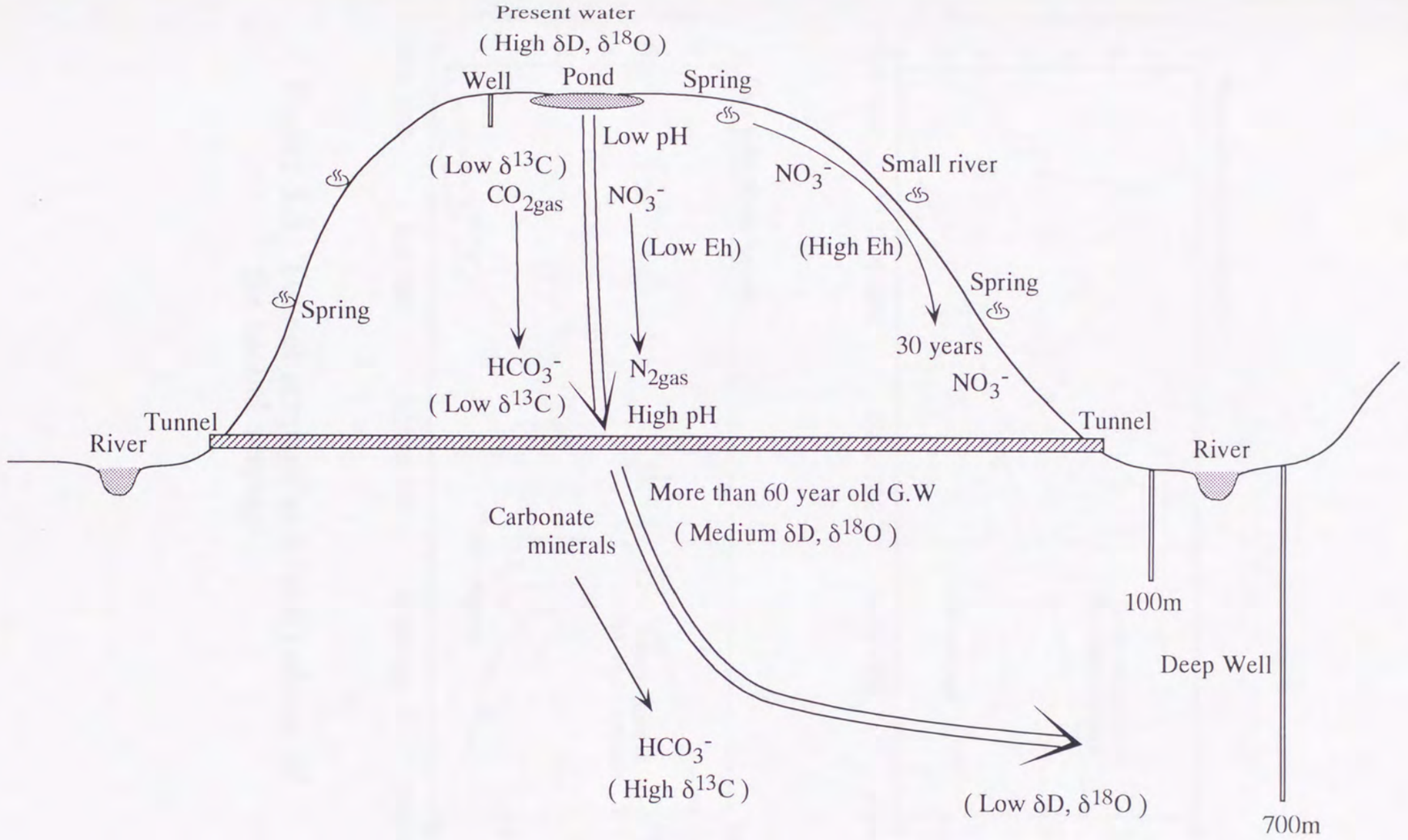


Figure 5.2 Changes in ground water chemistry within the plateau

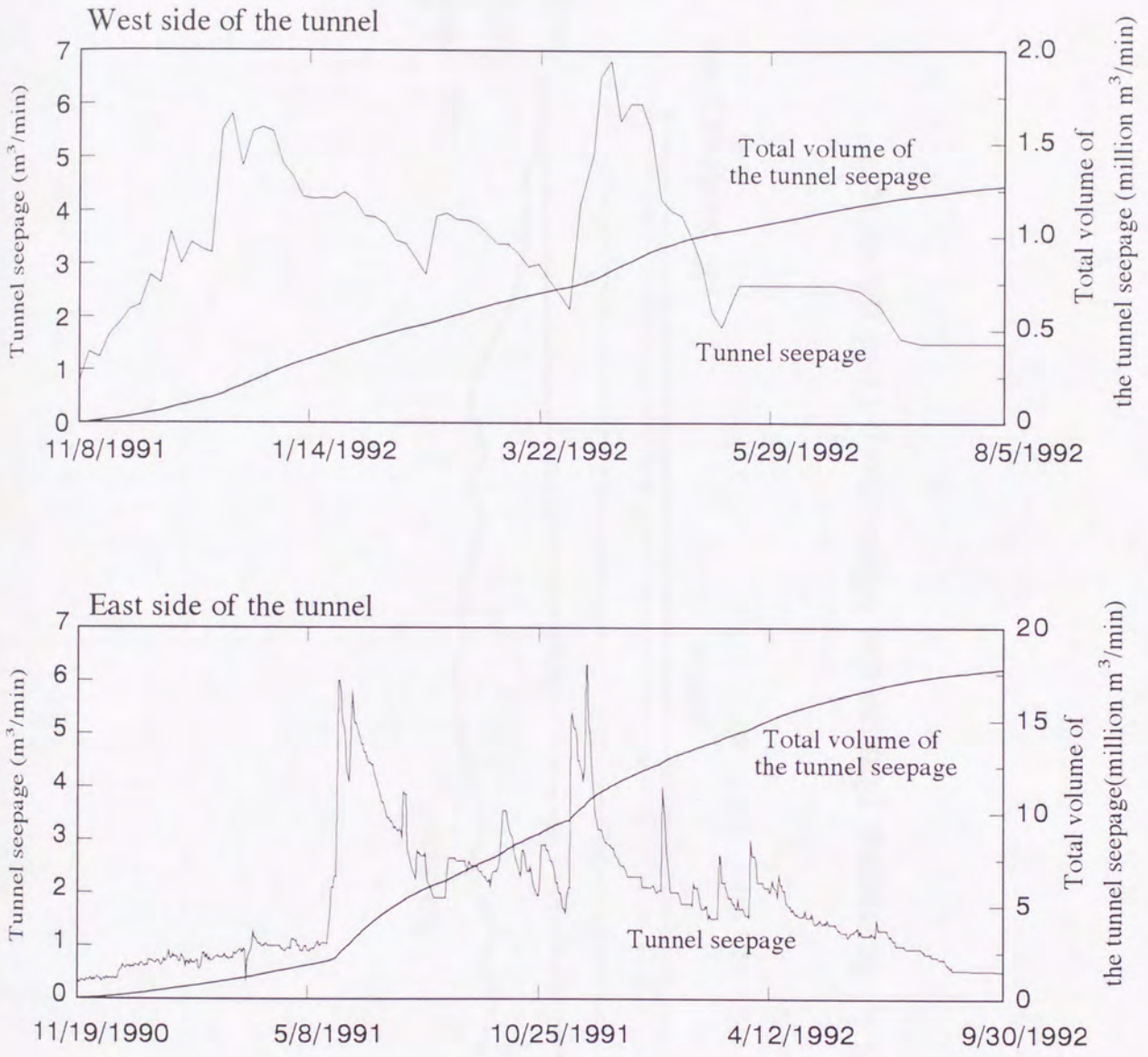


Figure 5.3 Tunnel seepage and total volume of the tunnel seepage

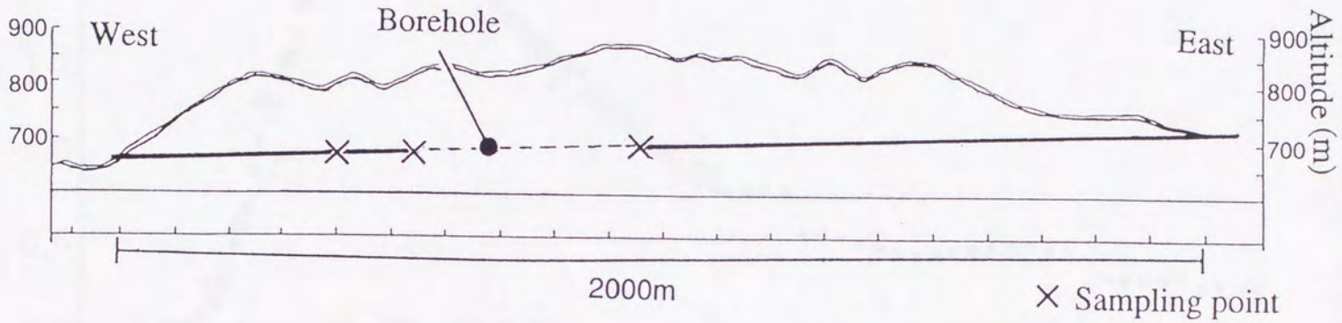


Figure 5.4 Sectional plan at the Matsumoto field tracer test

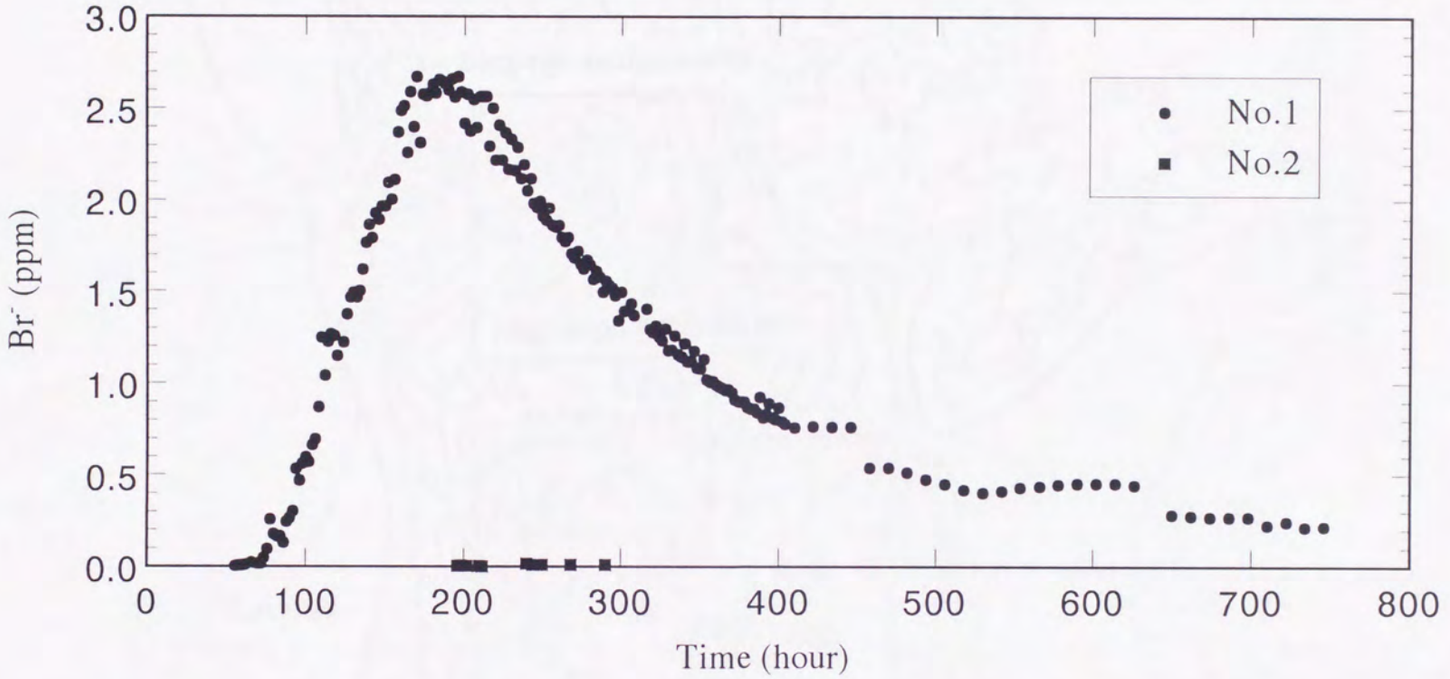


Figure 5.5 Relationship between elapsed time after the start of tracer injection and concentration of Br^- in the tunnel seepage

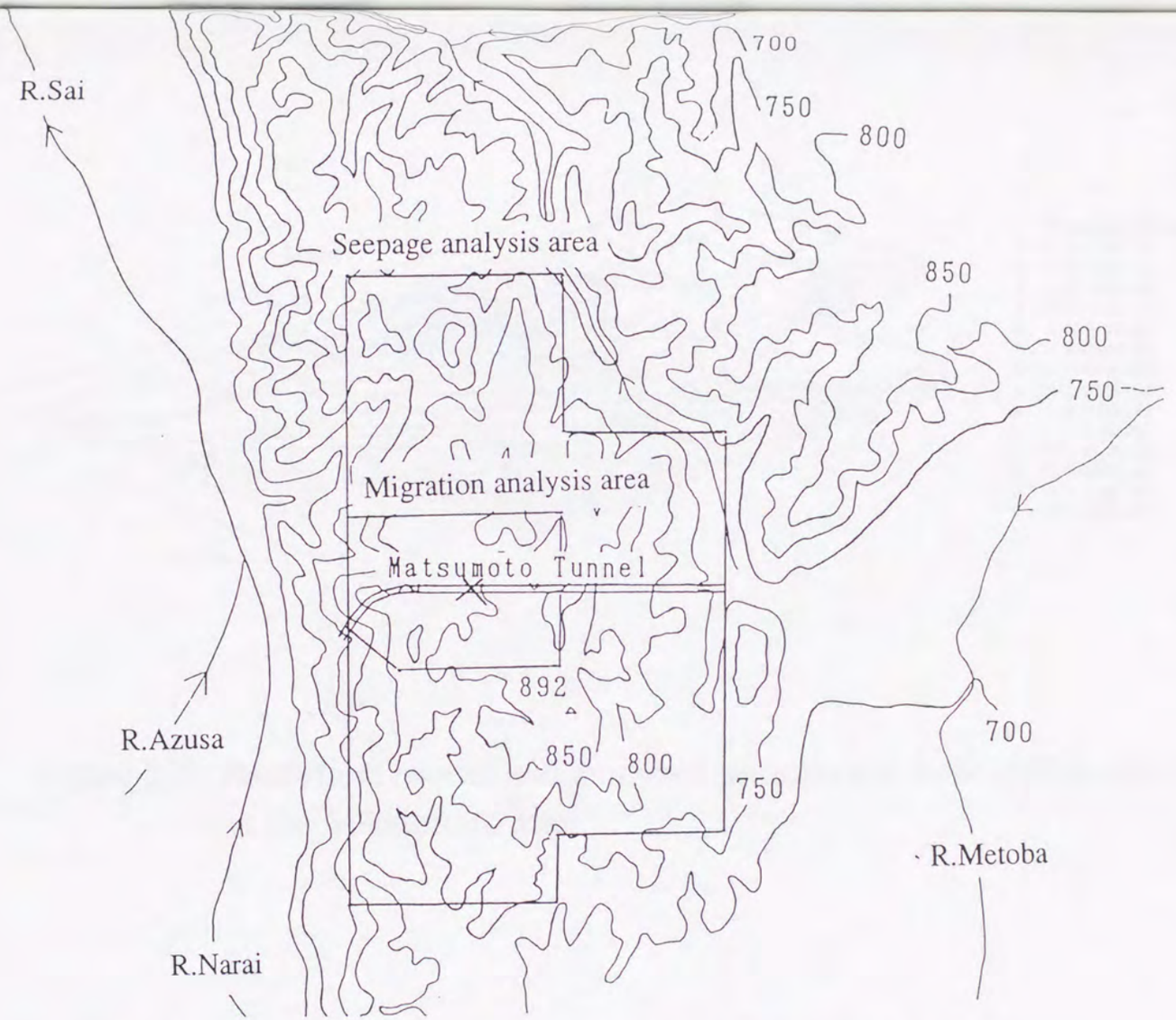


Figure 5.6 Seepage and migration analysis area
(×: Tracer injection borehole)

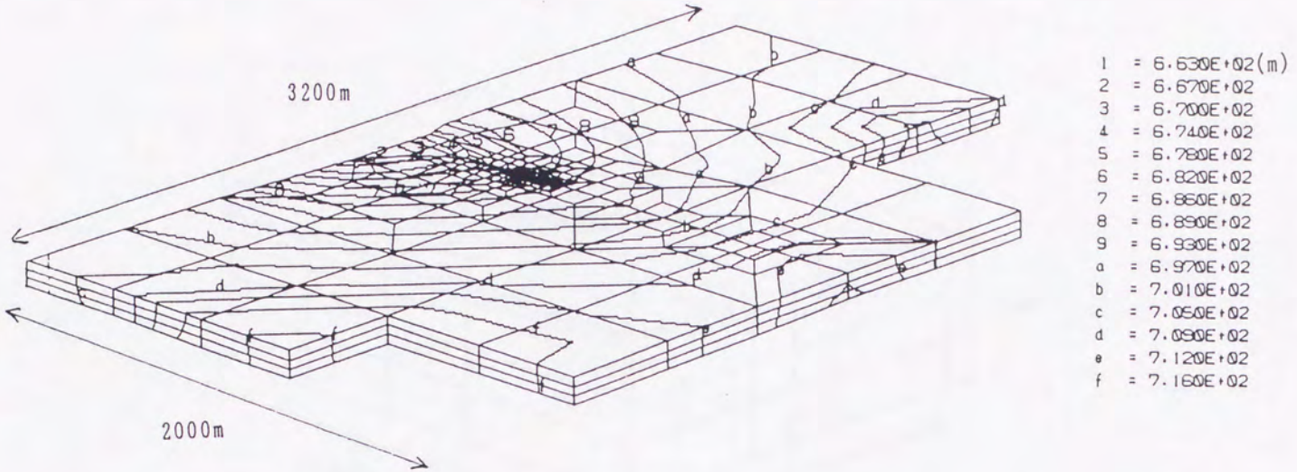


Figure 5.7 Analytical model and analyzed piezometric-head distribution at the Matsumoto site

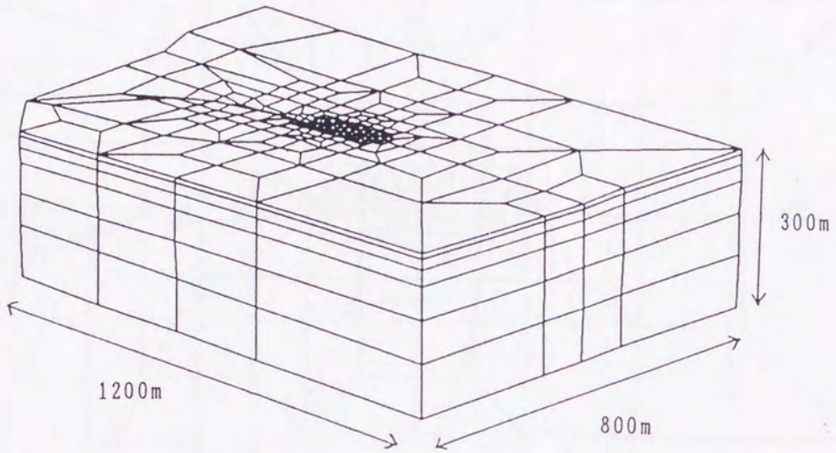
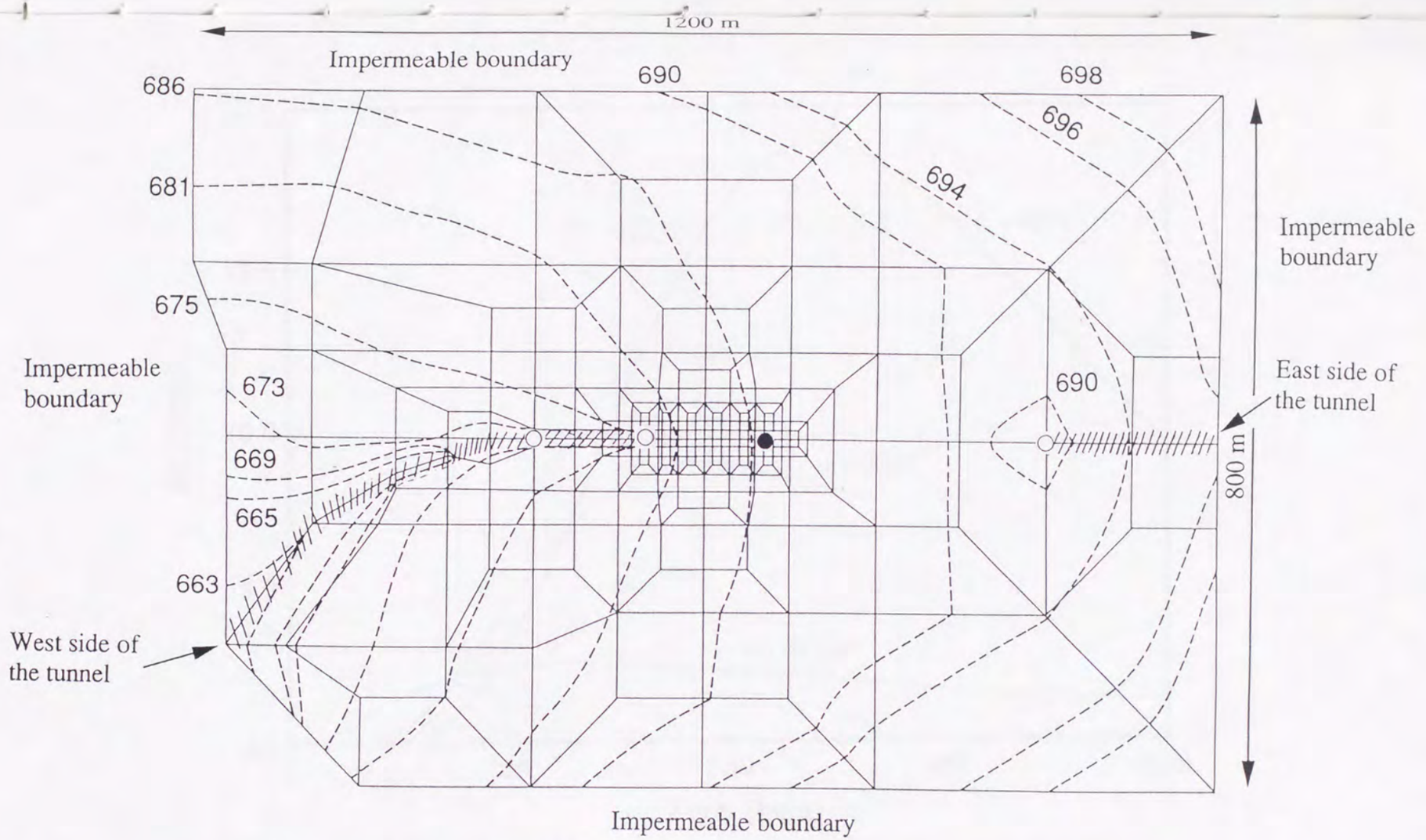


Figure 5.8 Analytical model for the migration analysis at the Matsumoto site



(○: Sampling point, ●:Tracer injection borehole, ////// :Tunnel,)

Figure 5.9 Analytical model for the migration analysis and analyzed piezometric-head distribution at the Matsumoto site (Horizontal section)

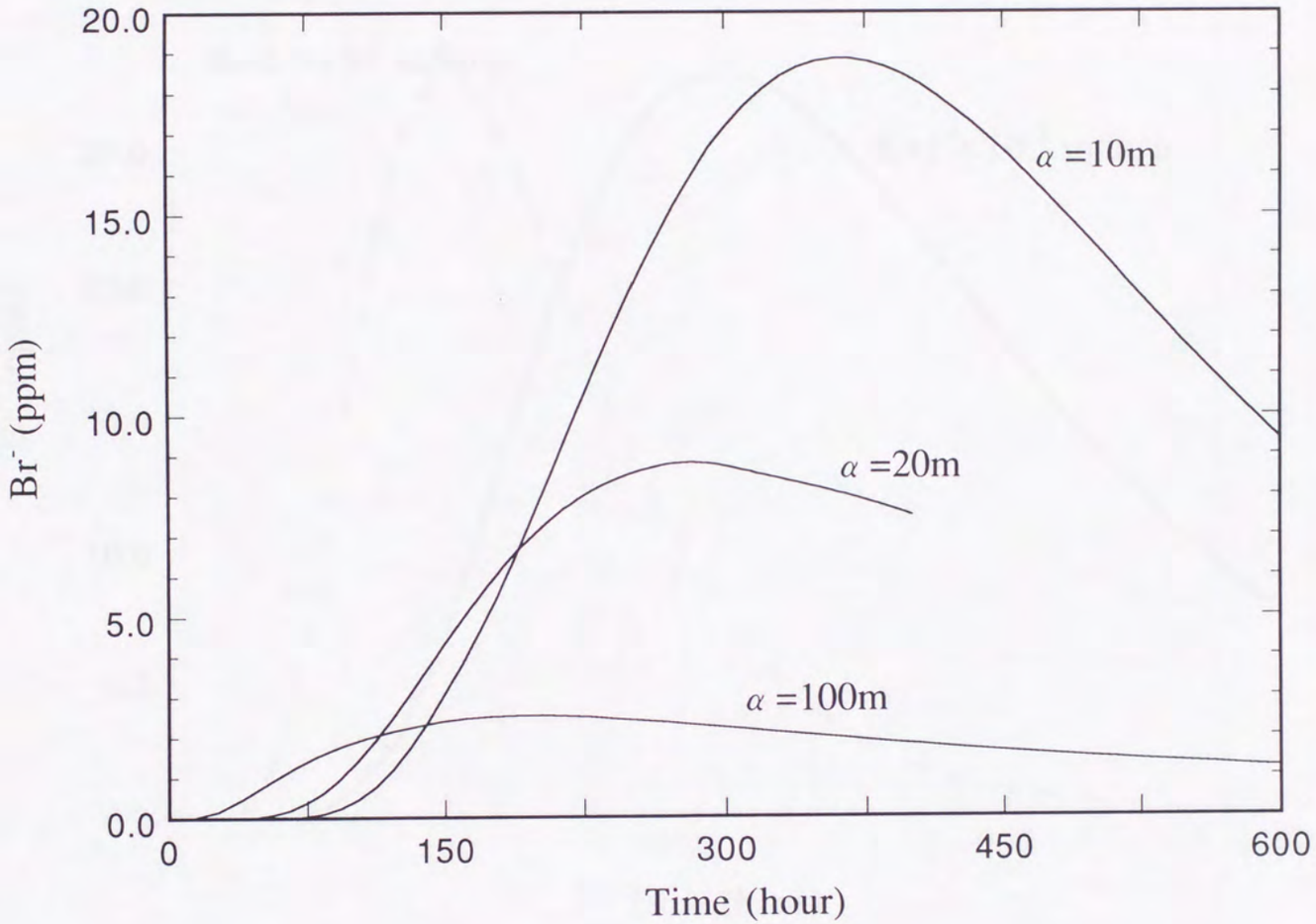


Figure 5.10 Relationship between elapsed time and concentration of Br^-.
Comparing different longitudinal dispersivities (10, 20, 100m) at the constant condition of effective porosity (0.08%) and hydraulic conductivity (8×10^{-3} m/hour).

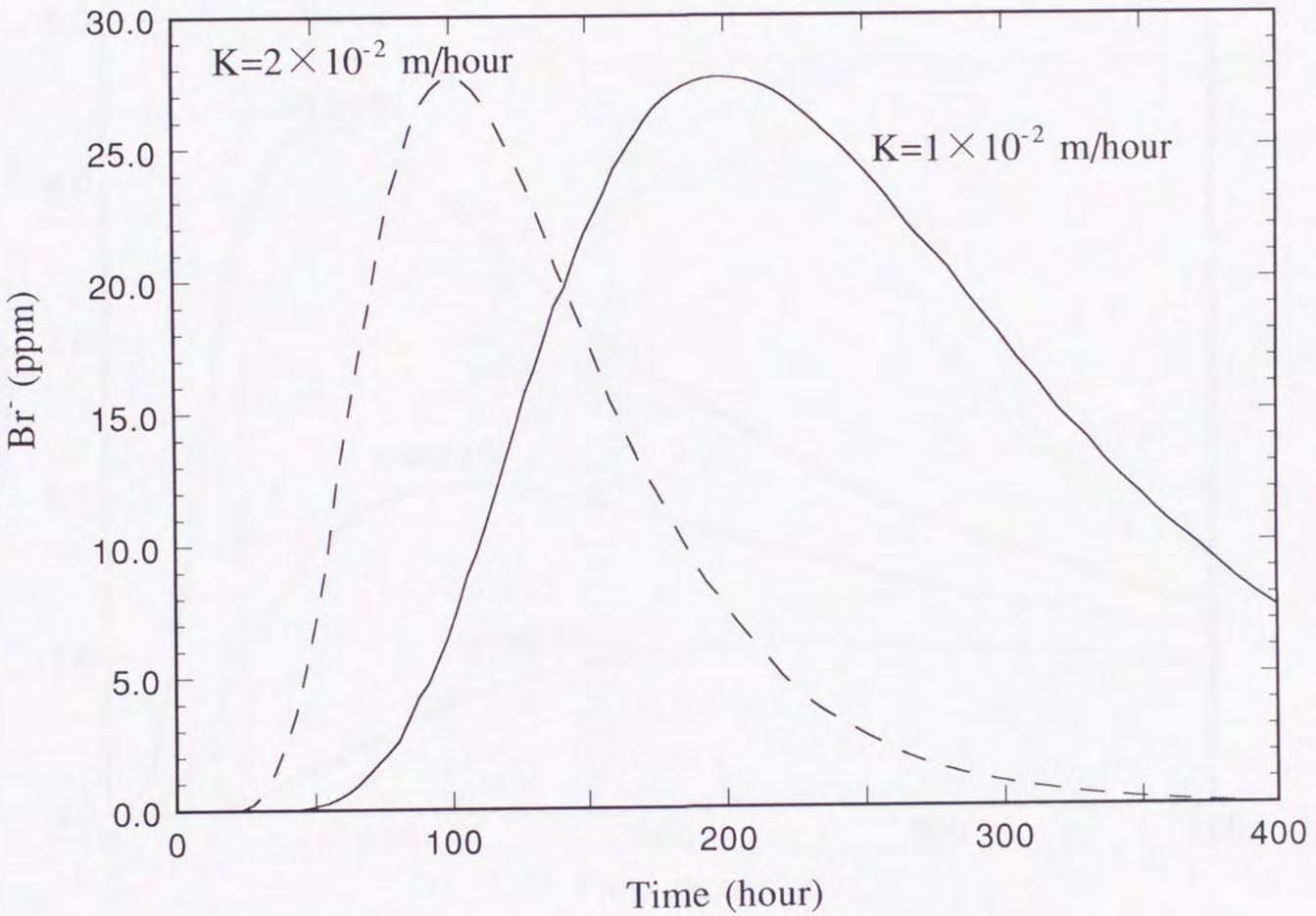


Figure 5.11 Relationship between elapsed time and concentration of Br^-.
Comparing different hydraulic conductivities (1×10^{-2}, 2×10^{-2} m/hour) at the constant condition of effective porosity (0.056%) and longitudinal dispersivities (10m).

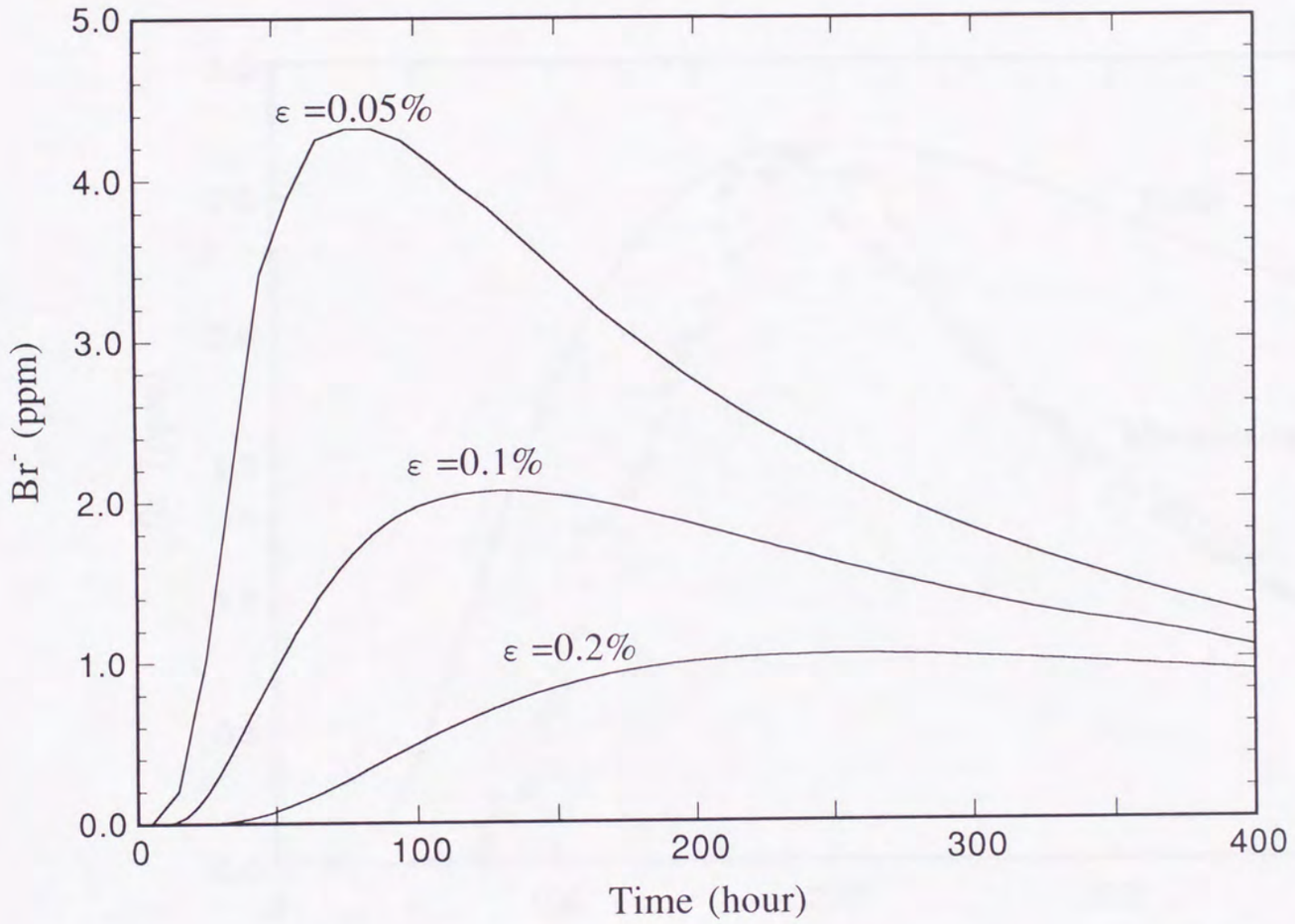


Figure 5.12 Relationship between elapsed time and concentration of Br^-.
Comparing different effective porosities (0.05, 0.1, 0.2%) at the constant condition of hydraulic conductivity (8×10^{-3} m/hour) and longitudinal dispersivity (100m).

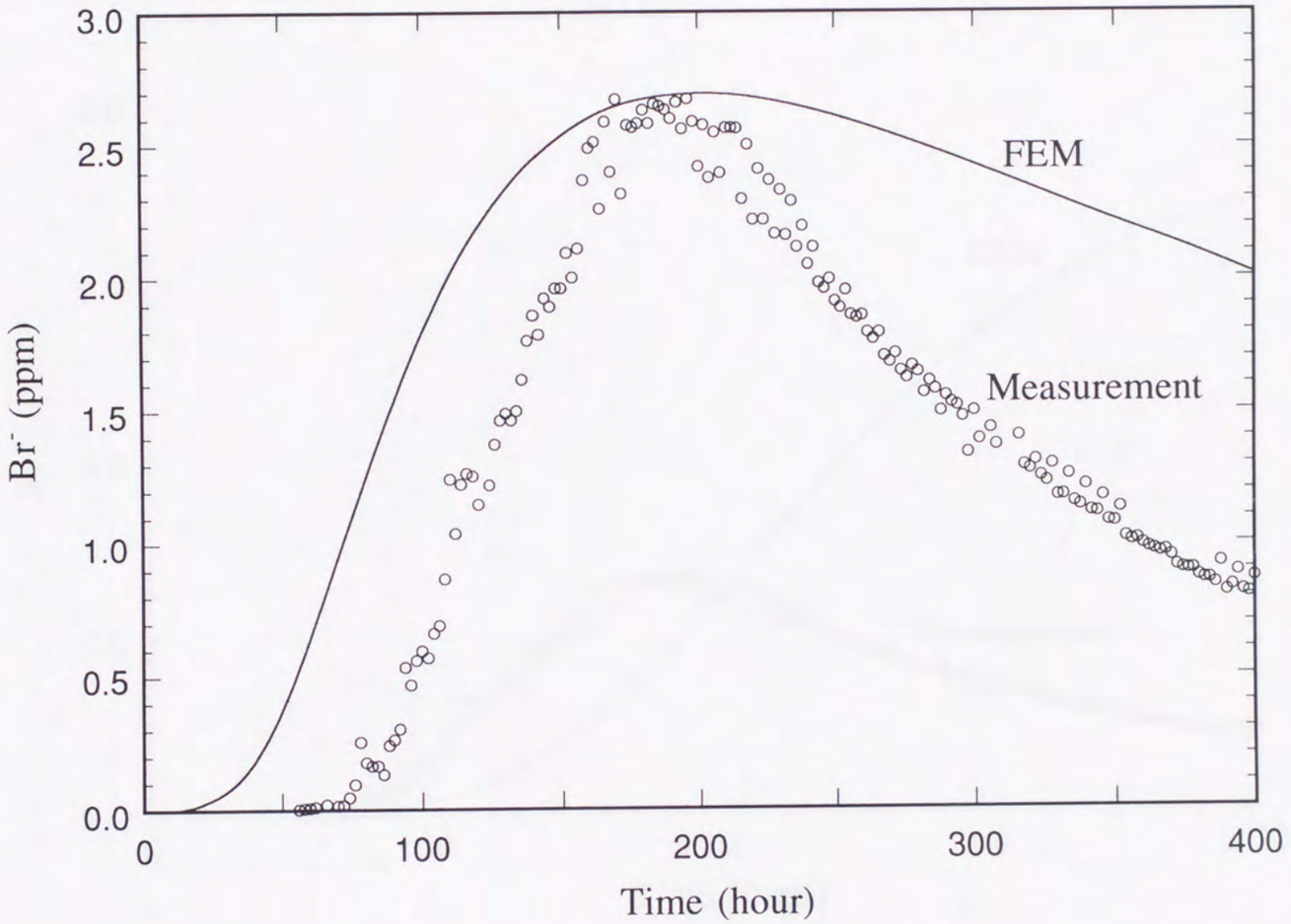


Figure 5.13 Relationship between elapsed time and concentration of Br^-.
(Case1 : $K=6.4\times10^{-3}$ m/hour, α =70m, ε =0.1%)

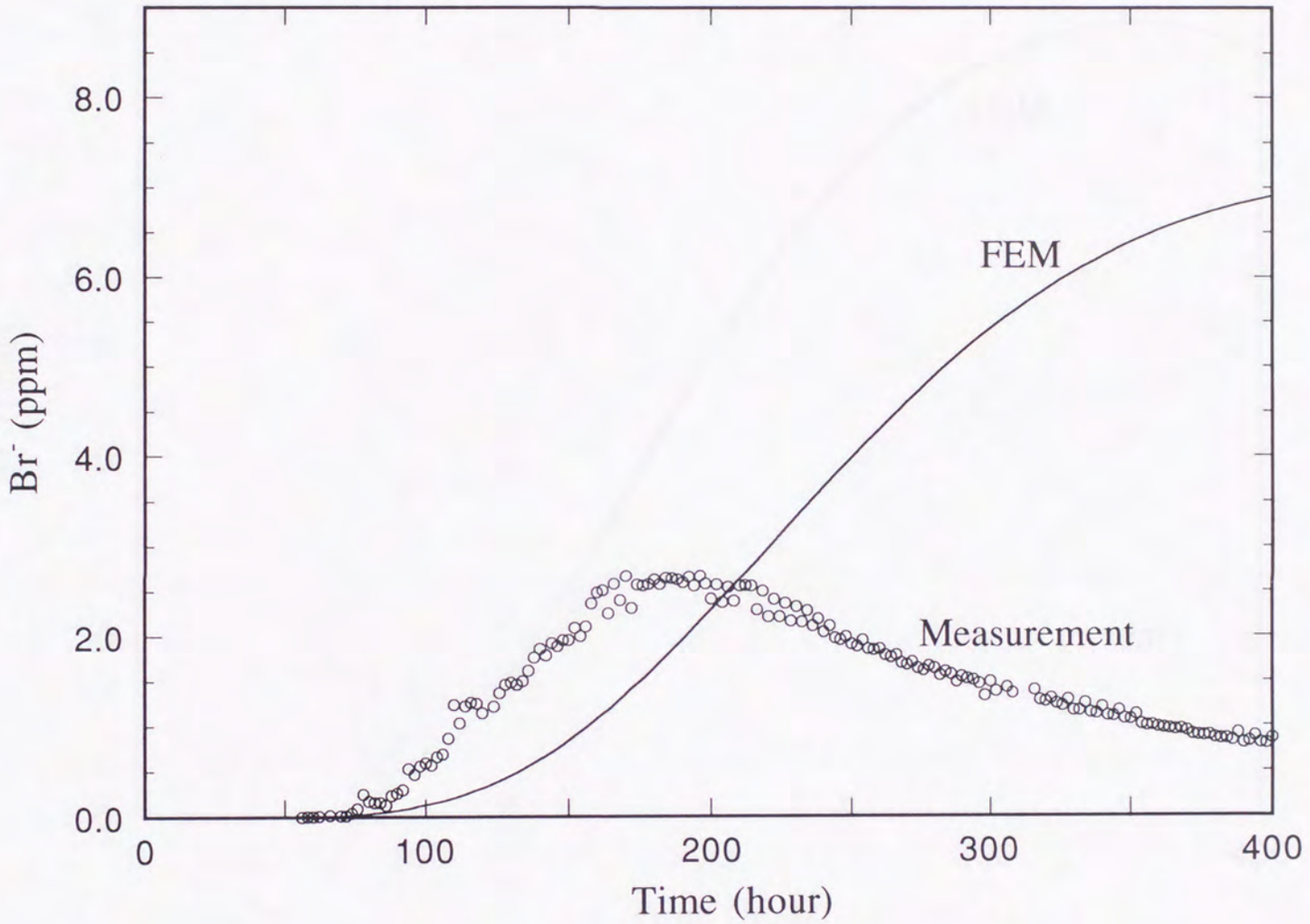


Figure 5.14 Relationship between elapsed time and concentration of Br^-.
(Case 2 : $K=6.4\times10^{-3}$ m/hour, α =20m, ε =0.1%)

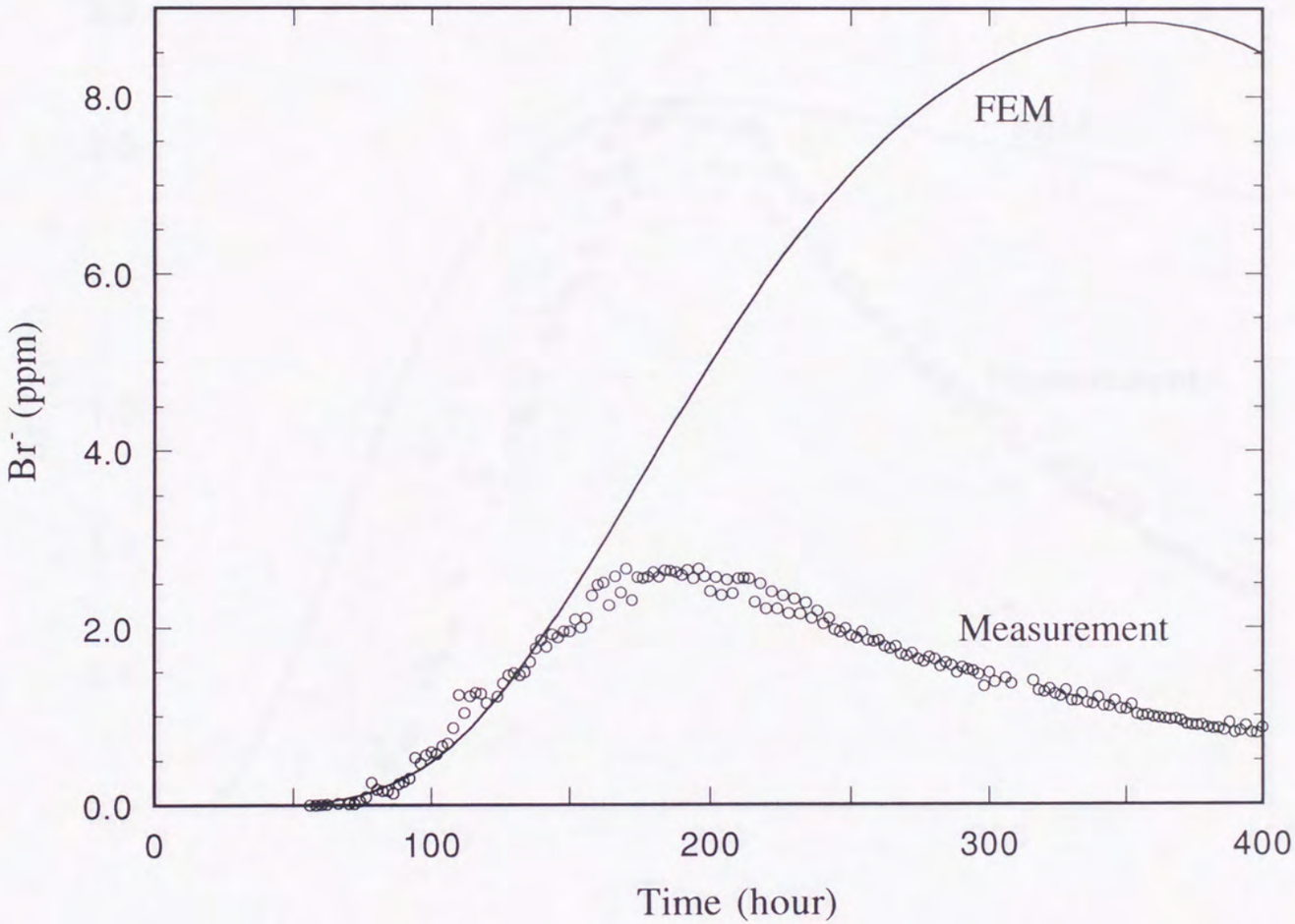


Figure 5.15 Relationship between elapsed time and concentration of Br^-.
(Case 3 : $K=6.4\times10^{-3}$ m/hour, α =20m, ε =0.08%)

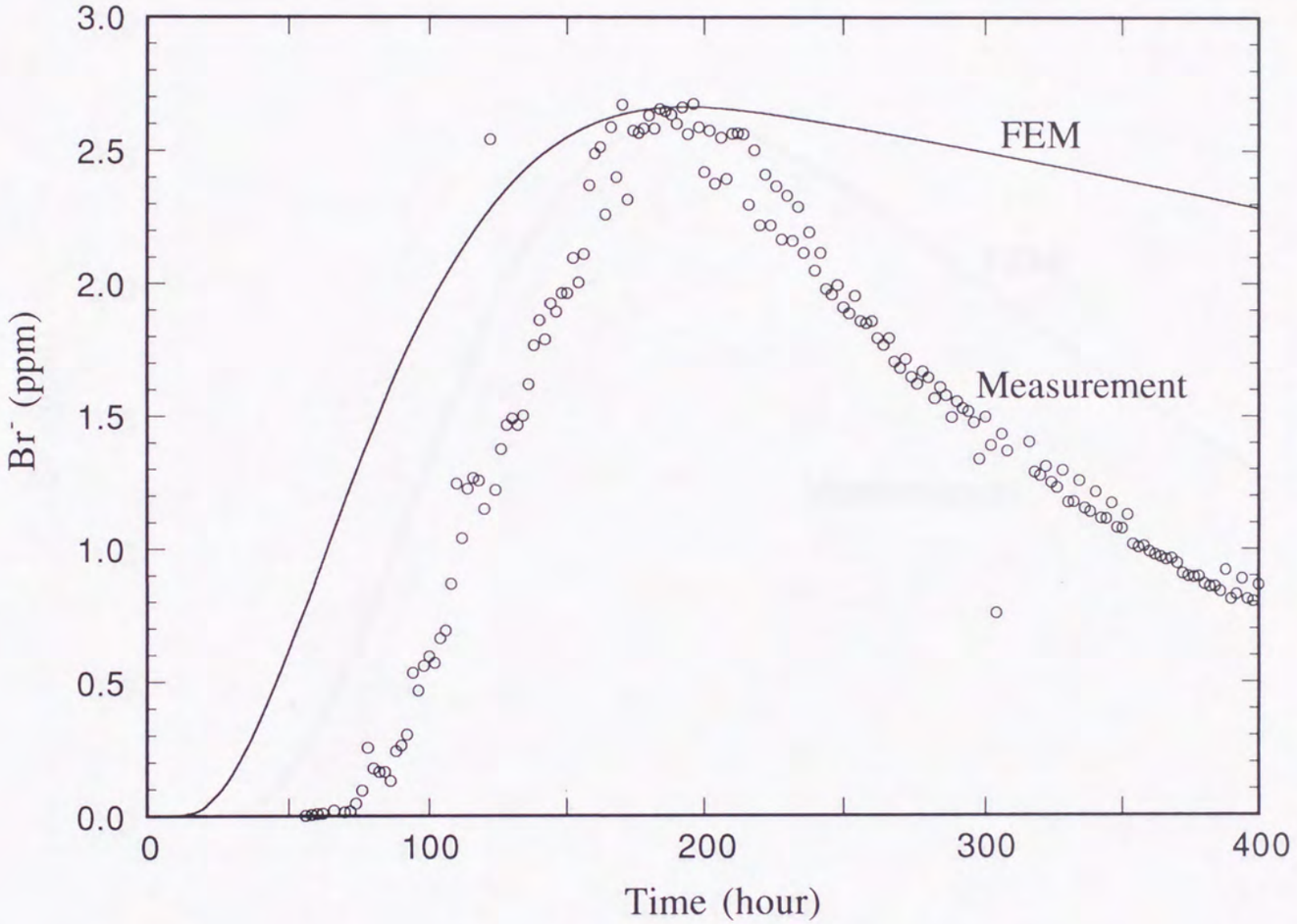


Figure 5.16 Relationship between elapsed time and concentration of Br^-.
(Case 4 : $K=2.4\times10^{-4}$ m/hour, α =190m, ε =0.064%)

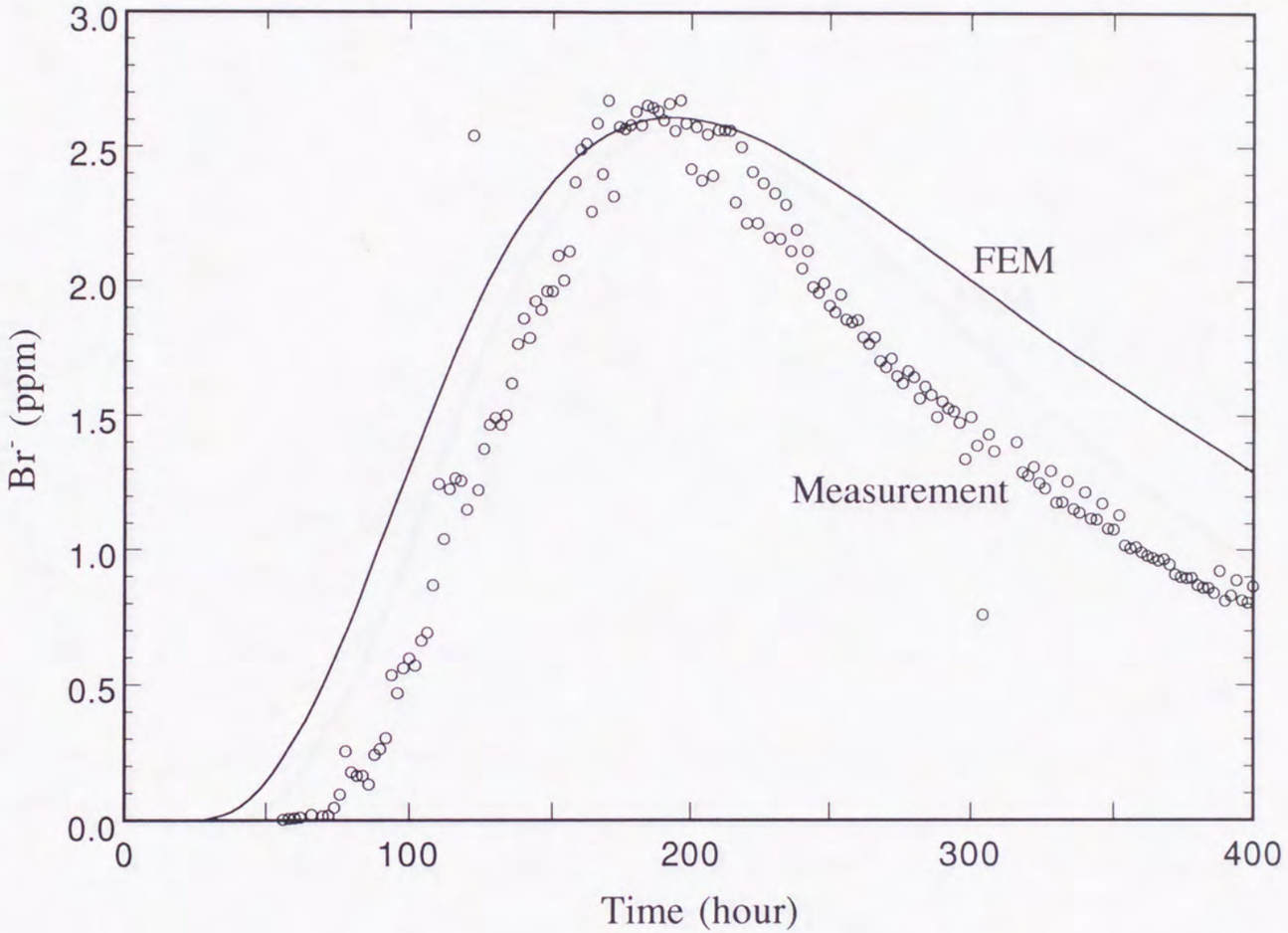


Figure 5.17 Relationship between elapsed time and concentration of Br^-.
(Case 5 : K=4.1×10^{-2} m/hour, α =20m, ε =0.27%)

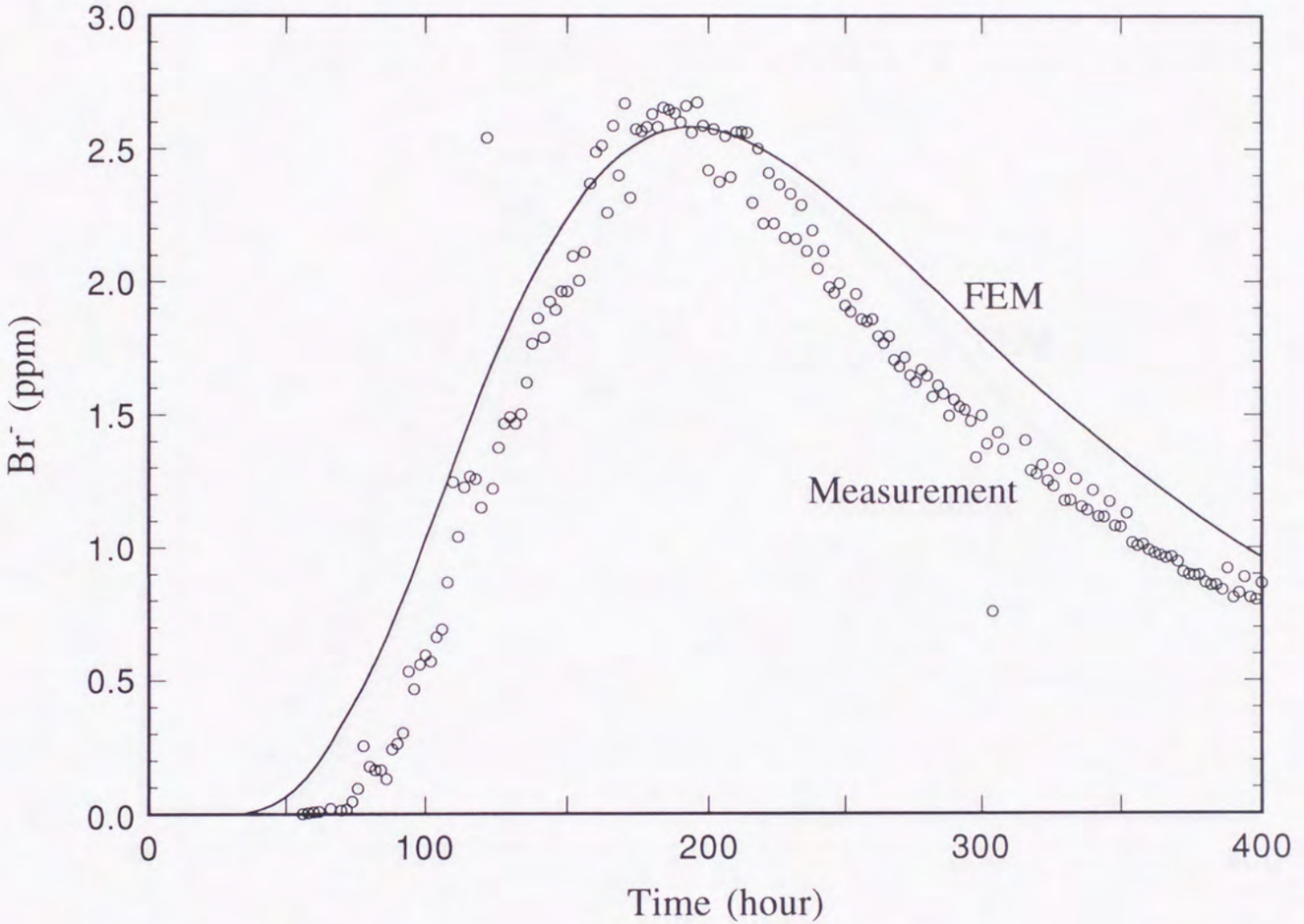


Figure 5.18 Relationship between elapsed time and concentration of Br^-.
(Case 6 : $K=6.8\times10^{-2}$ m/hour, α =14m, ε =0.4%)

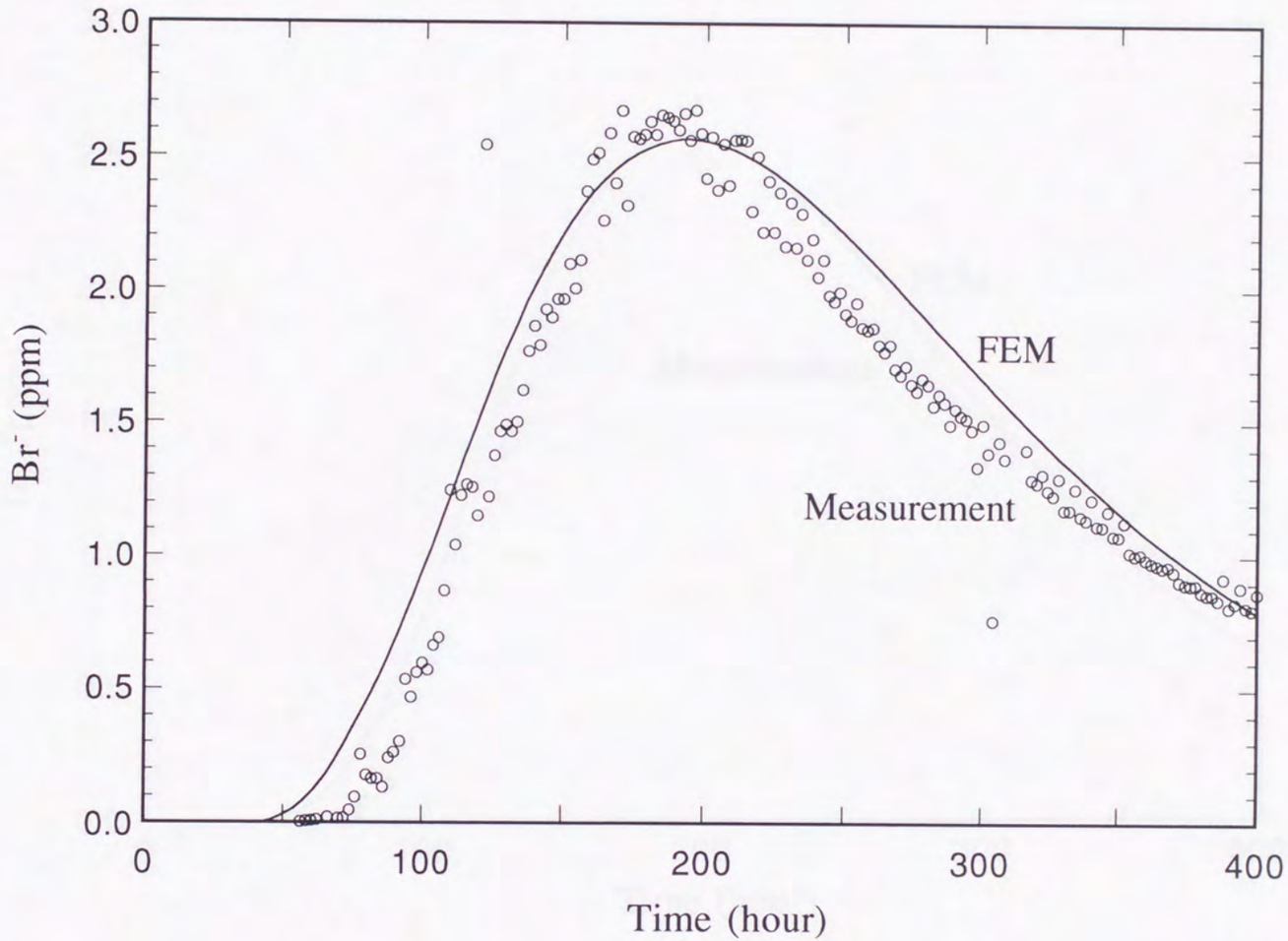


Figure 5.19 Relationship between elapsed time and concentration of Br^-.
(Case 7 : $K=8.6\times10^{-2}$ m/hour, α =12m, ε =0.48%)

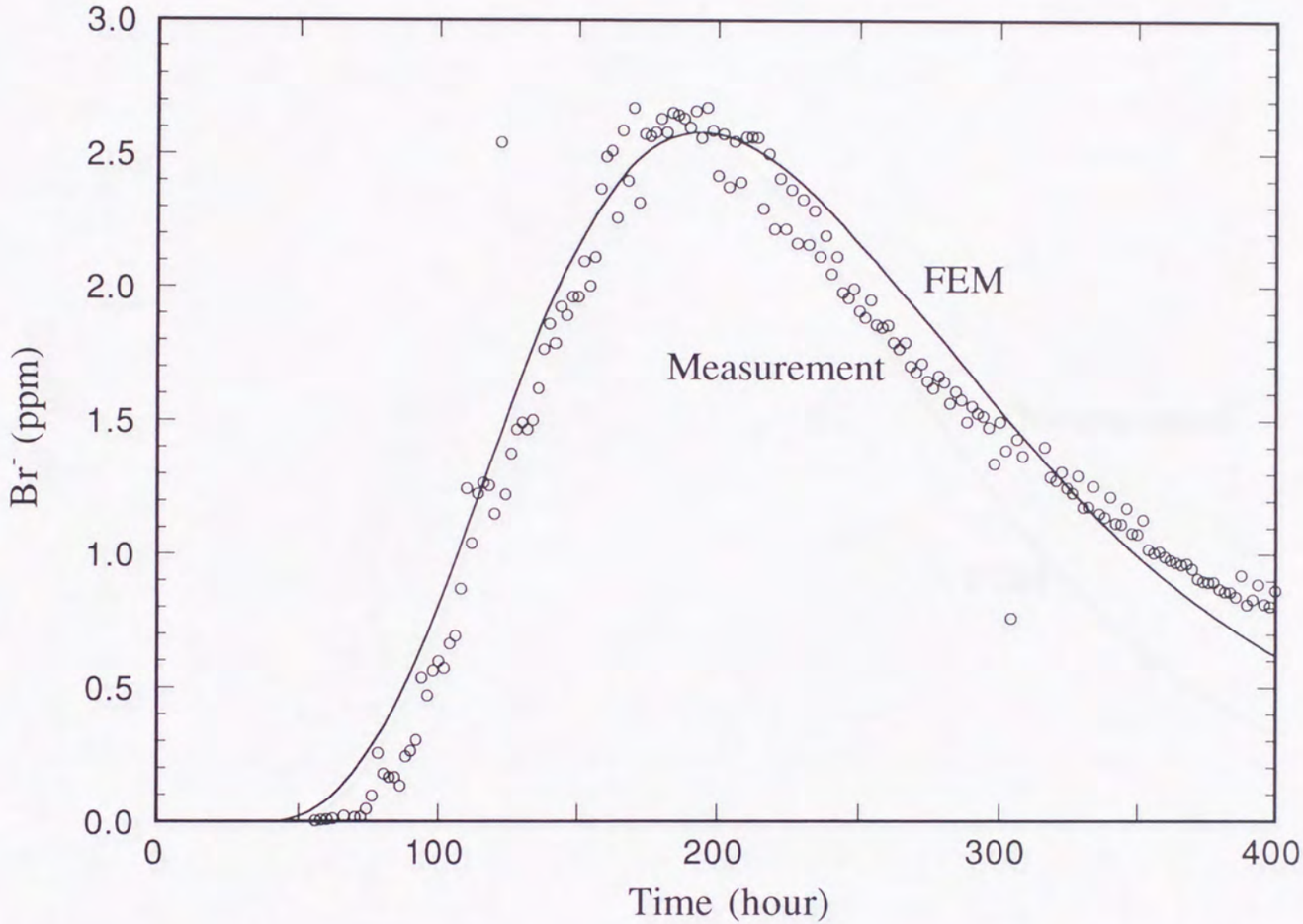


Figure 5.20 Relationship between elapsed time and concentration of Br^-.
(Case 8 : K=1.1×10^{-1} m/hour, α =10m, ε =0.59%)

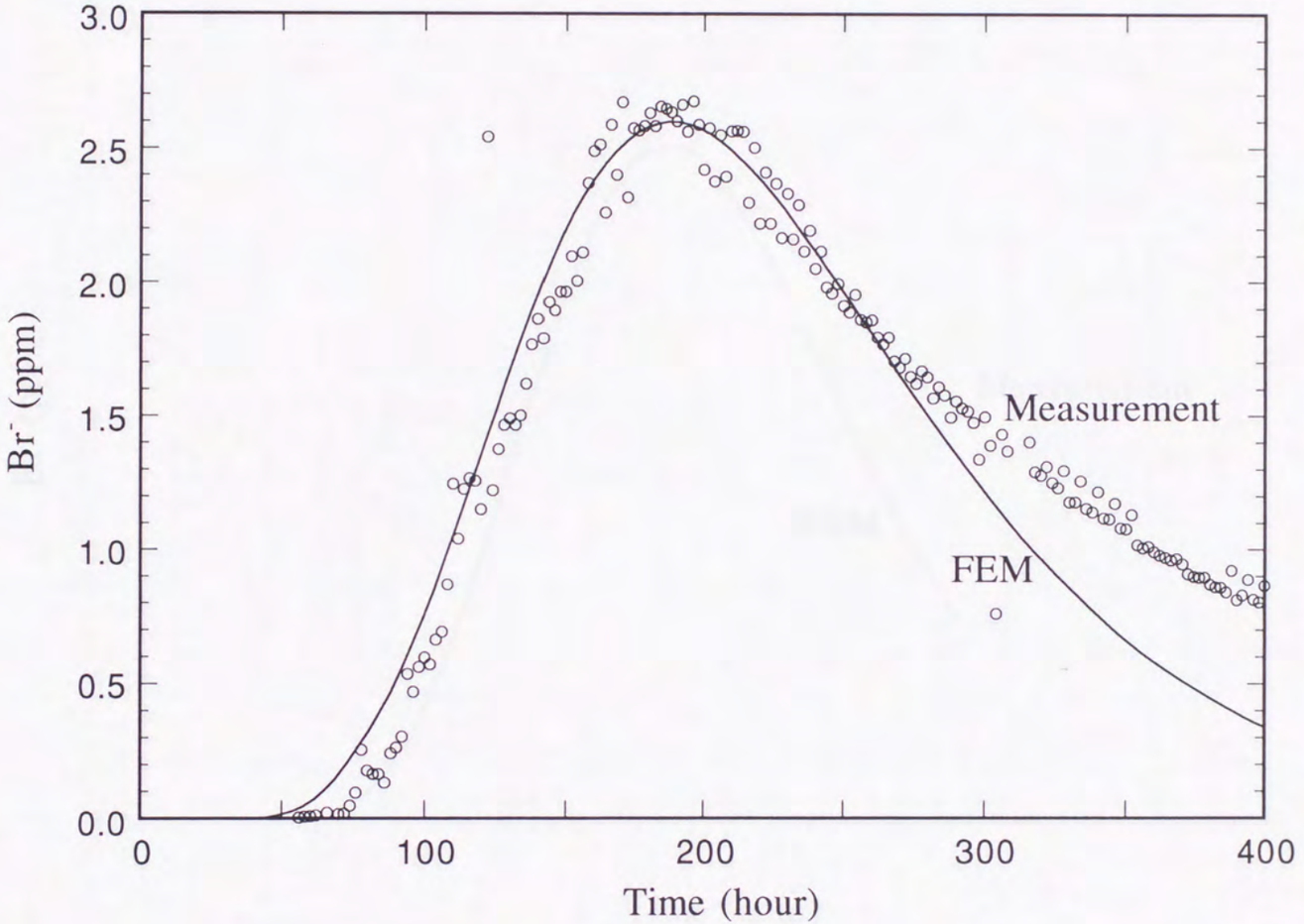


Figure 5.21 Relationship between elapsed time and concentration of Br^-.
(Case 9 : K=1.5×10^{-1} m/hour, α =8m, ε =0.76%)

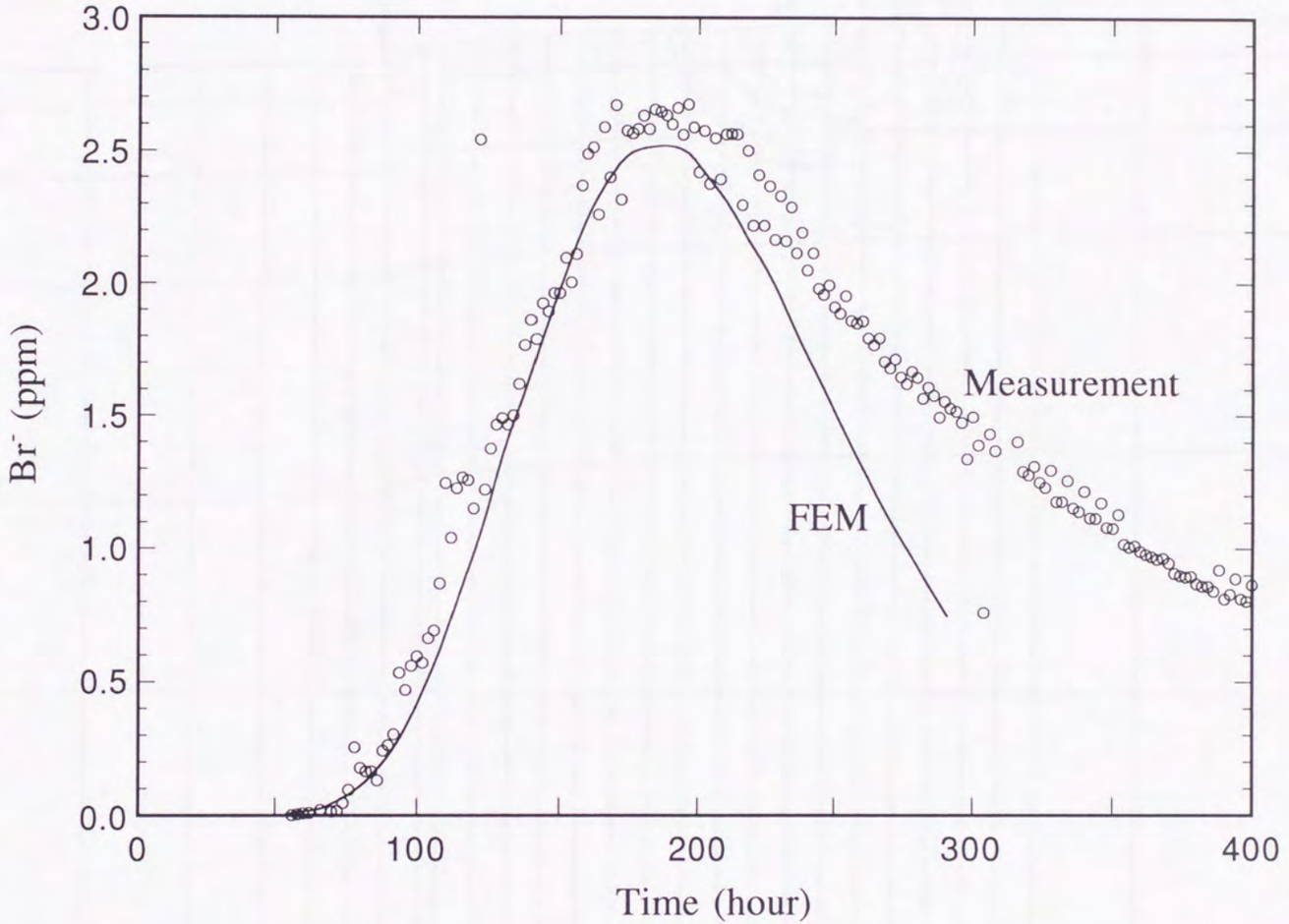


Figure 5.22 Relationship between elapsed time and concentration of Br^-.
(Case 10 : K=2.8×10^{-1} m/hour, α =5m, ε =1.4%)

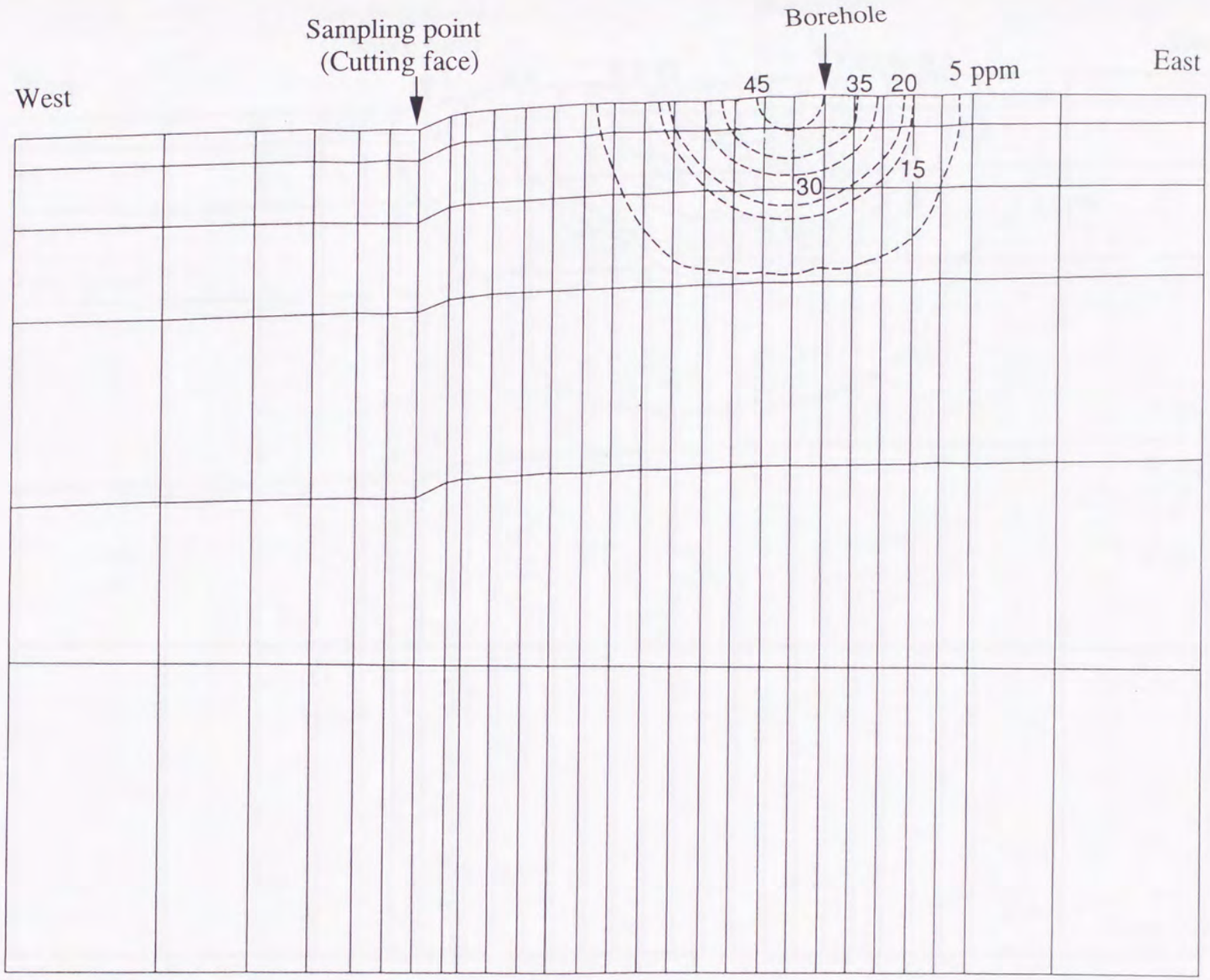


Figure 5.23 Analyzed Br^- concentration distribution 40 hours after the start of tracer injection at the Matsumoto site

(Sectional plan, ε=0.48%, α=12m, K=8.6 $\times 10^{-2}$ m hour^{-1})

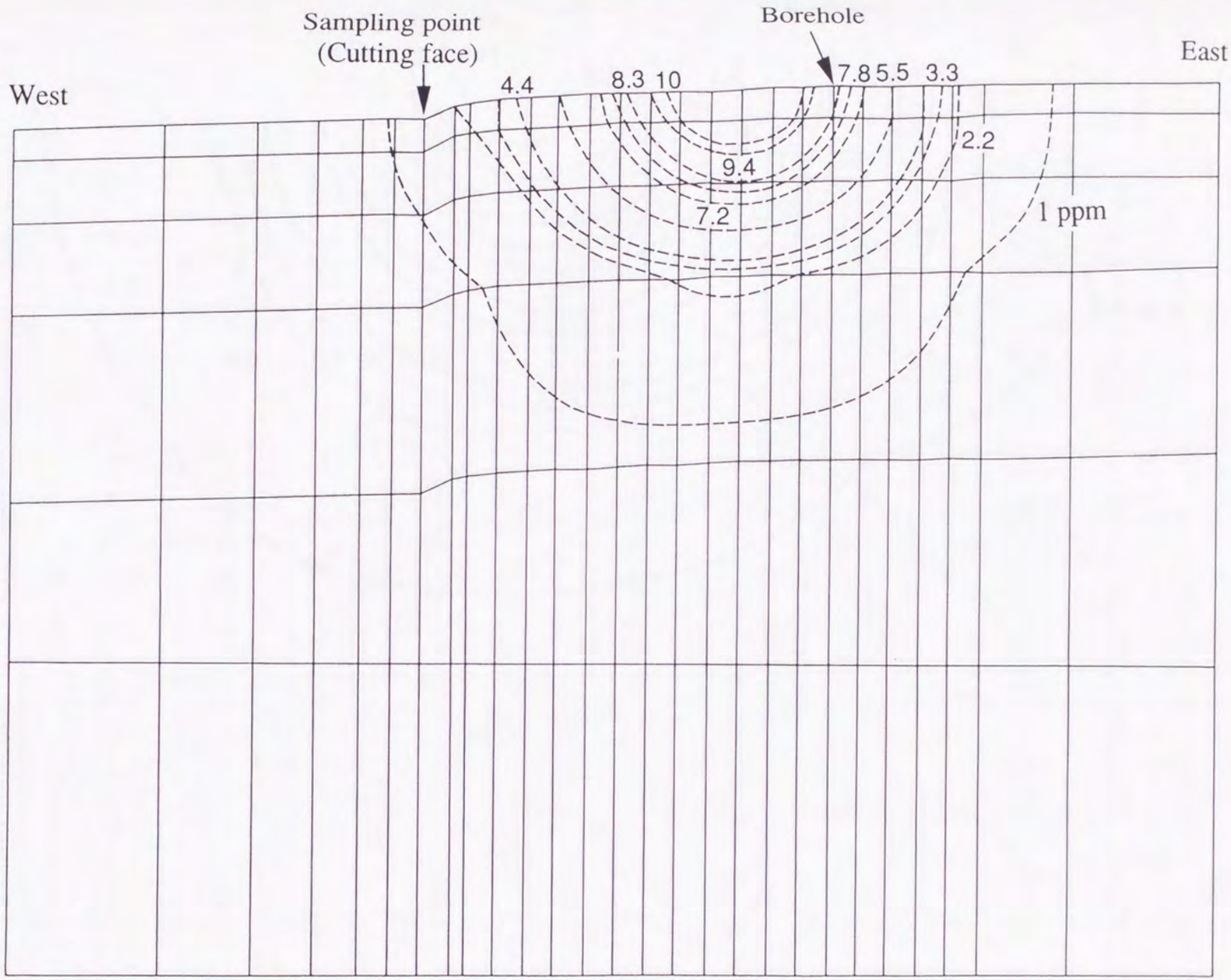


Figure 5.24 Analyzed Br^- concentration distribution 100 hours after the start of tracer injection at the Matsumoto site

(Sectional plan, ε=0.48%, α=12m, K=8.6 $\times 10^{-2}$ m hour^{-1})

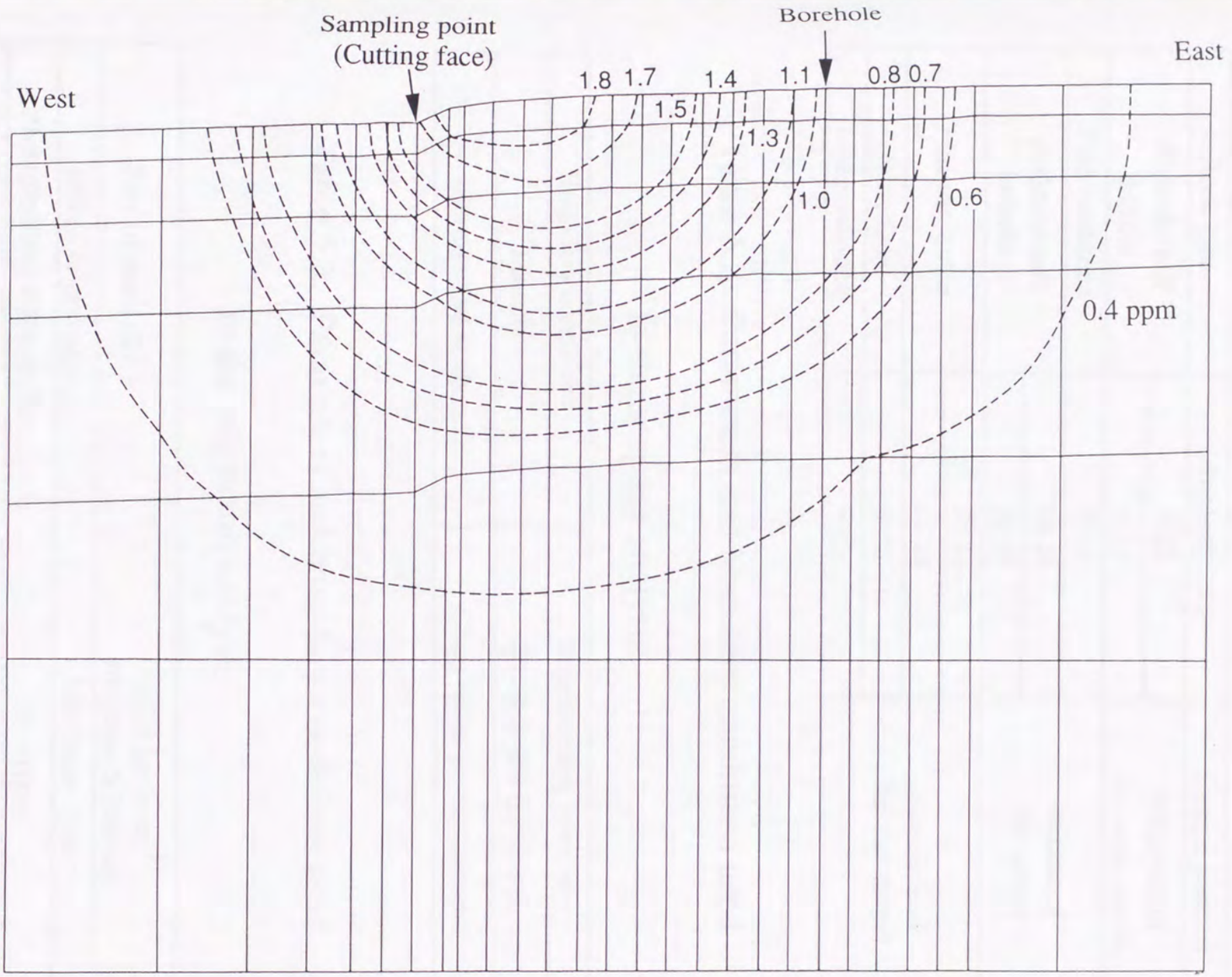


Figure 5.25 Analyzed Br^- concentration distribution 300 hours after the start of tracer injection at the Matsumoto site

(Sectional plan, ε=0.48%, α=12m, K=8.6×10^{-2} m hour^{-1})

Table 5.1 Porosity values at the Matsumoto site.

Rock type	Porosity (%)	Sample position
Andesite tuff breccia	9.23	Entrance of the west tunnel
	9.34	
Fine sandstone	7.16	Middle of the tunnel
Andesite tuff breccia	10.46	
	10.03	
Fine sandstone	15.43	Entrance of the east tunnel
	15.05	
Sandstone	9.52	
Fine sandstone	9.03	

Table 5.2 Parameters and boundary conditions used in the seepage analysis.

Boundary conditions	Impermeable boundary
Tunnels	Drain levels (constant)
Springs and wells	Observation levels (constant)

Table 5.3 Parameters and boundary conditions used in the migration analysis.

Flux of mass (Br^-)	46579.2g $hour^{-1}$ ($0 \leqq time \leqq 30min$)
Effective porosity	Maximum 15%
Longitudinal dispersivity	5 ~100m
Boundary condition	Impermeable
Hydraulic conductivity	$2.4\times10^{-4} \sim 2.8\times10^{-1}$ m $hour^{-1}$

Table 6.1 Conditions and results of column experiment of bentonite and quartz-sand mixture

Porosity (%)	Dry density (g cm^{-3})	Mixture ratio	Flow rate (cm^3 sec^{-1})	Tracer	Actual velocity (cm sec^{-1})	Dispersion coefficient (cm^2 sec^{-1})	Effective porosity (%)	Hydraulic conductivity (cm sec^{-3})
43	1.5	10:90	1.1×10^{-4}	Cl^-	1.3×10^{-5}	2.3×10^{-5}	43	1.0×10^{-8}
			5.0×10^{-4}	Cl^-	1.1×10^{-4}	5.0×10^{-5}	23	4.4×10^{-8}
			6.1×10^{-4}	Cl^-	1.7×10^{-4}	2.2×10^{-4}	18	5.2×10^{-8}
			5.8×10^{-4}	Cl^-	2.4×10^{-4}	1.7×10^{-4}	13	1.0×10^{-7}
				Br^-	2.3×10^{-4}	1.8×10^{-4}	13	
			1.6×10^{-3}	Cl^-	6.1×10^{-4}	7.7×10^{-4}	13	2.4×10^{-7}
		7:93	3.1×10^{-4}	Br^-	6.5×10^{-5}	1.2×10^{-4}	24	2.5×10^{-8}

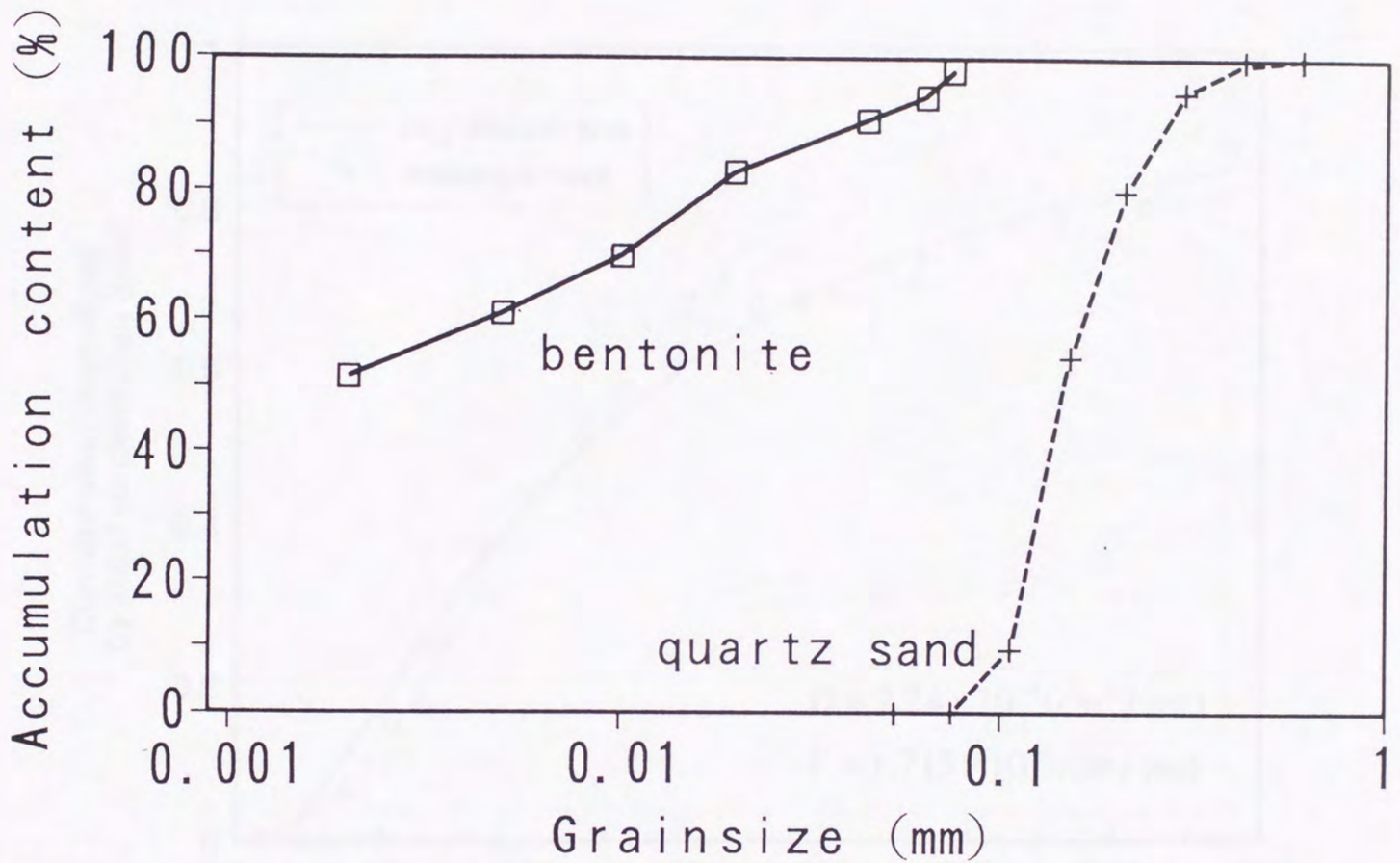


Figure 6.1 Grain size distribution curve of bentonite and quartz sand

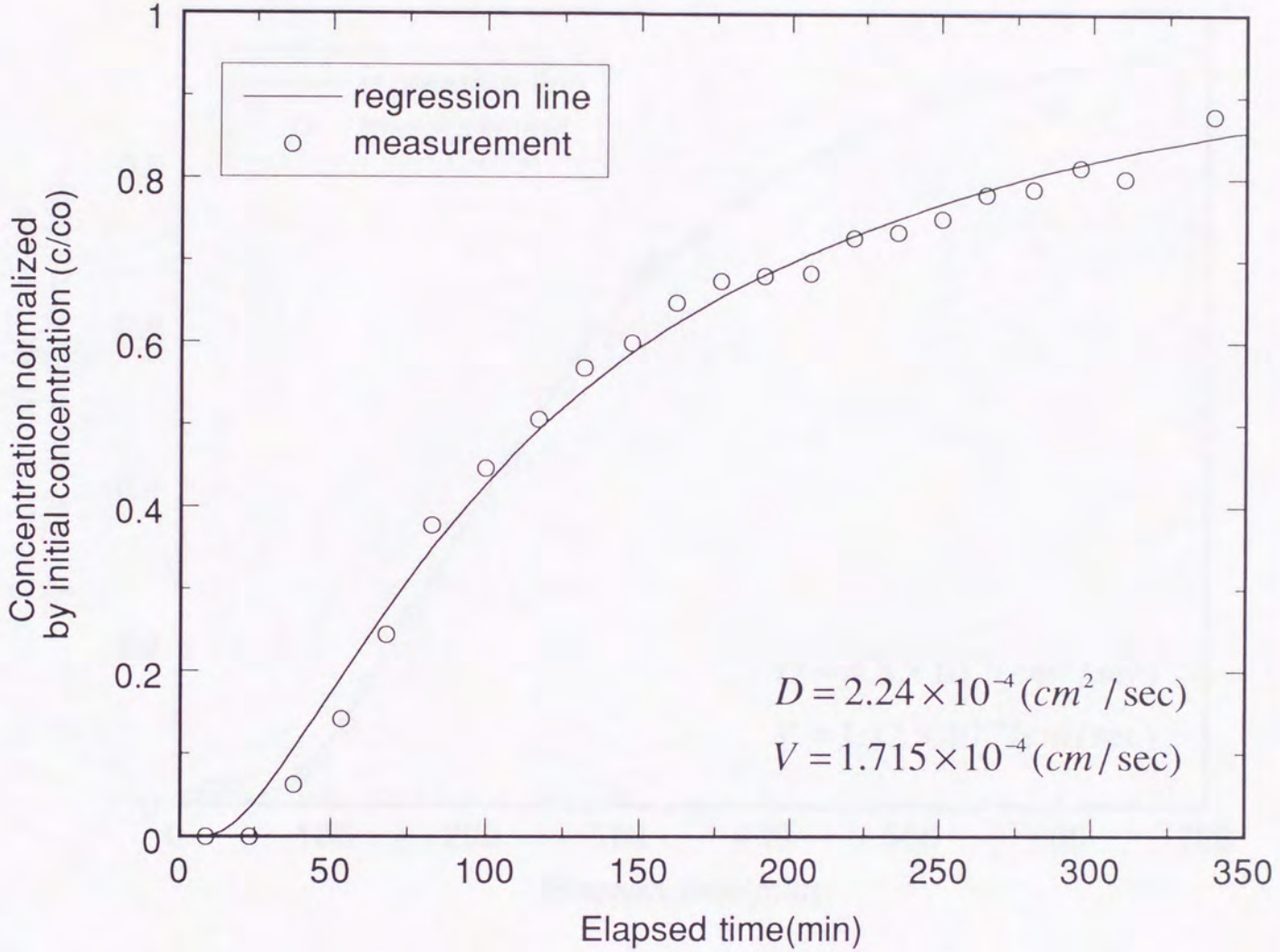


Figure 6.2 Breakthrough curve in bentonite and quartz-sand mixture laboratory tracer tests

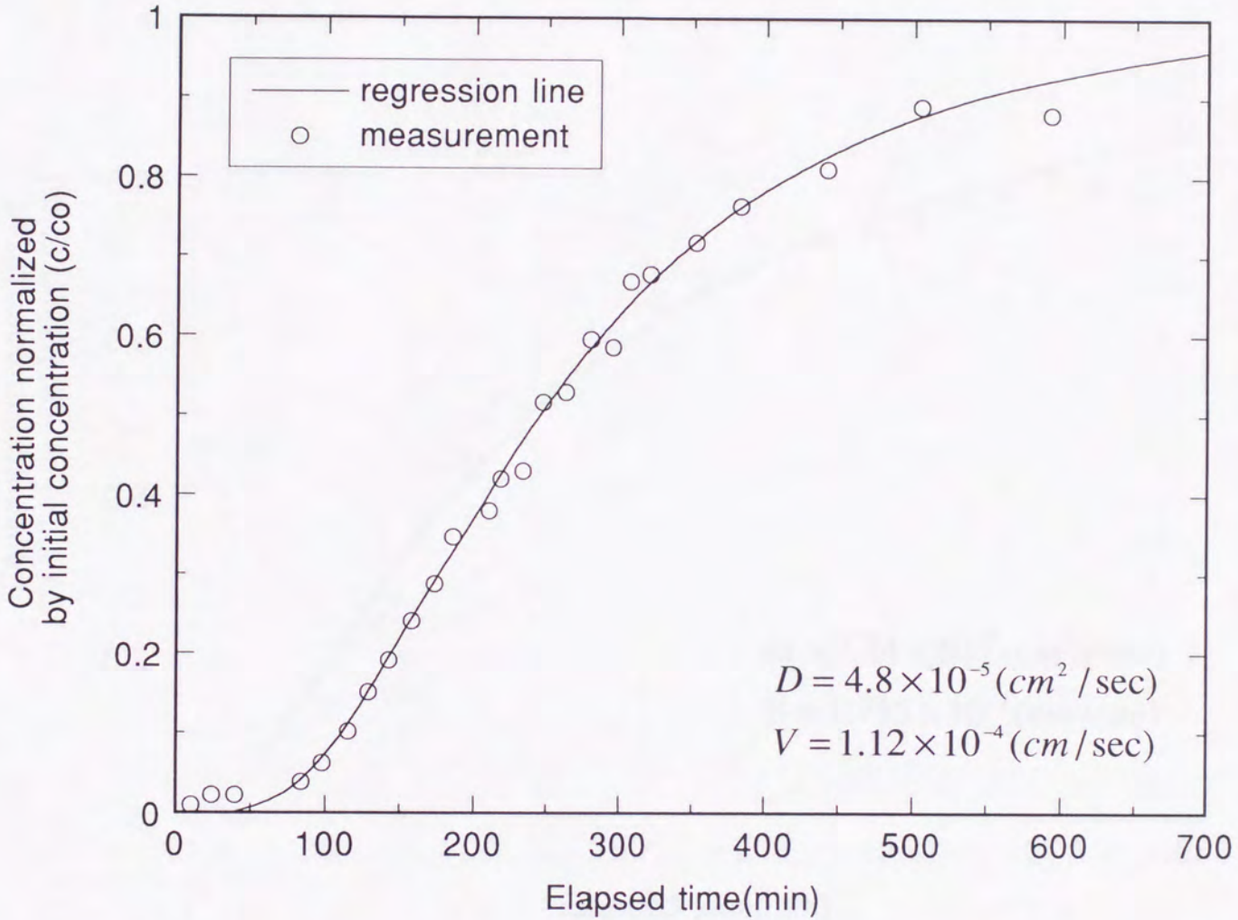


Figure 6.3 Breakthrough curve in bentonite and quartz-sand mixture laboratory tracer tests

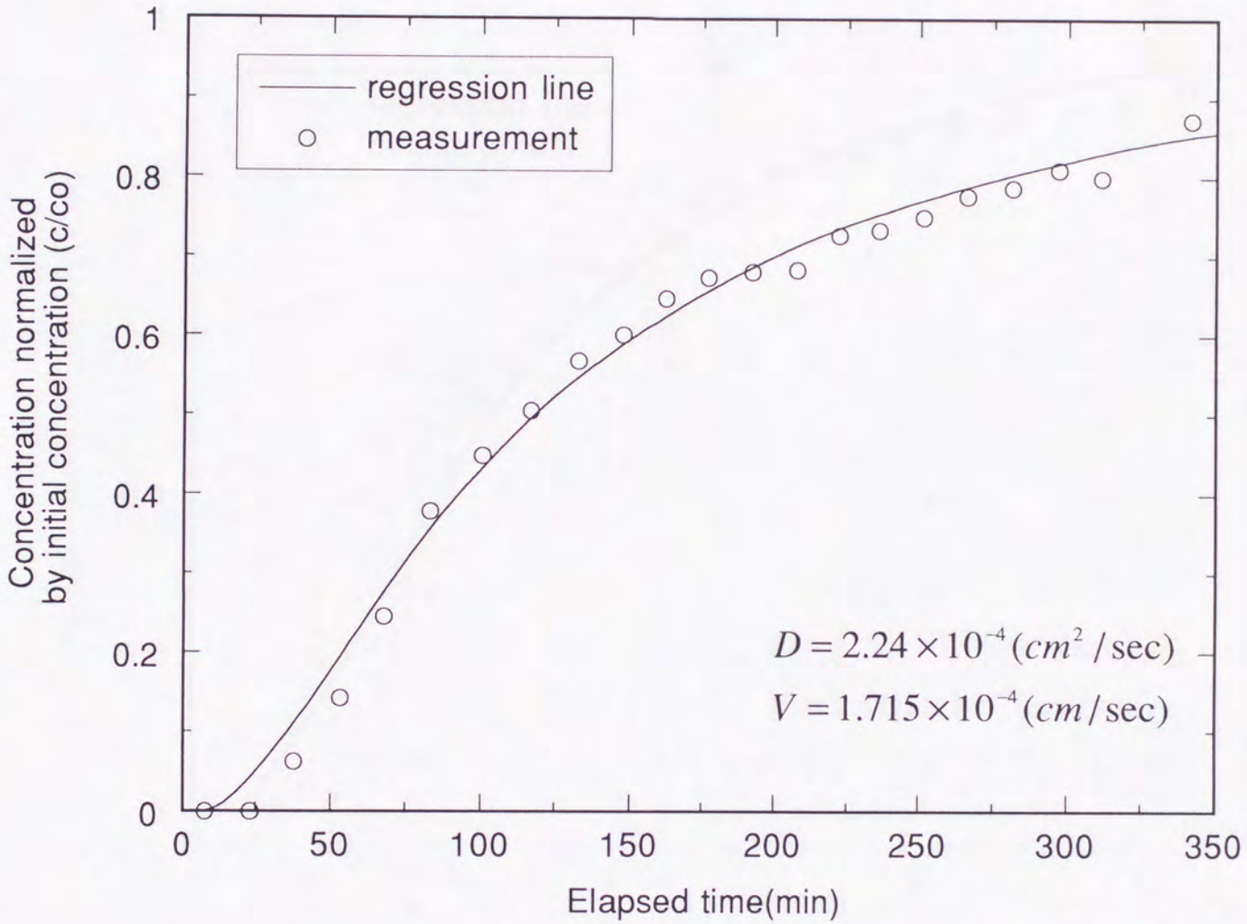


Figure 6.4 Breakthrough curve in bentonite and quartz-sand mixture laboratory tracer tests

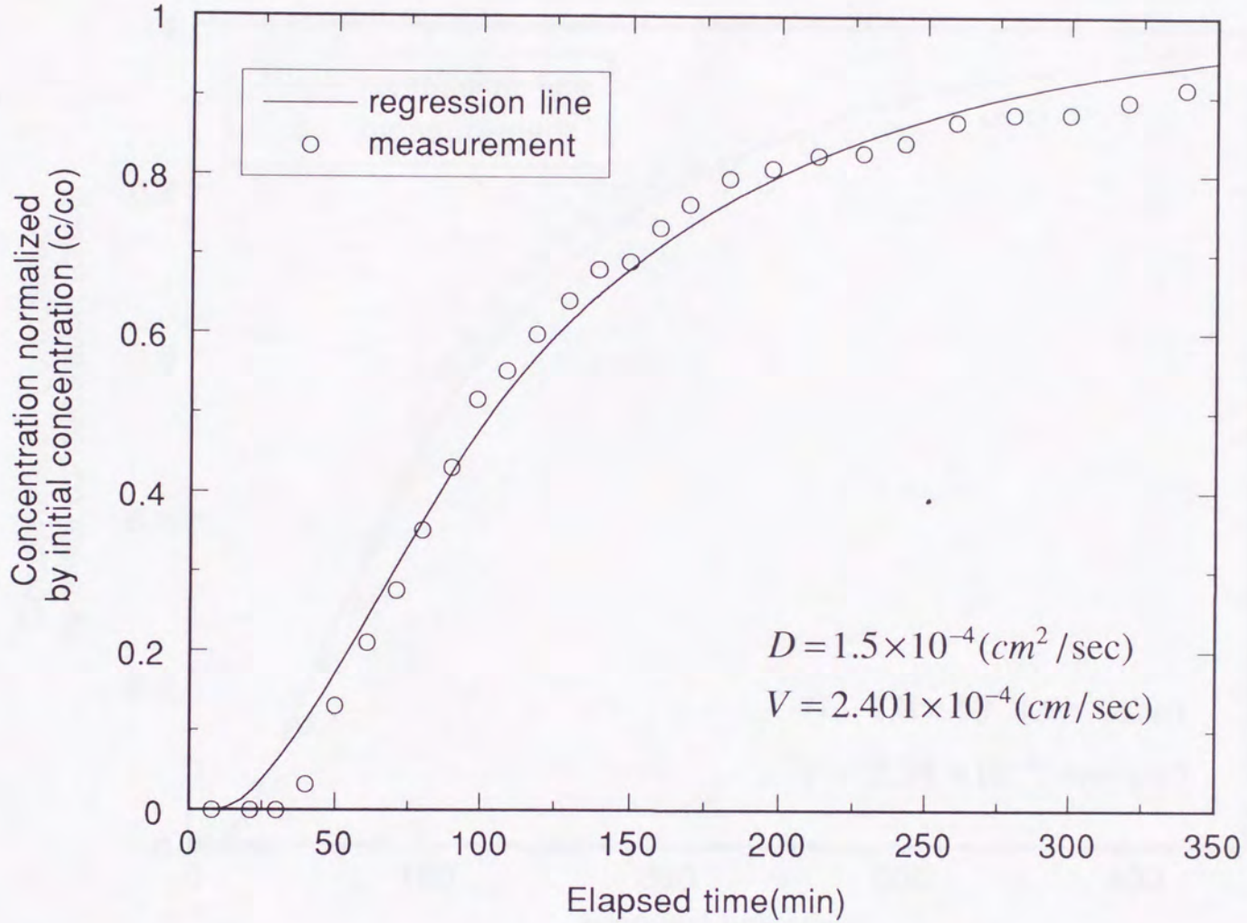


Figure 6.5 Breakthrough curve in bentonite and quartz-sand mixture laboratory tracer tests

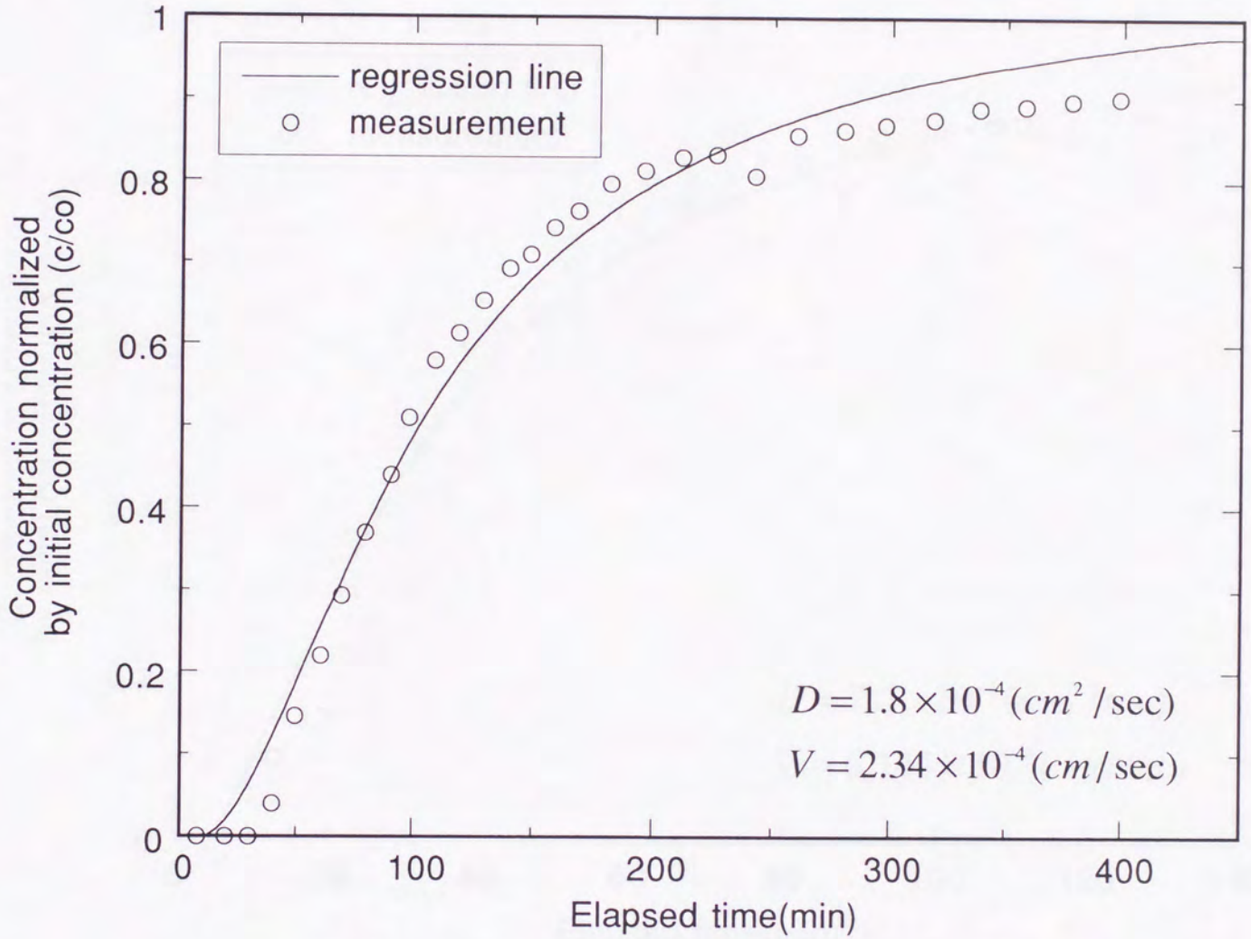


Figure 6.6 Breakthrough curve in bentonite and quartz-sand mixture laboratory tracer tests

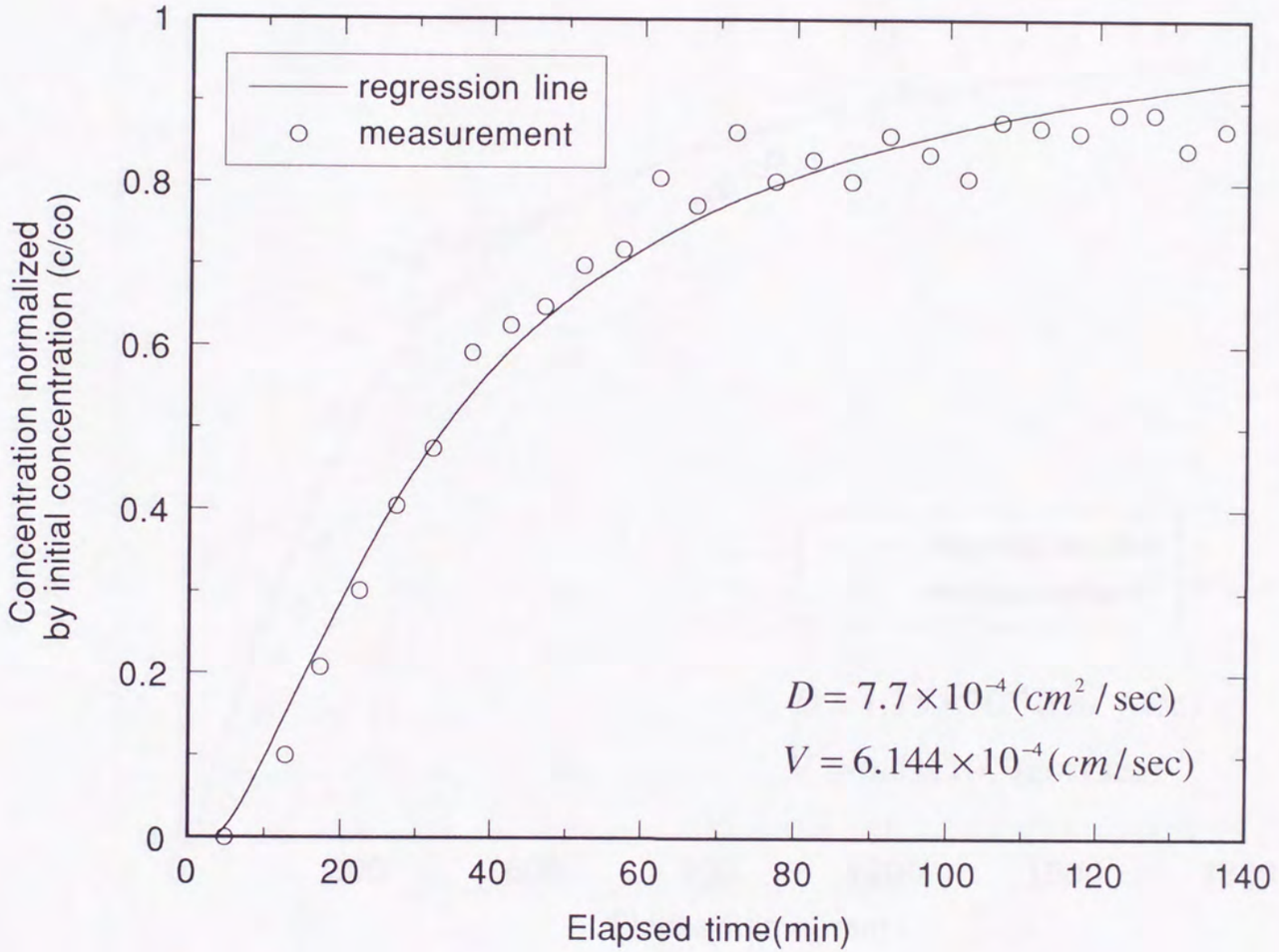


Figure 6.7 Breakthrough curve in bentonite and quartz-sand mixture laboratory tracer tests

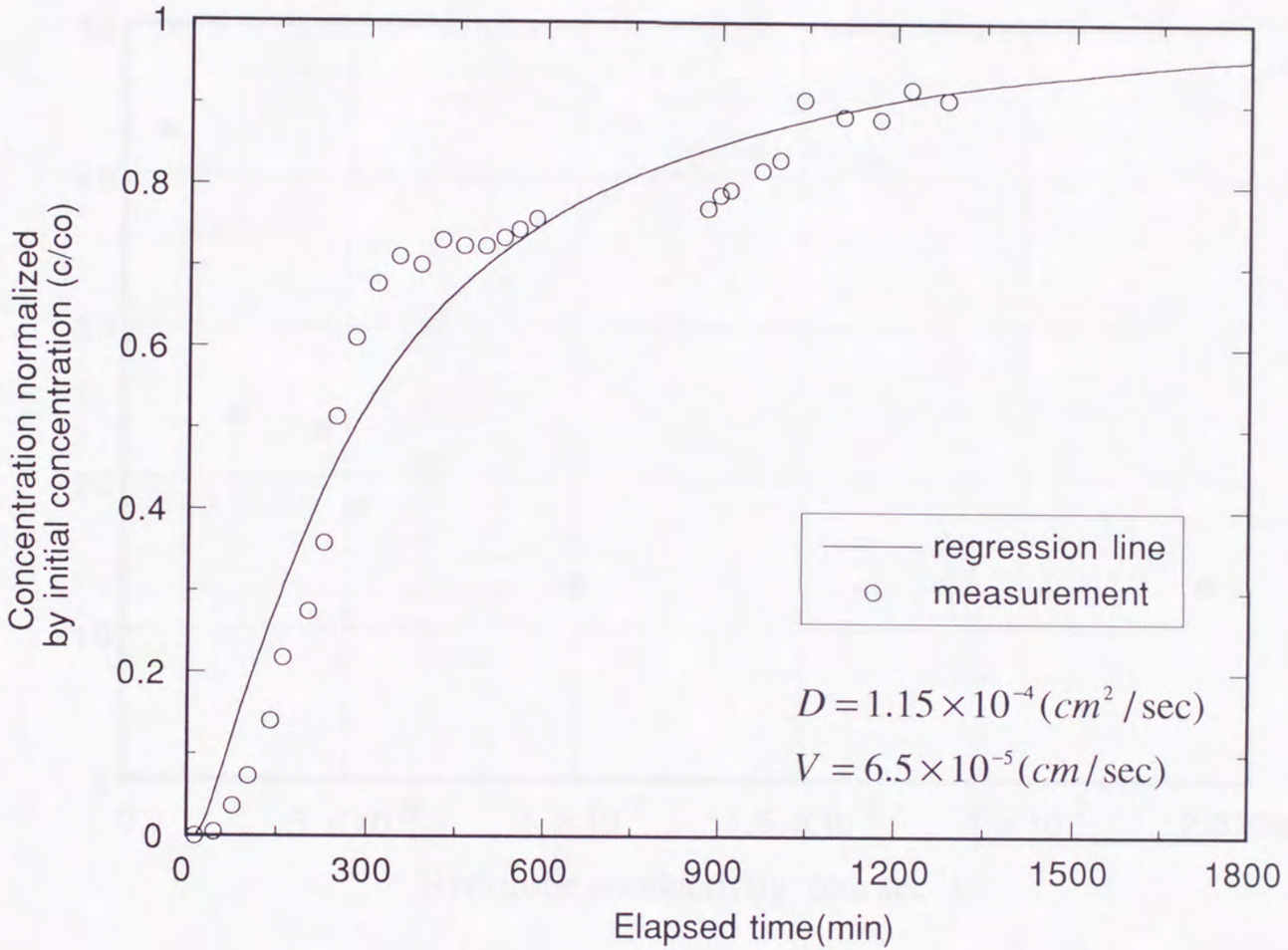


Figure 6.8 Breakthrough curve in bentonite and quartz-sand mixture laboratory tracer tests

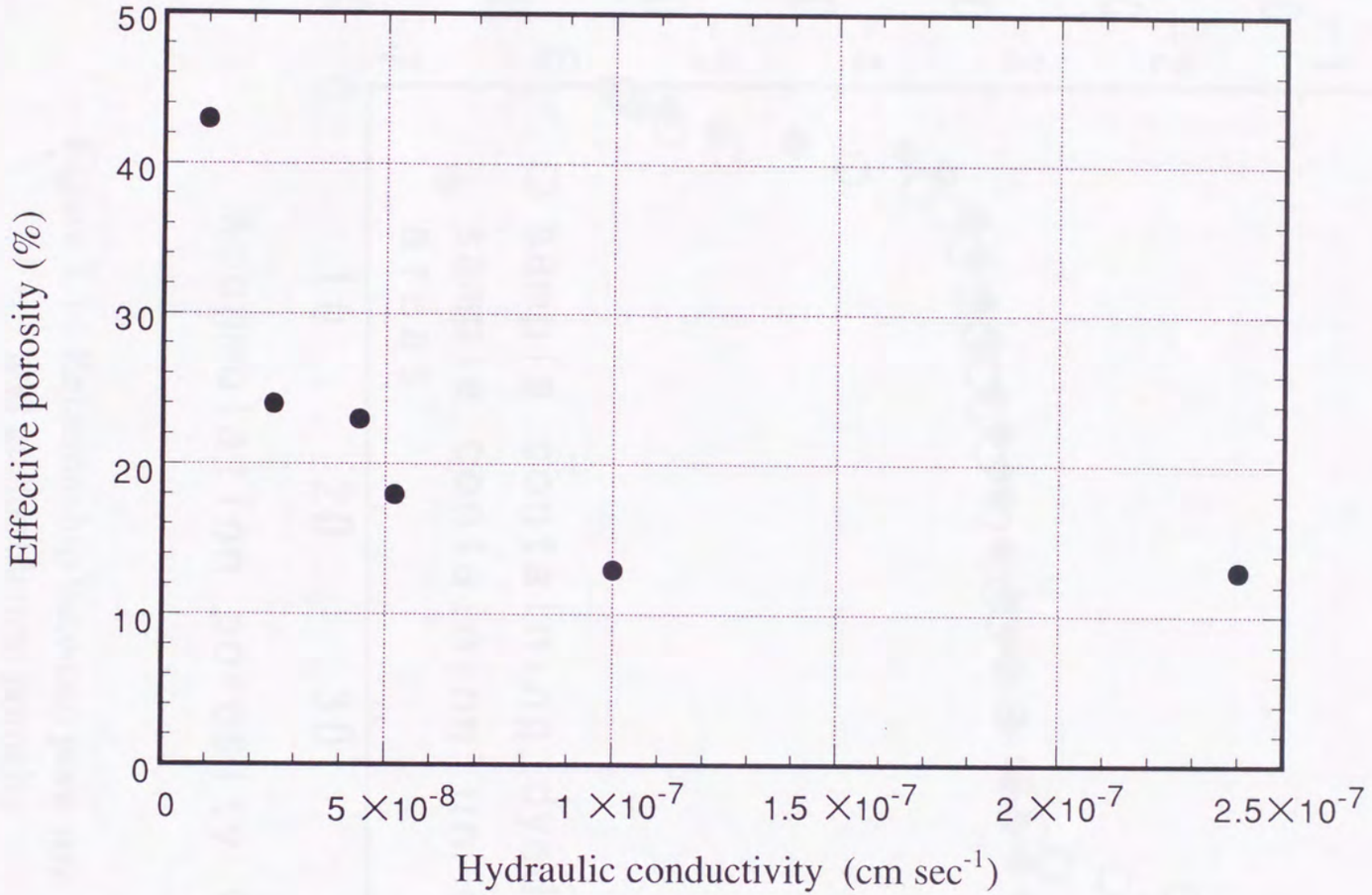


Figure 6.9 Relationship between effective porosity and the hydraulic conductivity of the bentonite and quartz sand mixture

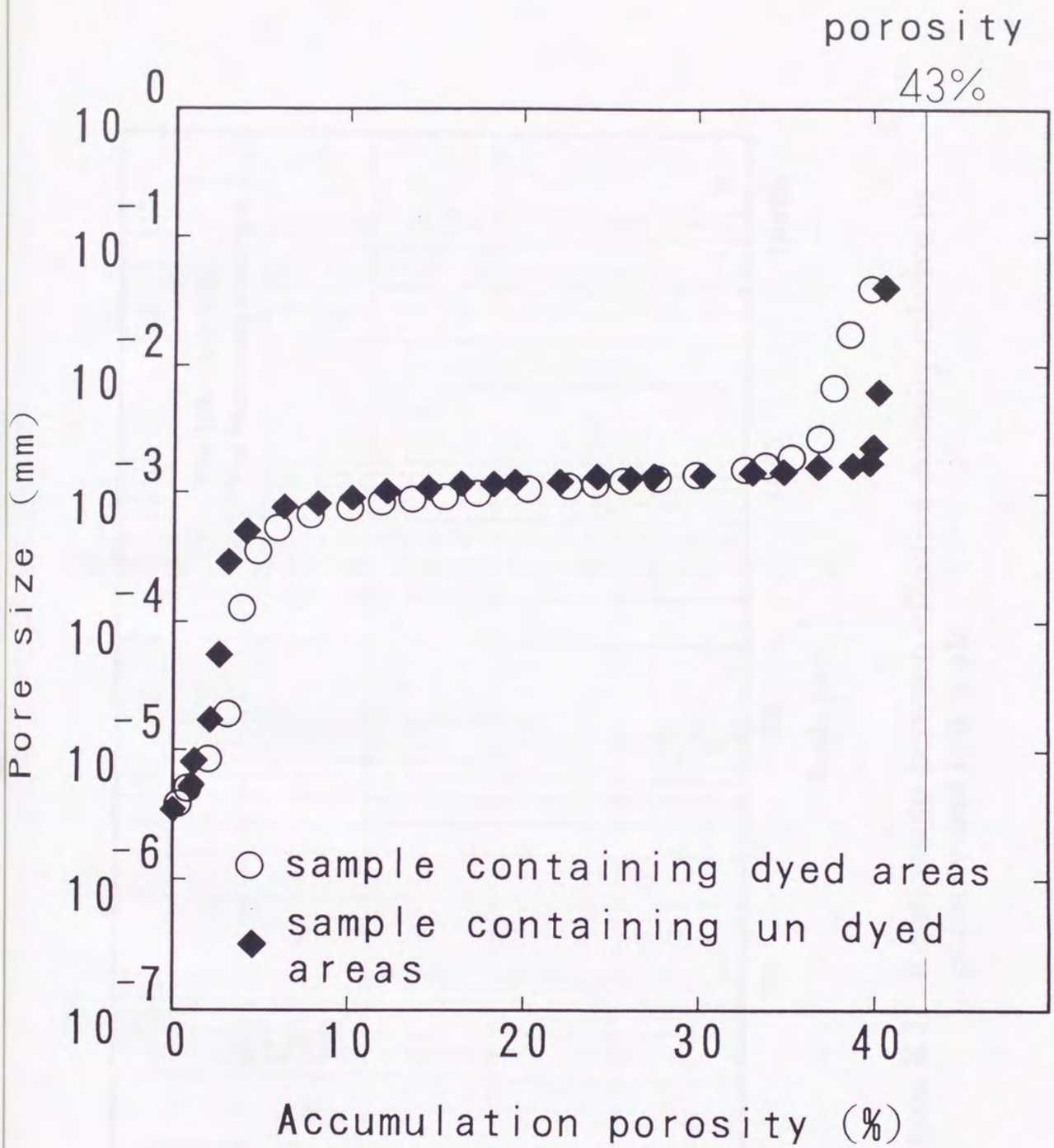


Figure 7.1 Relationship between pore size and accumulation porosity

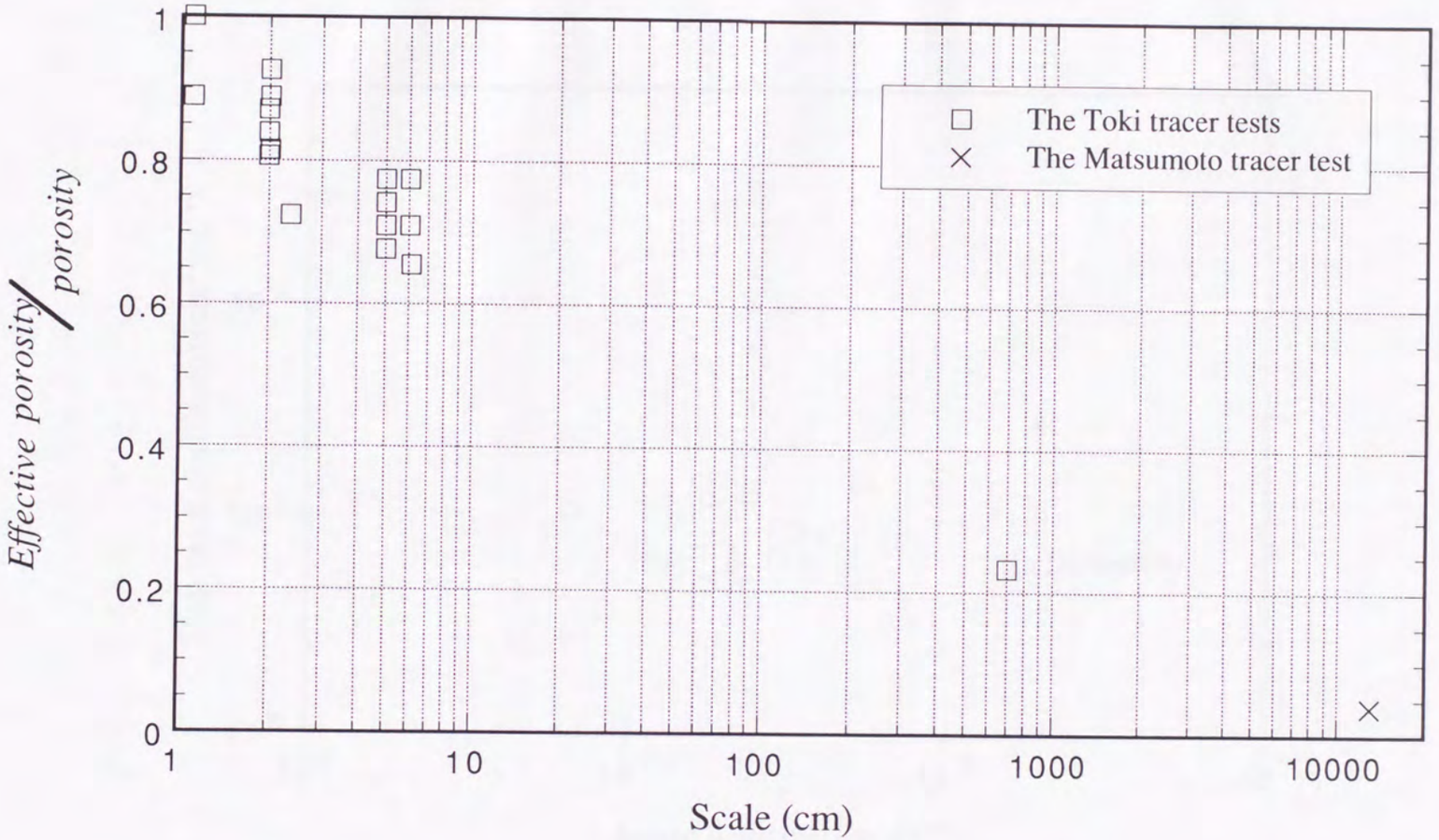


Figure 8.1 Relationship between effective porosity relative to porosity and test scale

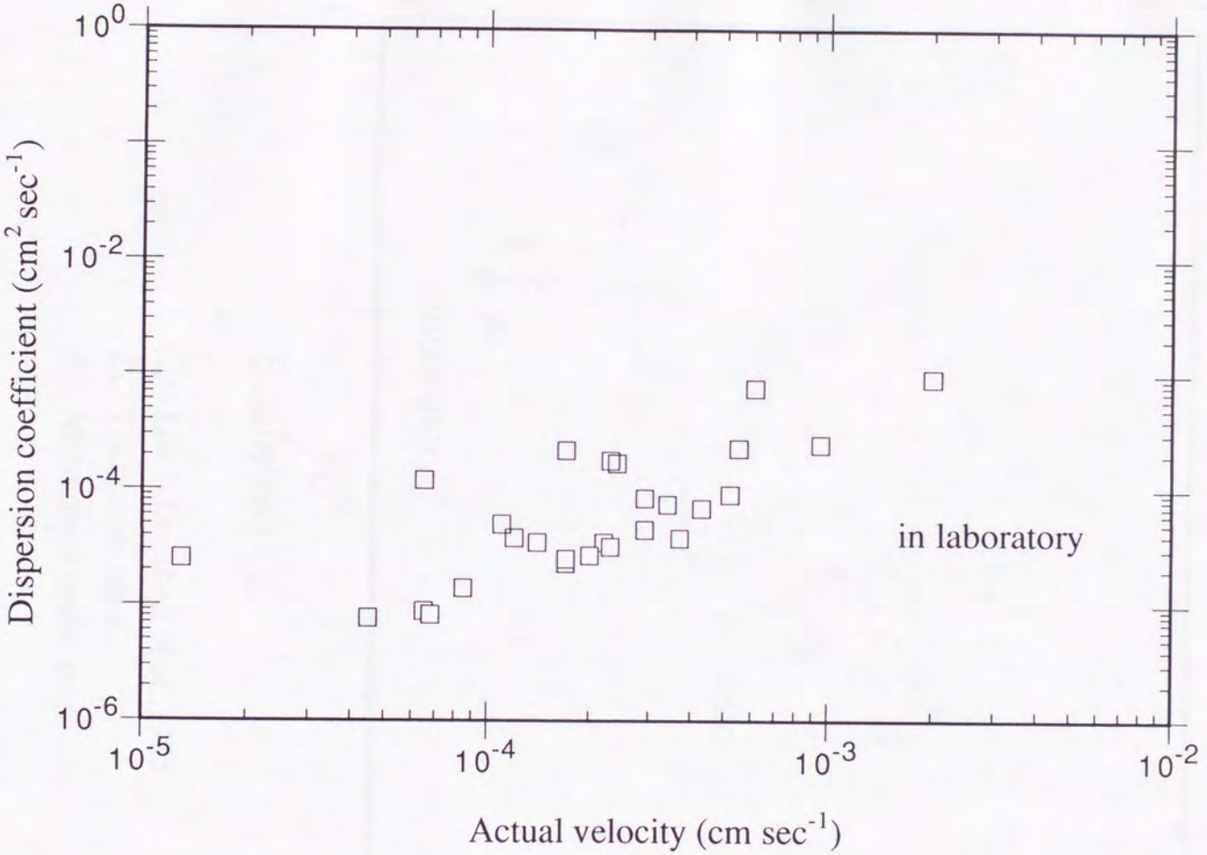
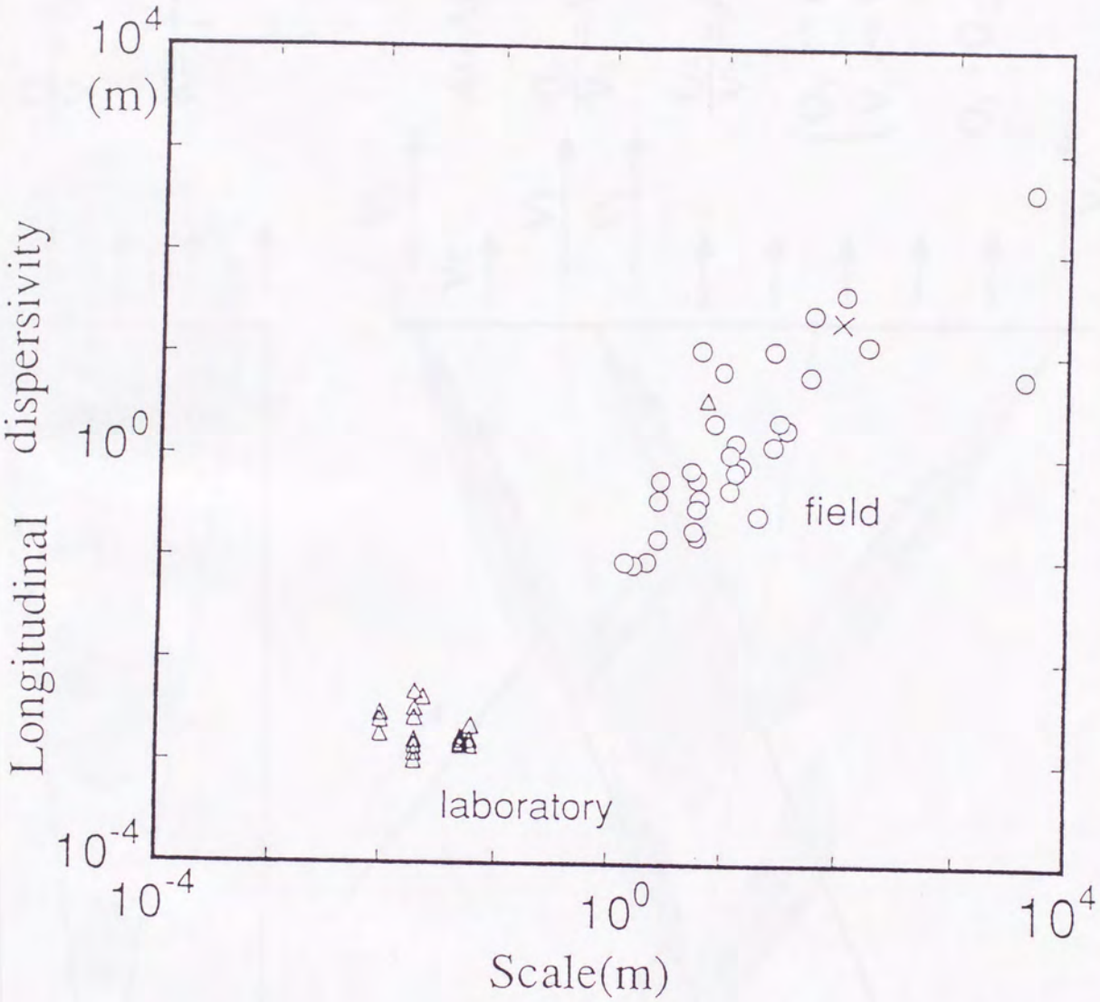


Figure 8.2 Relationship, estimated in laboratory tests, between the disper sion coefficient and actual velocity



○ : Leo S.Leonhart et al.,1985
△ : Toki tracer tests
× : Matsumoto tracer tests

Figure 8.3 Relationship between longitudinal dispersivity and test scale

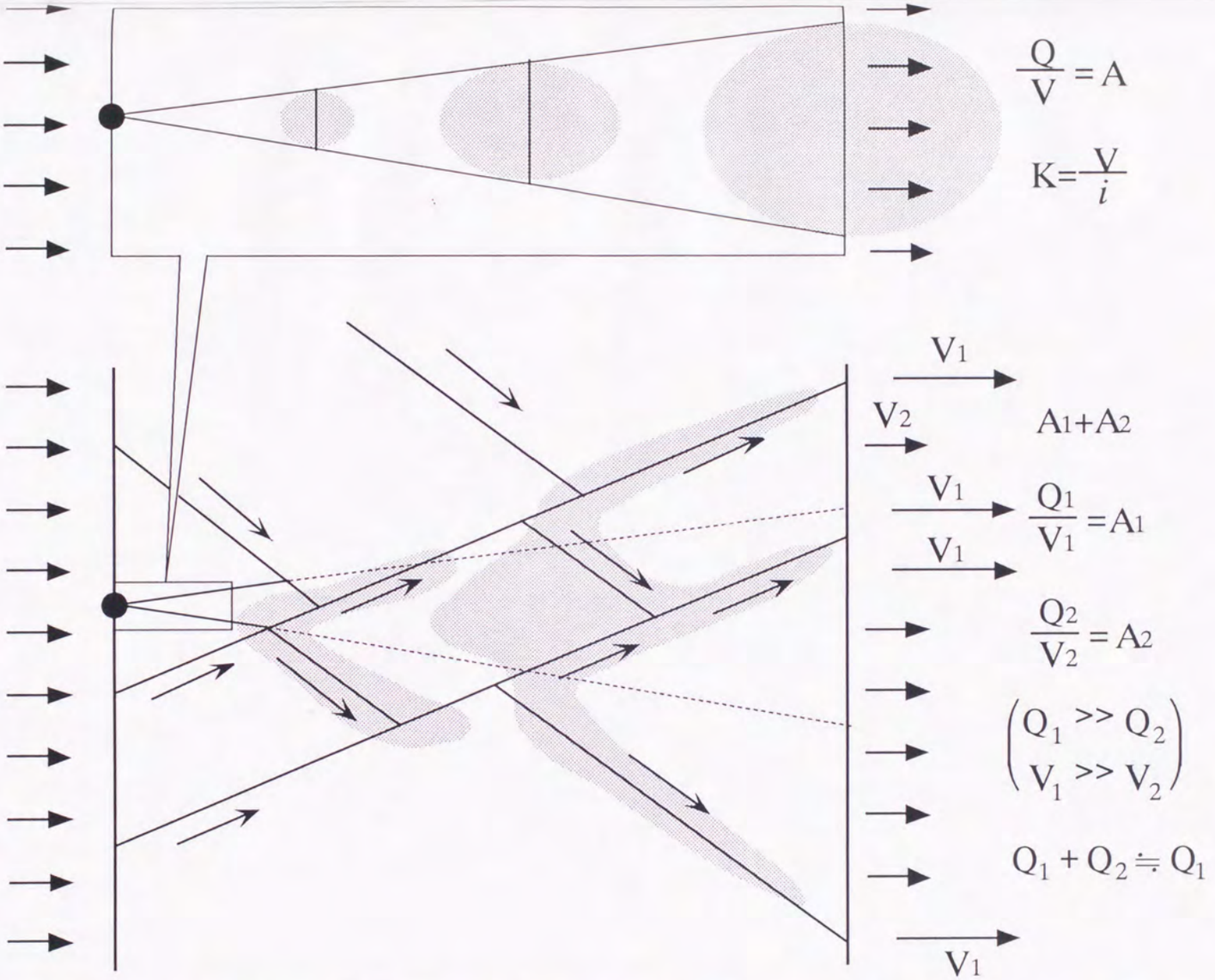
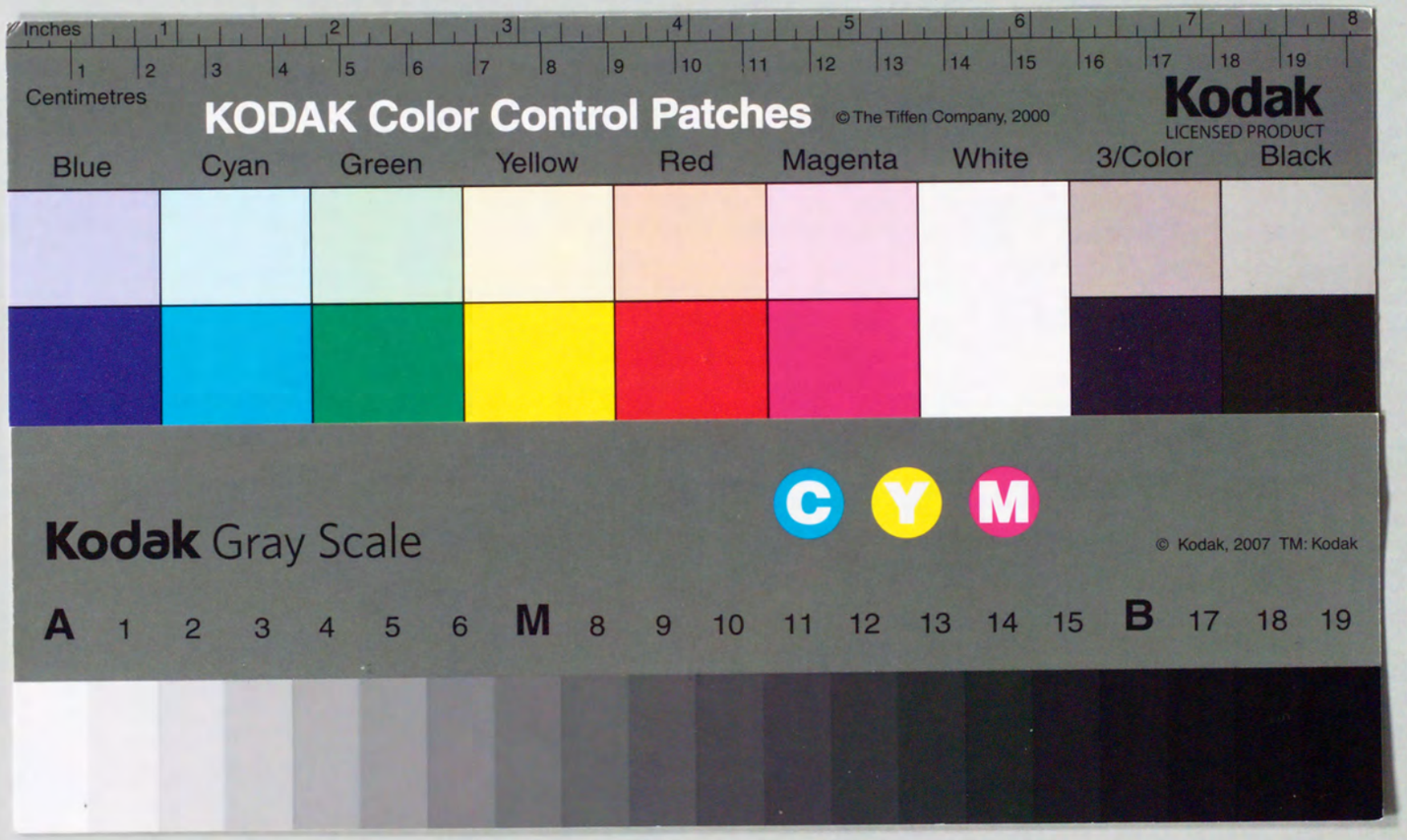


Figure 8.4 Schematic representation of the dilution process caused by mechanical dispersion in homogeneous media and heterogeneous media


Inches
Centimetres
KODAK Color Control Patches
© The Tiffen Company, 2000
Kodak
LICENSED PRODUCT
Blue
Cyan
Green
Yellow
Red
Magenta
White
3/Color
Black
Kodak Gray Scale
C
Y
M
© Kodak, 2007 TM: Kodak
A 1 2 3 4 5 6 M 8 9 10 11 12 13 14 15 B 17 18 19